Thesis for the degree of Doctor of Philosophy in the Natural Sciences

Breaking the cage – Implementing photocages to address spatiotemporal challenges in chemical biology

Emil Sandelin

Department of Chemistry and Molecular Biology, Gothenburg
2024

UNIVERSITY OF GOTHENBURG

Thesis for the degree of Doctor of Philosophy in the Natural Sciences

Breaking the cage – Implementing photocages to address spatiotemporal challenges in chemical biology

Cover: Adaptation of the album cover ”The Dark Side Of The Moon” – Pink Floyd illustrating the *ba*$_3$-type cytochrome c oxidase as it is illuminated by light and X-rays to yield a diffraction pattern.

Emil Sandelin

978-91-8069-707-1 (PRINT)
978-91-8069-708-8 (PDF)
Available online at http://hdl.handle.net/2077/80247

Department of Chemistry and Molecular Biology
Division of Biochemistry and Structural Biology
University of Gothenburg
SE-405 30, Göteborg,
Sweden
Printed by Stema Specialtryck
AB Borås, Sweden, 2023.

SVANENMÄRKET
Tryckssak
3041 0234

ABSTRACT

Visualizing atoms and molecules in motion remains a formidable challenge within structural chemical biology. Significant advances in the generation of ultrashort and bright X-ray pulses have provided the technical framework to facilitate the study of complex biomolecules with atomic resolution. For the first time, it was possible to convince nature's machinery to reveal their temporal structural dynamics by initiating native reactions in photoresponsive systems and observe the molecular dance of life by ultrafast time-resolved serial femtosecond crystallography. However, given the exceedingly small fraction of naturally photoactive proteins within nature's diverse repertoire of proteins, the vast majority remain elusive to detailed, time-resolved structural studies.

A major objective in the forefront of structural biology is to extend the scope of time-resolved X-ray diffraction beyond light responsive proteins to include substrate dependent systems. Photocages constitute a generic method of introducing a biologically relevant substrate to its associated protein with spatiotemporal control. Numerous challenges remain, some of which are addressed in this thesis.

In this work, the native reaction between cytochrome c oxidase and oxygen released from an oxygen photocage is studied by time-resolved serial femtosecond crystallography. These are difficult experiments, both from a theoretical and technical perspective. Nevertheless, we can provide structural evidence for enzymatic turnover following the release of oxygen from the photocage. In this thesis, novel oxygen photocages and singlet oxygen responsive materials have been developed towards addressing contemporary challenges in various scientific fields. An unexpectedly successful study of structural rearrangements in a pH-responsive ion channel following acidification by a photoacid via time-resolved X-ray solution scattering further cements the scientific versatility provided by photocages in the study of temporal dynamics of proteins.

SVENSK POPULÄRVETENSKAPLIG SAMMANFATTNING

För att förstå livets minsta byggstenar står strukturbiologin inför en enorm utmaning i att visualisera atomer och molekyler i rörelse. Denna enorma uppgift är motiverad av den direkta kopplingen mellan proteiners dynamiska struktur och funktion. Tack vare nyliga teknologiska innovationer har vi kunnat belysa och observera den molekylära dansen av proteiner i rörelse. Detta har möjliggjorts med hjälp av ultrakorta och intensiva röntgenpulser som genereras av moderna synkrotron- och frielektronlaserfaciliteter runt om i världen. För första gången har vi, genom att utlösa den naturliga reaktionen i ljuskänsliga proteiner, kunnat följa deras rörelser med hjälp av tidsupplöst röntgenkristallografi för att förstå vilka strukturella delar av proteinet som leder till dess funktion. Men eftersom endast en bråkdel av alla proteiner i naturen är ljusaktiverade, är större delen av proteinernas universum fortfarande dolt för oss. Ett stort mål inom strukturbiologin är att bredda forskningsfältet till att även omfatta proteiner som inte är ljuskänsliga och som i stället har som uppgift att reagera med diverse molekyler i kroppen och i vår omgivning.

I denna avhandling används fotokapslar, molekyler som kemiskt kan frisätta en biologisk aktiv substans genom belysning, som ett hjälpmedel för att möjliggöra studier av naturens fulla repertoar av proteiner. Genom att använda fotokapslar kan vi kontrollerat introducera biologiskt relevanta ämnen till diverse proteiner, och på detta sätt styra när och var reaktionen sker. Denna metod öppnar nya dörrar för att utforska den stora majoriteten av proteiner som tidigare varit utanför vårt räckhåll, och ger oss nya verktyg för att förstå de grundläggande processerna i livet genom att möjliggöra tidsupplösta studier mellan protein och substrat.

Med varje andetag reagerar miljontals av cytokrom c oxidas och konverterar syre till vatten, samtidigt som den frigjorda energin kan användas för essentiella biokemiska processer. Denna livsviktiga reaktion studeras i denna avhandling genom att frigöra syre från en fotokapsel och studera den strukturella dynamiken hos cytokrom c oxidas med tidsupplöst seriekristallografi. Vi tillämpar även liknande fotokapslar för syres energetiska kusin, singlettsyre, i utvecklingen av funktionella gel-material. Avslutningsvis demonstrerar vi att strukturella förändringar kan induceras hos en jonkanal när vi sänker lösningens pH på en mikrosekundskala med hjälp av en pH-fotokapsel som frigör protoner efter belysning.

ACKNOWLEDGMENTS

Five years would have seemed like an excruciating long time if it was not for the great people who made time fly. It really takes a village to raise a child and the same is true for a PhD student. The list of people who deserves the utmost thanks for making these years the most formative time of my life is long. The supervisor has a great impact on the student and here are many ways to teach. **Failure** has been a most present teacher, and it takes great confidence from the supervisor to allow their student to repeatedly; fail and try, try, try again. With that said, few people can match the confidence of my main supervisor. **Calle**. I was allowed great independence in my various projects, sometimes working multiple weeks without as much as a worried glance in my direction. Perhaps this is not entirely true considering that most times I ran out of ideas, you managed to realize this before I did and promptly aim me in the right direction (and sometimes just in another direction). **Thank you** for the opportunity to do my PhD in your group and for showing the confidence in letting me learn how to solve my own problems. **Richard and Gisela**, my official and unofficial co-supervisors. It really requires a special type of character and scientific bravado to take on such a herculean project as the oxidase project. It was a turbulent journey with many ups and downs. Thank you for taking me on this journey and for all the good times, often involving whiskey, and the bad times mostly involving ERC timesheets and fighting the good fight against bureaucracy. **Henrik**, thank you for an engaging and productive collaboration. Your passion for chemistry and cheerful words of encouragement always made it easy for me to find the motivation to push through streaky columns. I really appreciate all the time and effort you put into reading, re-reading and re-re-reading the gel paper. Let's hope that none of us ever needs to read that again. **Julia,** you are the least "PI-ish" PIs I have worked with (and yes, that is a compliment). The KscA project was unexpectedly successful with some of the most enjoyable beamtimes of my PhD and I hope that the continuation of this work lives up this standard moving forward. Thank you for the great collaborations and advice along the way! **Gergeley**, my examiner. Thank you! You did a great job!

Rickard. I recall the bearded vegetarian hiding in the bathroom, dreading the first meeting with me, the master student you never asked for. Our mentor-student relationship has certainly evolved during the years, recently reaching a full circle with the student becoming the teacher. Building character is a process catalyzed by productive suffering and you are one amongst few who truly understand and appreciate this art. Thanks for showing me how proper character development is done. **Jonatan**, "suffering builds character", and I think it is fair to say that our friendship could be categorized as one grown though shared suffering. We could always find comfort in that we were not suffering alone during our numerous failed endeavors in the laser lab (aka dungeon). I think together, we have crashed more project than most people start during a PhD, and it was a pleasure to crash and burn together on every occasion. **Alica**, I know that it wasn't always easy to share an office with me. However, the whiskey office would not have been complete without you and Rickard. Sometimes, I need someone to tell me when I am being unreasonably stubborn, and you

never did shy away from this… (**thanks!**). Sharing offices during a PhD you share the good and the bad days, and we always managed to make the best out of even the worst days! **Arpitha** from the Kabbinale village! You are really one of a kind. I have never met a bigger character in such a small package. It is impossible to understand how you endure the endless chaos of working with Jonathan and I, while maintaining such a cheerful positive attitude. You and I are an unstoppable beamtime team, and most of this stems from your limitless energy and ability to find joy in even the smallest things. **Yeersen**, there is no other way to describe you but as the pillar stone of the Wallentin group. I hope that sharing a lab together with me has left you with some sanity left and hopefully some additional character (not that you need more). **PS:** Don't you to forget to buy me flowers! And yes, roses are fine. **Leo, Leo, Leo**! You are my second favorite master student in our lab. (The first spot needs to be given to Bea or I would never hear the end of it). I am worried for some of the things you still did not manage to learn under my strict supervision, such as cleaning the lab-dishes and making fresh coffee for you supervisor. However, I have zero doubt with regarding your chemistry skills and I am eager to see what you achieve during your PhD. It was an absolute joy to mentor/torment you (pick whatever suits you best). **Bea.** Although you were not mine, you were always my favorite master student. Not because you always made sure to make fresh coffee for your supervisor or that you did more than your fair share of the lab dishes, but because you are such a fun person to work with. It was rare to see anything but a smile on your face when entering the lab and you always made a great effort to spread joy around you. I wish you the best of luck in the final stages of your PhD and remember; never work with cobalt. **Hogan and Andreas**, the Chip 'n Dale of the group during one exhausting year, which I have to admit was probably the most fun year of my PhD. I wish you both the best of luck in your own PhD journeys. **Bhaskar**, welcome to the Wallentin group. You picked the worst time to join (Natrium move) but it was great to have an extra set of hands around!

To the current and previous members of the oxidase group: Swagatha, thank you for putting up with the occasional mess in the spectroscopy room that I might have participated in creating. Also thank you for all the help when I started my PhD and the great beamtime company along the way! **Adams**, I could never really understand what it is that you do and I suspect you feel the same about me! Now at least you can read what I do and I look forward to doing the same soon! **Doris,** I hope that you have recovered from all the syringe related trauma I might have caused and that none of us ever again needs to look at a Hamilton syringe ever again. **Peter Dahl**, you were my first beamtime partner! Thanks for all the help with 3D printing and redesigning over the years! **Cecilia & Rebeca,** you left the oxidase project for us to continue, are you not sad now upon reading this that you did not stay for an additional five years? **Lucija** and **Johan**, I don't know how they managed to fool you into coming for our beamtimes, **I am sorry**! But it was great to have you guys around! **Per.** You have displayed a great amount of patience while sharing a lab with me. Thank you for always helping when asked and for all the great company during beamtimes and beer club. **Greger**, we had some eventful beamtime adventures which might or might not have included some near-death experiences. It was tons of fun! Thanks for the great company and your dedication towards the KscA project! **Ylber** and **Jens**, it has been a blast hanging out with you guys and thanks for all the great beer club nights, board game nights and other

various extracurricular activities over the years! **Andrea**, great work with the KcsA project, I was never worried for one second that you would not manage to get all the protein we needed. **Monika B.** Thank you for all the assistance during our numerous MAX IV beamtimes, we did have some fun even when things were not really working! Further thanks to all the inhabitants of the Lundberg Lab; **Filippo, Leona, Giorgia, Hanna, Ann, Taru, Bozidar, Szabolcs** and all other beer club enthusiasts for this time!

To the members of the old floor 8. Clara, you suffered in the trenches with me during multiple KEM030s and although it was painful at times, I have many fond memories! It was a blast brewing together which I hope we will do soon again! **Alex**, I have a weak memory of us crushing it at Beer-Pong and considering my weak recollection, I suppose it is you I have to thank? **Andrew**, you are the most and only British person I know, I don't think I need to say more. **Bijan**, you were the first person to call me a "proper chemist!" upon completing my first column purification, no take backs. Thanks for keeping the NMR alive long enough for me to get my crappy spectrums! (No fault of yours). Morten, Oscar, Anna and other the members of the **Grøtli group**, thank you for letting us piggyback during the Natrum move and for being the organized group on the floor! Thanks to all that I fail to personally mention by name, I am sure there are a few.

To my "non-chemistry" friends and family: Thank you for the support these last five years! **Emil**, no one else would have put up with all my whining, complaints and relentless rants and I am truly impressed that you patiently listened on (almost) every occasion. Thank you for proof-reading the thesis and everything else! You will soon have the pleasure of developing all the character that is associated with finishing a PhD yourself!

Julia. I am very fortunate to have met such a fun, kind and caring person. Thank you for your patience while supporting me through the final time of my PhD and for being the wonderful person that you are!

To my family. Not once has anyone expressed the slightest doubt that I would complete this thesis, and as I trust your judgement, it made me more confident in myself also. Thank you for your endless encouragement and support. Going through a PhD with such incredible family support is really playing the game on the easiest setting! **To my little sister,** I can always rely on you when I need an honest opinion, **tack för det! Och för att du är den jobbiga skitungen du är!**

List of publications

This thesis is based on the following studies, referred to in the text by their Roman numerals.

I. Characterization and evaluation of photolabile (μ-peroxo)(μ-hydroxo)bis[bis(bipyridyl)cobalt caged oxygen compounds towards enabling time-resolved crystallographic studies of cytochrome c oxidase

Emil Sandelin; Jonatan Johannesson; Ola Wendt; Gisela Brändén; Richard Neutze; Carl-Johan Wallentin. (**2024**) *Accepted for publication in Photochemical & Photobiological Sciences*.

II. Structural changes in cytochrome c oxidase following the reduction of dioxygen to water

Doris Zorić[†] ;Jonatan Johannesson[†]; Adams Vallejos ; **Emil Sandelin** ;Arpitha Kabbinale; Swagatha Ghosh; Aaron Flink ;Monika Bjelčić ;John Rönnholm; Peter Dahl; Emma Victoria Beale; Christoph Bostedt; Claudio Cirelli ;Camila Bacellar Cases da Silveira; Philip Johnson; Dmitry Ozerov; Alex Batyuk; Sebastien Boutet; Chris Kupitz; Ariana N. Peck; Fred Poitevin; Ray Sierra; Stella Lisova; Carl-Johan Wallentin; Gisela Brändén; Richard Neutze. *Manuscript* (**2024**) [†]These authors contributed equally to this work.

III. Spatiotemporal release of singlet oxygen in low molecular weight organo-gels upon thermal or photochemical external stimuli

Emil Sandelin; Leonard Schilling; Ekata Saha; Andrea Ruiu; Richard Neutze; Henrik Sundén; Carl-Johan Wallentin. *Manuscript* (**2024**). *(Submitted for publication in Small and is currently under peer review).*

IV. Time-resolved studies of pH induced conformational changes in a potassium channel

Andrea Cellini[†]; Greger Hammarin[†]; Analia Banacore; **Emil Sandelin**; Jonatan Johannesson; Beatrice Keller; Lucija Ostojic; Leona Cesar; Ayaan Ali; Giorgia Ortolani; Taru Larkiala; Céline Mariette; Mikhail Kozhaev; Kévin Pounot; Matteo Levantino; Carl-Johan Wallentin; Richard Neutze; Julia Morud. *Manuscript*, (**2024**). [†]These authors contributed equally to this work.

Further research articles of the author, which are not included in the thesis.

I. **Time-resolved serial crystallography to track the dynamics of carbon monoxide in the active site of cytochrome c oxidase**

Cecilia Safari; Swagatha Ghosh; Rebecka Andersson; Jonatan Johannesson; Petra Båth; Owens Uwangue; Peter Dahl; Doris Zoric; **Emil Sandelin**; Adams Vallejos; et al. Sci. Adv. (**2023**); 9(49).

II. **A simple goniometer-compatible flow cell for serial synchrotron X-ray crystallography**

Swagatha Ghosh; Doris Zorić; Peter Dahl; Monika Bjelčić; Jonatan Johannesson; **Emil Sandelin**; Per Borjesson; Alexander Björling; Analia Banacore; Petra Edlund et al. J. Appl. Cryst. (**2023**); 56, 449-460.

III. **A Facile Access to Novel (5+5) Annellated Heterocycles: Synthesis of a Furopyrrole, an Imidazoimidazole and a Pyrroloimidazole**

Pavol Zlatoidský; Elisa Martinelli; **Emil Svensson**; Alexis Pruvost. Synthesis. (**2019**); 51(18): 3491-3498.

Contribution report

Paper I: I performed the work described in the paper and wrote the manuscript. The protein measurements were conducted together with Jonatan Johannesson (J.J) who produced the protein and assisted with the time-resolved spectroscopic measurements.

Paper II: My contribution to this work involves: spectroscopic characterization and validation of the reaction initiation (much work is based on the findings of Paper I), strategic planning of the experiments and execution of the experiments. The work is based on four XFEL based SFX experiments at the European XFEL, 2x SwissFEL and LCLS in the time period from May 2019 until November 2023. In addition to this, some data was also collected at MAX IV at different times in the project where I participated at the experiments.

Paper III: I supervised a master student (Leonard Schilling, L.S) and together we performed all the work in the paper, involving the synthesis of all the compounds and carried out the characterization of the relevant properties for singlet oxygen binding and release in the gel phase. The rheology was performed by Andrea Ruiu and constitutes the only part of the experimental work not performed by me. I wrote the manuscript.

Paper IV: I was responsible for developing and verifying the reaction initiation protocol and setup together with J.J. I also optimized and performed the synthesis of the relevant photocage. I participated in the collection of the X-ray scattering data in the manuscript at ESRF during three separate experiments from May 2022 - July 2023. I assisted in writing the manuscript.

Contents

ABBREVIATIONS

Abbreviation	Full name
$^1O_2$	Singlet oxygen
$^3O_2$	Triplet oxygen
ADP	Adenosine diphosphate
ATP	Adenosine triphosphate
BNC	Binuclear center
bpy	Bipyridine
CcO	Cytochrome c oxidase
DBU	1,8-Diazabicyclo(5.4.0)undec-7-ene
DTBA	Dithiobutylamine
DTT	Dithiothreitol
HCO	Heme-copper oxidase
HOMO	Highest occupied molecular orbital
HPBC	(μ-hydroxo-μ-peroxo)bis[bis(bipyridyl)cobalt(III)]
ISC	Intersystem crossing
KcsA	K-channel Streptomyces A
LCP	Liquid cubic phase
LMCT	Ligand to metal charge transfer
LMWG	Low molecular weight gelators
LUMO	Lowest occupied molecular orbital
MB	Methylene blue
MGC	Minimum gelation concentration
MVCO	Carbon monoxide bound mixed valence
NaAsc	Sodium ascorbate
NaDt	Sodium dithionite
NHC	N-heterocyclic carbene
NMR	Nuclear magnetic resonance
NPE	Nitrophenylethyl
PA	Phenyl-anthracene
PDT	Photodynamic therapy
PLS	Proton loading site
PS	Photosensitizer
rt	Room temperature
SAXS	Small angle X-ray scattering
SET	Single electron transfer
SFX	Serial femtosecond crystallography
TR	Time-resolved
WAXS	Wide angle X-ray scattering
XFEL	X-ray free electron laser
XSS	X-ray solution scattering

AIM OF THIS THESIS

The aim of this thesis has been to develop and implement photocages towards structural studies of substrate dependent proteins. One scientific objective was to utilize an oxygen photocage to initiate the native reaction between cytochrome c oxidase and molecular oxygen and to study the structural dynamics with the use of time-resolved serial femtosecond crystallography. Furthermore, we developed novel oxygen photocages derived from molecular oxygen and the excited singlet state oxygen. We also aimed to explore various other photocages in structural studies of substrate dependent systems.

THEORY AND BACKGROUND

A breath of fresh air has not always consisted of what we today take for granted; 78 % nitrogen (N_2), 21 % oxygen (O_2), about one percent argon and 0.04 % (and growing) carbon dioxide (CO_2). I don't like change. Whether it's relocating to a new building in the final months of a Ph.D. education or adjusting to the consequences of the changes in the composition of the air we breathe. Such changes bring little but aches and hardships. Yet, there's one distant change that must be considered somewhat of an improvement, a change that led to our oxygen rich environment.

2.5 billion years ago, photosynthetic cyanobacteria evolved do something that we currently struggle with: making good use of the abundant CO_2 in the atmosphere. This was a successful strategy, considering that cyanobacteria, or rather their descendants, continue to thrive to this day. One major by-product of this evolutionary event was the reconstitution of atmospheric gases, marked by the formation of vast amounts of O_2. This marked the beginning of the era of aerobic organisms, often referred to as the "Great Oxidation Event" or "the "Rusting of the Earth".[1] Annually, around 200 billion tons of CO_2 is converted into various organic building blocks via the photosynthetic process and leads to the liberation of about 140 billion tons of O_2.[2] The formation of molecular oxygen through photosynthesis is an endergonic process, meaning it requires energy. Very few things of value come without effort or work, and the same is true for the chemistry of life. A debt of energy must be paid and the accepted currency within living cells is adenosine triphosphate (ATP). Upon ATP dephosphorylation into adenosine diphosphate (ADP) the energy conserved within the chemical bond in liberated. To settle the various biochemical energy debts in our bodies, a copious amount of ATP is consumed and needs to be resynthesized on daily basis, ~ 50 kg to be somewhat imprecise. A breath-taking > 90 % of the oxygen that we inhale is reserved for cytochrome c oxidase (CcO), the terminal electron acceptor in the electron transport chain, mediating the four-electron reduction of molecular oxygen to water.[3] During this process, protons are pumped across the inner mitochondrial membrane, generating a proton motive force that settles the various energy debt associated with the synthesis of ATP. It is imperative that the pumped protons move unidirectionally, that is; once a proton has been transported across the membrane it should not leak backwards. How does nature prevent this? Why does nature do it this way? These are questions that despite decades of rigorous scientific investigations remains to be resolved. It would be inappropriate to attribute this to a lack of effort considering the numerous explanations that have been proposed so far.[4,5] A better question one might ask is; what tool has been missing that could finally settle this debate. For years, measuring the output and input into nature's black box has only been able to tell us so much.

The primary research objective for this thesis has been to employ time-resolved X-ray crystallography—a tool with the potential to unveil the inner workings of nature's black box and put it in the spotlight. Ultrafast time-resolved crystallography is enabled by recent scientific breakthroughs in the generation of X-rays with high intensity and short duration, mediated by synchrotron and X-ray free electron laser facilities around the world. The

nature of the technique and the radiation source used demands a sophisticated method of initiating the native reaction of interest. What is still lacking is a chemical director to synchronize the millions of identical black boxes. We hypothesized that the incorporation of a photocage, an inactive derivative of the natural substrate, that can be activated upon light illumination, could act as this director and with blast of a laser, initiate and synchronize the chemical orchestra of life.

1.1 VISIBLE LIGHT

Twelve years ago, during a high school visit to Chalmers University, I found myself face-to-face with a "nerdy" Ph.D. student of physics (or so I assumed). The question he posed (repeatedly) still lingers vividly in my memory: "What is light?". Armed with a rare moment of having done my homework, I answered silently in my own head, regurgitating what I had studied late the previous night – "Light is both a particle and a wave." To my surprise, a classmate echoed my response, and the Ph.D. student, with a mischievous grin, exclaimed, "Yes! This is true... but... What is light?" Little did I know, this playful game would stretch on for another 10 - 15 minutes.

In 1865, in his seminal work, "A Dynamical Theory of the Electromagnetic Field", Maxwell took on the goliath task to unravel the fundamental laws governing light. While he didn't explicitly define light itself, he made an astounding prediction - the existence of electromagnetic waves that travel at the speed of light. This led Maxwell to propose that light is fundamentally an electromagnetic phenomenon and a form of electromagnetic radiation.[6] Light, as described by Maxwell, propagates as a wave characterized by its frequency (f), wavelength (λ), and speed (c), inherently tied together as described by **Equation 1** ; where c = the speed of light.

$$\lambda f = c \qquad \textbf{(1)}$$

Light has an associated energy, which was subsequently demonstrated by two scientific giants, Max Planck and Albert Einstein, who demonstrated that light comes in quantized bundles referred to as photons. This energy (E) of a photon is a product of its frequency (f) and Planck's constant ($h = 6.626 \cdot 10^{-34}$ J s) according to **Equation 2**.

$$E = h f \qquad \textbf{(2)}$$

Light interacts with matter and of particular importance is the interaction between light and another fundamental particle, the electron. The properties and behavior of the electron is fundamentally tied to the very core of chemistry as it is typically the actions of electrons that dictates the outcome of chemical reactions. When a photon and an electron interact, there is a chance that a chemical change will occur. This change is dependent of the energy of the photon and the chemical and physical environment of the electron. If the photon possesses sufficient energy, it can excite an electron to a higher energetic state, more commonly referred to as an excitation. The chemistry of these excited states, mediated by light, is what is studied in the field of photochemistry and is governed by two rather intuitive laws[7]:

(1) Only light absorbed by a substance is effective in bringing about a chemical change. (The Grotthuss–Draper law)
(2) For every single photon absorbed, only one substrate can react. (The Stark–Einstein law)

When an electron is excited, it transitions to a higher energy orbital from its highest occupied molecular orbital (HOMO) to the lowest unoccupied molecular orbital (LUMO). This generates an excited singlet state that upon intersystem crossing (ISC) yields an excited triplet state. Typically, it is the chemistry of the excited triplet state that is involved in bimolecular reactions due to its extended lifetime compared to the corresponding singlet state, prolonged by the spin forbidden transition between singlet and triplet states.[7] The study of these various transitions is commonly performed by ultraviolet/visible (UV/Vis) spectroscopy. When a molecule, typically dissolved in a solvent with minimal light absorbing properties, is exposed to light of varying wavelengths it will absorb photons with the appropriate energy that matches a specific electronic transition. This is exploited in UV/Vis spectroscopy where the sample is exposed to a range of wavelengths (typically between 200-800 nm) to probe for all possible electronic transitions in this region. The absorption of light by a molecule is expressed through the Beer-Lambert law, shown in **Equation 3**, where A is the absorbance, l is the pathlength where light travels through the sample, and ε is the molar attenuation coefficient.

$$\mathbf{(3)} \qquad A = \varepsilon \, l \, c$$

The absorbance of light across selected wavelengths is measured as the difference in detected transmittance between the sample (I) and a reference sample typically only containing solvent (I_0), shown in **Equation 4**.

$$\mathbf{(4)} \qquad T = \frac{I}{I_0}$$

In the realm of light interactions, there exists a region of particular importance for life, where the energy difference between two molecular orbitals aligns with the energy of photons within the visible spectrum of electromagnetic radiation. Molecules that exhibit absorbance in the visible light range, between 400 – 700 nm, are termed chromophores. In accordance with the Grotthuss-Draper law, the detection of light requires an interaction between light and a molecule. The absorbance of light has a transformative power to induce further chemical change, utilizing the energy acquired from the photons to signal and facilitate various biochemical functions. In human vision, the spectral range of light interaction is governed by the absorbance of specific chromophores, such as retinal. When a photon with the appropriate wavelength is absorbed by retinal it leads to an isomerization reaction which prompts a signaling cascade reaction by inducing a conformational change of the associated protein. This is how our eyes knows that a photon of a specific wavelength has made it to the right place. It is important to note that not every absorbed photon necessarily results in a chemical reaction or change. The likelihood of a chemical reaction upon photon absorption is quantified by the quantum yield (ϕ). If ϕ = 1, it indicates that one absorbed photon leads to one chemical reaction representing a 100 % quantum efficiency. The

quantum yield is a valuable measurement of how efficient a photochemical process is. The most common method of determining the quantum yield is to benchmark the unknown process to a chemical reaction with a known quantum efficiency by chemical actinometry.[8,9] While the visible spectrum is important for many biological processes, looking beyond it reveals a plethora of other novel interactions, particularly with higher energy photons like X-rays. Unlike photons in the visible spectrum, X-rays have substantially more energy, allowing them to interact with materials that visible light cannot.

1.2 X-RAY CRYSTALLOGRAPHY – BUT THIS ONE GOES TO ELEVEN

Light indeed has quite some tricks up its sleeve. It's intriguing how even within the visible spectrum, light's behavior can vary dramatically, from the precision of a short-pulsed laser beam to the illumination by a gentle stream of photons provided by a lit candle.

The electromagnetic spectrum is divided into different regimes, from gamma rays to radio waves, as illustrated in **Figure *1***. As we venture beyond the visible spectrum, increasing the frequency and energy of electromagnetic radiation, we traverse through ultraviolet light and ultimately step into the enigmatic world of X-rays. The rules of the game change as the high energy allow for novel interactions with matter. X-rays have wavelengths ranging from 10^{-12} to 10^{-9} m and is typically categorized into soft X-rays, X-rays, and hard X-rays, from longer to shorter wavelengths. To visualize the interactions between atoms, molecules, and proteins, with atomic resolution hard X-rays with a wavelength between 0.1 – 1 Å, are ideally suited for this task.

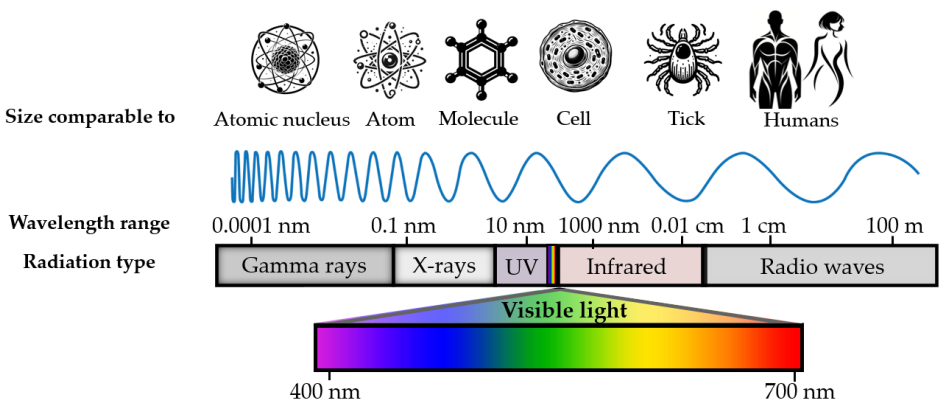

Figure 1. Electromagnetic spectrum ranging from gamma rays to radio waves. Black and white illustrations were generated with DALLE via ChatGPT 4.0.

The fundamental principle first formulated by the father and son team, Henry and Lawrences Bragg (both first name William) in 1913 termed Bragg's law. It is a simple yet powerful equation that provides the foundation for how X-rays diffract in a crystal lattice

(**Equation 5**). Where λ is the wavelength of the X-ray, d is the distance between the planes, n is an integer and θ is the incident angle of the X-ray.

$$n\lambda = 2d \sin(\theta) \quad (5)$$

When a crystal is exposed to X-rays of suitable wavelength and intensity, the dense cloud of electrons within the orderly crystal scatters the incoming X-rays. This interaction leads to constructive interference dictated by Bragg's Law, culminating in a discernible pattern with spots of varying intensity. The coherence of in-phase X-ray waves determines the strength of these spots captured by a detector, each carrying information about the crystal's dimensions, symmetry, and atomic coordinates. However, stationary crystals (**Figure 2**, top) limit the intersection with the Ewald sphere (**Figure 2**) —a conceptual sphere with a radius of $1/\lambda$— with the crystals reciprocal lattice, capturing only a portion of potential diffraction data. By rotating the crystal, the reciprocal lattice is likewise rotated, bringing different atomic planes into reflective positions, allowing new reciprocal lattice points to intersect with the Ewald sphere. This continuous rotation allows a comprehensive dataset to be collected by the diffractometer, essential for constructing the three-dimensional model of the crystal. The Ewald sphere originates at the X-ray source with a size depending on the wavelength of the incident X-rays: the shorter the wavelength, the bigger the sphere.[10] The collected data, while rich in intensity information, do not convey the phase of the scattered waves, giving rise to the infamous phase problem.

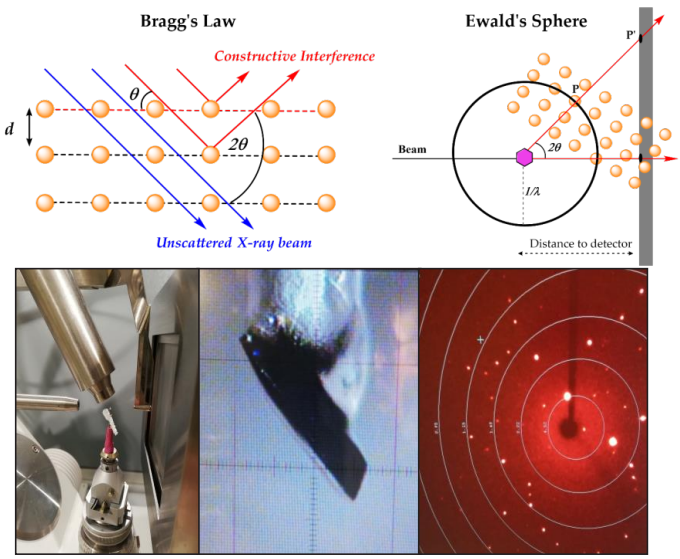

Figure 2. Top: ***Left)*** A schematic representation of the principle of Bragg's law where an incoming X-ray beam is diffracted by a crystal where the spheres represent atoms within the crystal. ***Right)*** Ewald's sphere illustrating when Braggs law has been satisfied which results in diffraction which can be collected with a detector. **Bottom:** ***Left)*** A crystal mounted in a traditional X-ray diffractometer cooled with a stream of liquid nitrogen. ***Middle)*** A close up of the crystal which is rotated and **right)** the diffraction pattern obtained after 30s of continuous exposure to the X-ray source.

To reconstruct the three-dimensional structure, crystallographers rely on indirect methods to estimate these missing phases such as; Molecular Replacement (MR), Multiwavelength Anomalous Diffraction (MAD) and Single Isomorphous Replacement (SIR).[10] In crystallographic studies, the size of the crystal under examination, can significantly influence the experimental requirements and complexity of data collection. For small organic molecules, "large crystals" are often more readily obtainable. These larger crystals scatter X-rays more effectively, yielding clearer diffraction patterns, which mostly can be resolved with standard X-ray diffraction equipment, shown in **Figure 2**. Smaller crystal will scatter X-rays less efficiently and with increasing molecular complexity such as biomolecules, this poses a significant challenge in attaining sufficient resolution without causing damage to the crystal. In protein crystallography, especially for membrane proteins, the crystals obtained are typically very small, often in the micrometer range. Membrane proteins are challenging to crystallize due to their amphipathic nature, having both hydrophobic and hydrophilic regions, and often have complex and dynamic structures.[11] These tiny crystals require more intense X-ray beams to produce high quality diffraction data and beams of this caliber are only readily available at technically advanced facilities such as synchrotrons or X-ray Free Electron Lasers (XFELs).[12] The facilities of relevance for this thesis are shown in **Figure *3***.

Figure 3. Top: Left) The European synchrotron and radiation facility (ESRF) located in Grenoble, France, supported by twenty-two countries and has been conducting X-ray based scientific measurements since 1994. In 2022 it received an impressive upgrade which increased the performance with a factor of one hundred.[13] **Middle*)*** The SACLA facility in Japan, co-located with the SPring-8 synchrotron, is renowned for its XFEL. **Right)** The MAX IV Laboratory in Sweden, operational as a user facility since 2016, succeeds the MAX-lab (1987-2015) and with its 16

beamlines offering advanced X-ray spectroscopy, scattering/diffraction, and imaging techniques.[14] **Bottom: Left)** The Linac Coherent Light Source (LCLS) XFEL at SLAC National Accelerator Laboratory in the United States, operational since 2009. **Middle)** the SwissFEL at the Paul Scherrer Institute (PSI) in Switzerland, operational since 2016. **Right)** The European XFEL, located in Germany has been operational since 2017.

The advent of synchrotron radiation marked a significant advance for X-ray crystallography. Synchrotron radiation is produced when a charged particle, such as an electron, is accelerated to near-light speeds and forced to travel in a curved path by a magnetic field.[15] This acceleration leads to the emission of extremely bright and intense X-ray radiation, which was initially deemed a nuisance by frustrated particle physicists as it represented a loss in energy. However, it did not take long until it was realized that this could be used to generate X-rays of exceptional brightness, with tunable wavelengths, and very short pulses. This made it ideal for a wide range of scientific applications. For crystallographic applications, the brilliance of the synchrotron radiation enabled the study of significantly smaller and more imperfect crystals than those typically required for traditional X-ray sources. The enhanced beam brightness significantly reduced the required exposure time to collect a diffraction pattern, allowing for rapid acquisition of large datasets. Furthermore, the ease at which the wavelength could be tuned has facilitated the routine use of specific analytical techniques and expanded the toolbox of X-ray based studies.

While traditional Cu-based X-ray diffractometers typically requires exposure times ranging from seconds to minutes, synchrotron-based experiments frequently employ exposure times in the range of microseconds to milliseconds. This reduction in exposure time and increase in brilliance not only yielded an increase in time efficiency; it also opened the door for completely new scientific avenues. Particularly, for the study of atoms in motion. This breakthrough is analogous to the advances made in camera technologies. From hours-long portrait sittings suffered through by early nobles and kings, to modern cameras capturing sub-microsecond events with high temporal and graphical resolution. A similar revolution has now transformed time-resolved crystallography. The brief duration of X-ray pulses in synchrotron sources intersected with the timescale of enzyme catalysis. The enzymatic turnover number (k_{cat}), varies widely from the very slow (10^{-2} s^{-1}) to the very fast (10^{5} s^{-1}), as seen in enzymes like carbonic anhydrases[16] and acetylcholinesterase[17] respectively. According to the BRENDA database, which compiles various kinetic parameters for enzymes, the median enzymatic reaction rate is approximately 13.7 turnovers per second (**Figure 4**).[18] The integration of synchrotron radiation into crystallography now allowed for the visualization of snapshots of these enzymatic events, correlating structural changes with functional outcomes at unprecedented speeds. However, this was still far away from the scale of rapid intermolecular movements during the timescale of the actual chemical reaction and the associated movements of the protein machinery.

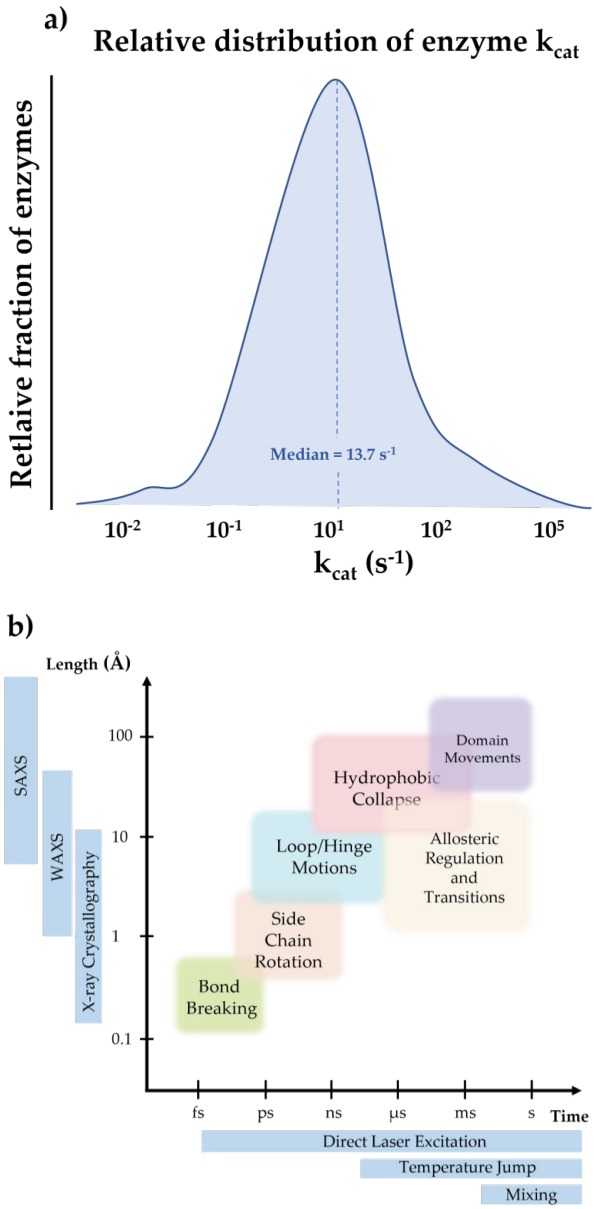

Figure 4. a) An overview of the relative proportions of enzymatic reaction rates. Figure adapted from ref.[18] **b)** Approximate time-scale of relevant events which are typically studied with the various X-ray based techniques in addition to traditional crystallography such as small angle x-ray scattering (SAXS) and wide angle x-ray scattering (WAXS) in time resolved studies. Additionally, it shows what method of reaction initiation is suitable for observing different types of molecular dynamics. Figure is adapted from ref.[19]

The advances of XFELs marked the final piece of the puzzle. This technology differs from how synchrotron radiation is generated by its linear configuration, generating X-ray pulses

by accelerating a high energy electron beam through an undulator magnet. The X-ray pulses generated by XFELs are of extraordinary intensity and ultrafast duration, enabling observations of molecular dynamics on the femtosecond timescale. Initially, there was skepticism regarding the feasibility of these high-intensity X-rays and protein crystals due to the inherently fragility, akin to firing a high caliber bullet though glass. Not a completely unfair comparison but fortunately it differs where it matters. It was predicted that diffraction resulting from the interaction of the X-ray and crystal occurs before the inevitable destruction of the crystal has had time to unfold. This phenomenon is central to modern protein crystallography and is referred to as the principle of "diffraction before destruction".[20,21]

Nothing is free in life or science; a price must be paid for this fortunate phenomenon. The destructive nature of the XFEL necessitates a different method for data collection. Unlike traditional methods where a single or handful of crystals are rotated to capture data from all angles, the crystals need to be replenished after each exposure to an XFEL beam. This led to the development of serial femtosecond crystallography (SFX). In a SFX experiment, a stream of crystals in aqueous or a viscous fatty matrix is extruded from an injector system and passed through an X-ray beam. This results in a more complex data analysis process as the diffraction patterns are collected from many different crystals in random orientations. However, as a consequence of the ultrafast duration of the X-ray pulse, the diffraction data is generated before the onset of radiation damage. Radiation damage is a common topic of discussion regarding synchrotron data of proteins containing redox sensitive moieties such as metalloenzymes.[22–24] After the initial success story of the first solved SFX structure with XFEL radiation, photosystem I, a light responsive protein complex responsible for bio-solar energy conversion, it was only logical to further push the limits of what this new technique could achieve.[25] Due to the ultrafast nature it provided novel access into the avenue of light induced structural changes in the picosecond range. Reaction intermediates quickly started to appear in the scientific literature following the implementation of time-resolved (TR)-SFX.[26,27]

In a typical TR-SFX experiment of a photo responsive system, the crystals are extruded from a microjet,[28] a pump-laser is used to initiate the photochemical reaction, which is then subsequentially probed by the X-ray pulse (illustrated in ***Figure 5***). For the first time, it was possible to visualize the molecular dance of life. This has been shown to be a very successful method for light responsive systems.[29] However, it left a lot on the table considering the miniscule proportion of light responsive proteins in the total repertoire of proteins in nature's toolbox.[19] To facilitate the study of substrate dependent proteins, with comparable spatiotemporal control, novel approaches to initiate the reaction of study have been suggested, such as: liquid mixing jets,[30] picolitre "drop on drop" rapid diffusion,[31] temperature jumps,[32,33] stimulation by an electric field,[34] each with its associated challenges. One particularly interesting approach is the implementation of photocages, where the natural substrate of the enzyme is chemically modified which renders the substrate unreactive. Until a light pulse activates the substrate which will be discussed in greater details later.

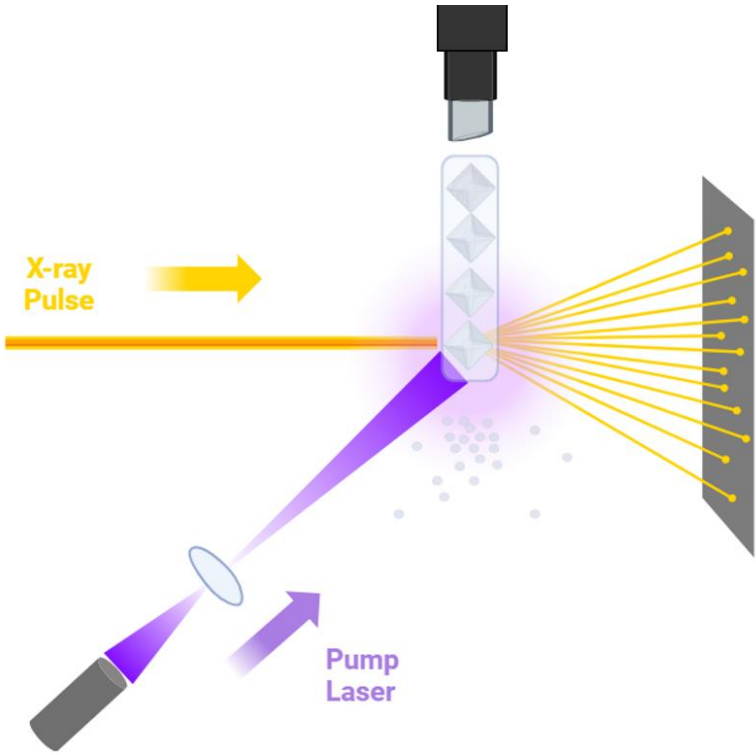

Figure 5. The typical experimental setup in a TR-SFX based experiment typically performed at XFELs where a sample injector delivers the protein crystals to the X-ray beam as a thin jet. Laser illumination is performed shortly prior to the interaction of the protein crystal and the X-ray beam at a determined time delay to trigger a photochemical reaction.

1.3 OXYGEN – A BREATH OF FRESH AIR

"Without darkness there can be no light." The same saying holds true for molecular oxygen as the excess of O_2 in our atmosphere is a consequence from light emitted by the sun. The tie between oxygen and light is biblical in the literal sense. Life as we know it starts with cellular respiration, and what other experimental method of study is more suitable to study the interplay between oxygen and light, but one dependent of light itself.

Oxygen manifests itself in many different shapes and forms in nature. It can be found in minerals, metal oxides, carbonates, phosphates, water, proteins, and carbohydrates. In the gaseous state it is a diatomic molecule comprised of two oxygen atoms bonded together. Much of its chemical versatility stems from its ability to adopt various electronic configurations. In contrast to other homonuclear molecules, the oxygen we breathe possesses a paramagnetic triplet ground state ($^3O_2$) with an open-shell electronic configuration featuring two unpaired electrons (**Figure *6***).

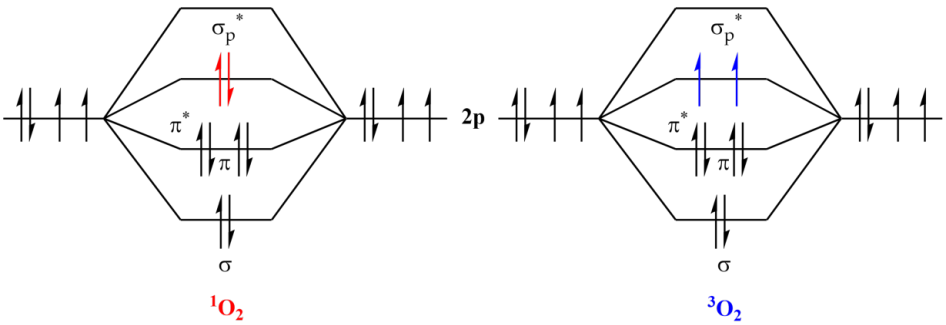

Figure 6. Electronic configuration of molecular oxygen in the ground state ($^3O_2$) and the singlet state ($^1O_2$).

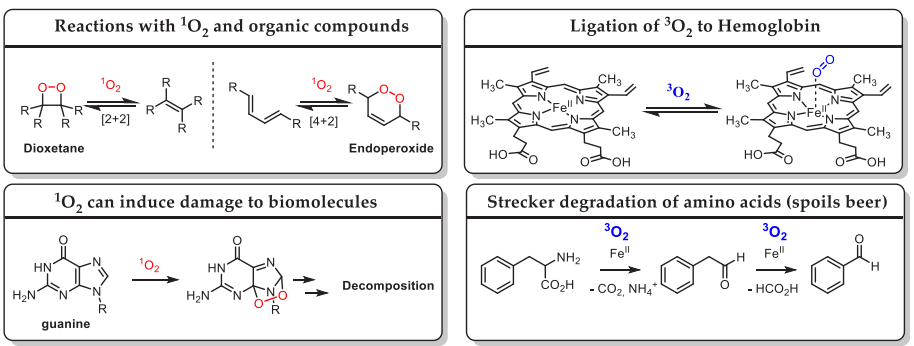

Figure 7. Various reactions between singlet oxygen and organic molecules. Also shown is the ligation of molecular oxygen to hemoglobin and the Strecker reaction of amino acid which is partially responsible for wet carboard tasting beer following improper packaging and storage with residual oxygen.

According to Hund's rule, electrons fill up molecular orbitals in a way that maximizes the number of unpaired electrons.[35] This arrangement helps explain why, despite being a diradical, molecular oxygen is surprisingly stable and unreactive under normal conditions.[36] However, it does react readily with other radicals. Oxygen reacts exothermically with almost all organic compounds, as one might expect for a substance which is added as an additive to rocket fuel. However, most chemistry students will remember that a balloon filled H_2 and O_2 will float around until it is ignited with a match, preferably attached to a very long stick, and go off with a loud bang due to a high energy activation barrier.[37] Reactive oxygen species derived from molecular oxygen are frequent in nature and in biological systems. A harsh lesson learned by most homebrewers is the autooxidation of beer by oxygen-driven reactions such as the Strecker degradation of amino acids (**Figure 7**) which leaves a lingering taste of wet carboard on the tongue.[38]

In the 1930s, Hans Kautsky proposed the existence of an "activated form" of molecular oxygen. However, this idea did not gain significant attention until three decades later when it peaked the interest of the broader scientific community.[39,40] The first excited singlet state ($^1O_2$) of molecular oxygen is reached when the two unpaired electrons are forced to combine within the same molecular orbital, which changes the reactivity drastically. The relative low excitation energy of $^1O_2$ (1.0 eV)[41] aligns seamlessly with its prevalence in nature. Singlet oxygen is produced by various routes, in the chemical laboratory it can be produced in large amounts by the reaction of peroxynitrite and hydrogen peroxide, a common chemistry demonstration to visualize the chemiluminescent properties of singlet oxygen.[42] It can also be formed as a by-product of enzymatic reactions such as peroxidases and oxygenases and directly in cells by direct energy transfer to ground state molecular oxygen by various excited species present.[43] Today, a more common method of singlet oxygen generation is the combination of light and a photosensitizer. The photosensitizer in the ground state (S_0) absorbs light and reaches an excited singlet state (S_1) which is rapidly converted to a long-lived triplet (T_1) state via ISC. This triplet state has a sufficiently long lifetime to participate in bimolecular reactions and will with high efficiency excite molecular oxygen to its excited singlet state.[44] Rather impatient with a short lifetime (~3 μs in water[37]), in the absence of a reaction partner, $^1O_2$ readily relaxes back to the ground triplet state $^3O_2$ via radiative or non-radiative processes. $^1O_2$ is a highly electrophilic species which readily participates in a variety of chemical reactions with alkenes, dienes, polycyclic aromatic rings, and frequently participates in ene-type reactions and cycloadditions (**Figure 7**).[43]

Singlet oxygen is produced endogenously in many biological systems, often to the detriment of the host. When concentrations exceed the cells endogenous $^1O_2$ scavenging system cytotoxic damage occurs and rapidly leads to necrosis.[45] Even upon generation of low concentrations of $^1O_2$ this tends to trigger a response that leads to programmed death of the cell.[46] Biological systems have evolved a response to destroy cells which are associated with $^1O_2$ production. Photodynamic therapy (PDT) is routinely used in the treatments of certain types of cancer. It relies on photochemical generation of singlet oxygen by illuminating the desired area with red light. Light is then absorbed by a photosensitizer (PS) which can further react with molecular oxygen to excite it to the singlet state. $^1O_2$ subsequently triggers

destruction of the cancerous cells via oxidative damage. However, wider implementation of this technique faces challenges. The hypoxic environment of certain tumors significantly restricts the efficiency of PDT. Furthermore, the excitation of the PS is dependent on light penetrating to the affected area in addition to the efficient accumulation of the PS in tumors.[47–49] Recent strategies to circumvent these limitations include the development of oxygen generating materials in conjunction with PDT.[50] Employing a singlet oxygen carrier for direct spatiotemporal release could address many challenges currently facing photodynamic therapy (PDT). Endoperoxides derived from acenes have recently been explored for this purpose by attachment to gold nanorods,[51] or incorporated into covalent organic frameworks[52,53]. Recently it was also shown that the release of $^1O_2$ could be triggered by chemically[54] or enzymatically[55] modifying an endoperoxide which then leads to an increase in the release rate.

1.3.1 THERE IS SOMETHING METAL ABOUT OXYGEN

Not all metals will readily form a bond with oxygen, but amongst the ones that do, one bond stands out as particularly intriguing. Not too strong, which would have had detrimental consequences for life as we know it, and not too weak as this would have severe consequences, especially for our blood. The cultural controversy surrounding blood has deep roots, given the duality as a disease transmitter and an indispensable necessity for life, transporting oxygen from our lungs to the rest of the body.

Oxygen plays a pivotal role in biological systems. Hemoglobin, a crucial protein found in blood, serves a vital function in the transportation of oxygen. The nomenclature is logical given its chemical composition as a globular metalloprotein containing heme groups. Of this we can be quite certain ever since the elucidation of its crystal structure which was awarded with the Nobel prize.[56] Nature ingeniously employs various metals in enzymes, each metal employed being fine-tuned by structural and electronic factors to fulfil a specific function. Within hemoglobin there is an atom of iron which serves a life essential task of binding, and equally important, releasing molecular oxygen. With every breath we take, oxygen gas is taken up in the lungs, diffused through the alveoli into the blood stream, and taken up by the iron metal to form a temporary bond, which is broken once the oxygen molecule has been delivered to the correct place in the body. As previously mentioned, oxygen can react exothermically with almost any substance, provided sufficient activation energy is available. Thus, the precise and controlled way in which nature binds and releases oxygen (**Figure 7**), avoiding unwanted chemical reactions, showcases remarkable spatial and temporal regulation of this potentially reactive species.

O_2 is highly effective as an electron acceptor in the oxidation of carbon-based fuels for several reasons. Firstly, the reduction of O_2 results in the largest free energy release per electron transfer, surpassed only by fluorine. Second, O_2 in its ground state is a diradical, possessing two outer electrons with parallel spins, which contributes to its stability and prevalence in Earth's atmosphere.[57] Unlike fluorine, which fortunately sat this one out. When oxygen emerged in abundance, nature quickly implemented it as an electron acceptor in various metabolic processes. Cytochrome P450 fixates and utilizes molecular oxygen in various biochemical hydroxylation, epoxidation and oxidation reactions.[58] Methane

monooxygenase catalyzes the biotransformation of methane to methanol, a reaction involving the cleavage of the O–O bond in O_2.[59] Other enzymes have been tasked with the harnessing of the energy conserved withing the dioxygen bond and utilize this to catalyze highly energetically demanding processes, one being cellular respiration. This resulted in a significant improvement in terms of energy yield demonstrated by the increased efficiency of aerobic contra anaerobic metabolic pathways. In aerobic metabolism, for each molecule of glucose, four times more energy is generated in contrast to the anaerobic pathways, ultimately leading to a more efficient synthesis of ATP.[57] Aerobic respiration is comprised of three main stages; glycolysis, the Krebs cycle, and oxidative phosphorylation. Glucose metabolism, initiating with glycolysis, culminates in the production of up to 38 ATP molecules per glucose molecule. A significant portion, approximately 32 ATP molecules, is generated through oxidative phosphorylation. This process involves a series of redox reactions where electrons from the reduced form of nicotinamide adenine dinucleotide (NADH) and flavin adenine dinucleotide ($FADH_2$) are transferred to O_2 facilitating the creation of an electrochemical proton gradient across the inner mitochondrial membrane. This gradient, known as the protonmotive force, is crucial for ATP synthesis, as it drives the ATP synthase enzyme to convert ADP into ATP, harnessing the energy released during these essential redox reactions.[60] In eukaryote organisms, this series of complex electron transfer events takes place in four protein complexes within the inner membrane of the mitochondria. Oxygen enters the stage in the third act, together with the third complex of the chain, cytochrome c oxidase.

1.4 CYTOCHROME C OXIDASE – WHAT IS MY PURPOSE? YOU PASS PROTONS

Cytochrome c oxidase (CcO) belongs to the terminal heme-copper oxidase (HCO) superfamily of enzymes responsible for the chemical reduction of molecular oxygen to water according to the reaction scheme below. This process involves the translocation of protons across a membrane, creating a protonmotive gradient used for ATP synthesis.

$$O_2 + 4\,e^- + 4\,H^+_{substrate} + 4\,H^+_{pumped} \rightarrow 2\,H_2O + 4\,H^+_{pumped}$$

(*Shown above is the pump stoichiometry for the aa$_3$-type oxidases*)

HCOs are divided into three families (A, B, and C), characterized by unique cofactors and subunits. Despite variations in pump stoichiometry and efficiency, these families share a conserved mechanism for oxygen reduction. Much of the chemistry associated with the redox chemistry of CcOs is governed by the different redox sites.[61] The *ba$_3$*-type CcO is comprised of a low-spin (heme b) and a high-spin heme (heme a$_3$) positioned near a copper, with two additional copper ions near the enzyme's surface (Cu$_A$). The two different copper sites play a pivotal role in the enzyme's function. Cu$_A$ is situated near the enzyme's surface and acts as the initial entry point for electrons that are delivered from reduced cytochrome c, the natural electron donor for CcO. The dinuclear copper center facilitates rapid electron transfer to a nearby heme via electron tunnelling.[62,63] The low spin heme b is characterized by a paired electron configuration together with a strong associated field ligand. It exhibits a smaller magnetic moment and has more subtle spectral characteristics due to its greater energy difference between the HOMO and LUMO. Conversely, high spin heme a$_3$ has an unpaired electron configuration with weaker field ligands and displays a larger magnetic moment with distinct spectral characteristics. This owing to a lower energy difference between the HOMO and LUMO. The low spin heme a$_3$ is crucial in redox reactions and form part of the binuclear center (BNC), comprised by low spin heme *a$_3$* and adjacent copper ion (Cu$_B$).

The BNC is where the crucial four-electron reduction of oxygen occurs. The strategic positioning of these copper ions, along with the heme groups, is essential for the efficient functioning of CcOs, enabling effective electron tunnelling within the enzyme. The difference in redox potential of the high and low spin heme in conjunction with its placement relative to the copper sites create a unidirectional chain where the electrons can traverse from the surface Cu$_A$ to the active site embedded within the enzyme (**Figure *8***).[3,64,65] A notable characteristic of CcO is a unique conserved structural feature of the Cu$_B$ site, where one of the three histidine ligands of Cu$_B$ is covalently bonded to a tyrosine residue. This cross-link is essential for the stability and catalytic activity of the enzyme.[66] Furthermore, it significantly influences the redox properties, which are essential for the chemistry of oxygen reduction. An important consequence of the cross-link is a lowering of the phenolic proton pKa from 10 to approximately 8.5 which is thought to facilitate a more efficient proton transfer.[67]

The *aa*$_3$-type oxidases belong to the A-family and are the largest and most well studied group of CcOs. The first crystal structure was solved from *Paracoccus denitrificans* almost two decades ago, achieving an impressive resolution of 2.8 Å at the time.[68] The first crystal structure of the *ba*$_3$-type oxidase was solved shortly thereafter at a resolution of 2.4 Å.[69,70] The *ba*$_3$-type CcO is the major topic of this thesis and further details about CcO will mainly be regarding the *ba*$_3$-type oxidase unless otherwise stated. One major difference is the lack of one of the distinct proton transfer pathways in the *ba*$_3$-type oxidase, which is thought to only contain one proton pathway, commonly referred to as the K-pathway analogue of the channel in the *aa*$_3$-type oxidase. This channel is thought to be the path for the protons which are to be pumped across the membrane in addition to the protons required to protonate the various intermediates in the catalytic reaction cycle to produce water.[71]

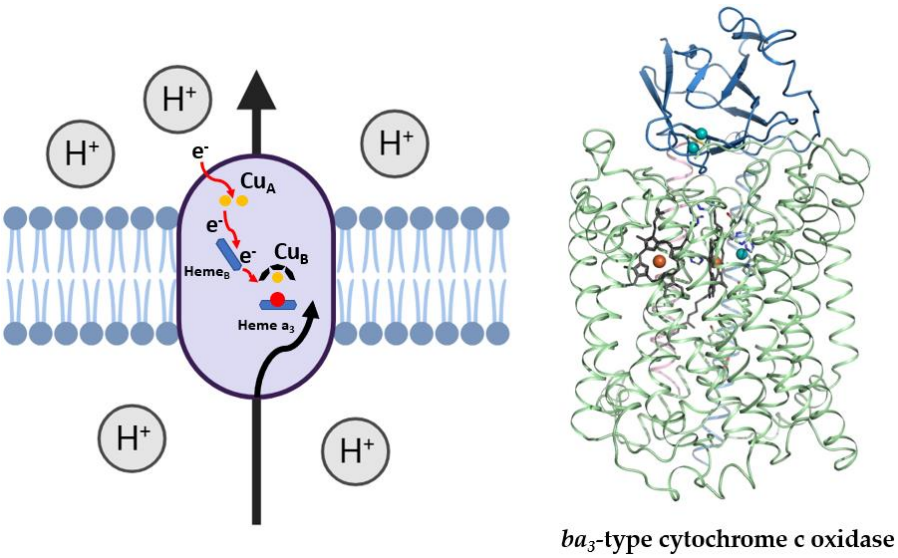

Figure 8. ***Left)*** *ba*$_3$-type CcO showing the unidirectional flow of electrons upon chemical reduction of the Cu$_A$ site followed by electron tunneling via heme b →heme a$_3$ →Cu$_B$. Also shown is the approximate route of proton transfer via the K-channel analogue. ***Right)*** Structure of *ba*$_3$-type cytochrome C oxidase from *Thermus thermophilus*.

The reaction mechanism for oxygen reduction has been a hot research topic for decades but still there are gaps of knowledge. Oxygen enters the catalytic cycle through a well-defined hydrophobic channel and makes its way to the BNC. The catalytic reaction cycle is initiated when O_2 binds and ligates to heme *a*$_3$ in the fully reduced enzyme (**R**). In **Figure 9**, the mechanistic cycle for oxygen reduction to water is shown for the aa$_3$-type cytochrome c oxidase. This results in the formation of a short-lived intermediate **A** (~10 μs) that upon cleavage of the dioxygen bond yields either the **P$_R$** or **P$_M$** state, depending on the initial redox state of the enzyme, and one proton is taken up in the active site from the cross-linked tyrosine.[67] In both **P**-type states, the BNC is oxidized, the iron in heme *a*$_3$ converts from Fe^{2+} to Fe^{4+} and the copper from Cu^{1+} to Cu^{2+}. The reaction proceeds directly to the **P$_R$** state when the reaction is initiated from the fully reduced state (four electrons), otherwise it proceeds

first via the $\mathbf{P_M}$ state. The $\mathbf{P_M}$ state is formed when there is no electron available immediately after oxygen ligation and is associated with a longer time constant (200 μs as opposed to 30 μs) for the transition from **A** → $\mathbf{P_M}$, presumably due to the requirement of a more demanding rearrangement withing the BNC. The $\mathbf{P_R}$ and $\mathbf{P_M}$ state both share the same optical absorbance properties but the $\mathbf{P_M}$ is unique due to its charge distribution and the fact that it is EPR active due to the interaction between Cu_B and ferryl heme a_3.[65] The subsequent protonation of the $\mathbf{P_R}$ state occurs on the time scale of 100 μs which results in the formation of the **F**-state, which is typically associated with a significant change in the optical absorbance properties due to the altering of the heme axial symmetry caused by either the protonation of the OH ligand of Cu_B or the loss of a newly formed water from the coppers coordination sphere.[3] However, the absence of optical absorbance changes associated with the $\mathbf{P_R}$ → **F** transition in the ba_3-type oxidase could indicate a distinctive feature of its reaction mechanism. Since the formation of the **F**-state does not cause a significant change in the absorbance spectrum it is likely that the proton acquired during the $\mathbf{P_R}$ to **F** transition is not located within the BNC and could instead be transferred to the crossed-linked tyrosine.[72] Alternatively, it could also be provided via the propionate groups of heme a_3 assisted by nearby histidine and aspartate residues, along with surrounding waters.[73]

The charge translocation associated with the transition from the **F** to **O** state in ba_3-type oxidase closely mirrors what is observed in the aa_3-type oxidases during the same transition. This similarity across the CcO enzyme family highlights a conserved mechanism in the proton pumping despite variations in the intermediate state characteristics.[72] The formation of the **F**-state is presumed to result in water leaving the BNC and one proton being pumped. The final step in the oxygen reduction process is the transition to the fully oxidized $\mathbf{O_H}$ state. This phase is marked by characteristic spectral changes, indicating that the $\mathbf{O_H}$ state formation coincides directly from the decay of **F**-state when an electron reaches the BNC from heme *b*. Interestingly, this oxidized state ($\mathbf{O_H}$) is not equivalent to the oxidized state of the enzyme as isolated (**O**). If no further electrons are present the $\mathbf{O_H}$ state can shift to a more stable form which is the **O** state. Single electron injection experiments of $\mathbf{O_H}$ and **O** showed that upon single electron reduction of $\mathbf{O_H}$ the electron makes it to the BNC rapidly while upon single electron reduction of **O** mainly ends up on Cu_A and the low spin heme over several milliseconds.[74] The resulting single electron reduction of the $\mathbf{O_H}$ state results in the pumping of one proton whereas in the **O** state there is no proton translocation. The $\mathbf{O_H}$ state is postulated to have a hydroxide ligand, with short Fe–OH–Cu bond distances, and the transition to the **O** state have been suggested to arise from hydration and mainly differ in the coordination of Cu with an additional fourth ligand in the form of a water molecule.[75]

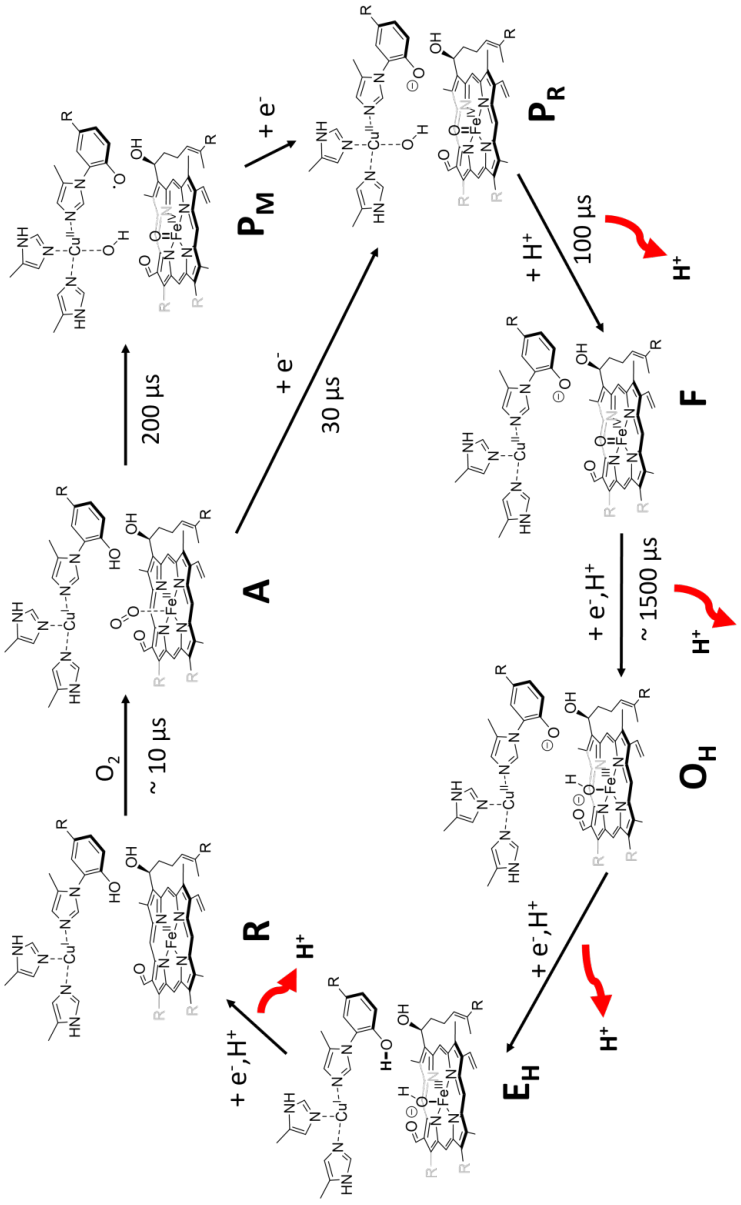

Figure 9. A proposed catalytic cycle for the reduction of molecular oxygen to water in the *aa*$_3$-type cytochrome c oxidase. Adapted from ref[65].

In the catalytic cycle of A-type CcO (**Figure 9**), each step associated with a single electron reduction is linked to the pumping of one proton. However, in B-type oxidases like the *ba*$_3$, the proton pumping is less efficient with only about 0.5 H^+ pumped per electron.[76] For effective proton translocation across the membrane, a proton must be picked up on one side and subsequently released on the other side of the membrane. This process is facilitated by the proton loading site (PLS), a crucial component in the proton pumping mechanism. The PLS is believed to consist of a group of residues that alter their proton affinity (pK_a) during the reaction sequence, enabling a "catch and release" mechanism for protons. The proton pumping mechanism is believed to first proceed through an initial single electron reduction and uptake of a proton to the PLS, and a proton is subsequently transferred to the BNC for the chemistry. It is postulated that electrostatic repulsion between the two protons eventually causes the release of the proton at the PLS.[76] A structural explanation for the intricacies of how redox events such as these reductions and oxidations of various metal centers translates into proton pumping still eludes researchers to this day. The precise nature and location of the PLS in CcO remains uncertain and is thought to vary among different oxidases. Several candidates for the PLS have been proposed, including the propionate of heme a_3 and nearby amino acids. In A-type oxidases, each electron reduction event in the catalytic cycle corresponds to both the loading and release of a proton at the PLS. In contrast, the *ba*$_3$-type oxidase likely associates one redox event with either the loading or release of a proton, contributing to its lower proton pumping stoichiometry.[73,77,78] Furthermore, a structural basis for the prevention of back-leakage of protons following proton pumping is still lacking.[79]

1.5 TIME IS OF THE ESSENCE

1.5.1 PHOTOCAGES

A photocage is a chemical compound engineered to undergo a light-mediated transformation and rendering the photoproduct an active substrate. This typically involves covalent attachment of a photolabile protective group on a reactant. The first utilization of a photocage in biological systems dates back to 1975 and is credited to Kaplan, Forbush, and Hoffman.[80] Their collective effort closed the gap between the synthetic organic chemistry community, where photolabile protective groups were already established, to other branches within the natural sciences. The first photocage based on a biomolecule was developed by attaching an *ortho*-nitrobenzyl protective group on ATP, utilizing a free hydroxyl moiety of the phosphate group as the chemical handle for attachment of the photocage (**Scheme *1***). This also established a convention within the photocage community by naming this new protected substrate "caged ATP". The authors demonstrated the caged-ATP to be chemically inert towards an ATP dependent Na/K-ATPase under "dark-conditions", meaning the typical experimental conditions while excluding exposure to light. Following light illumination and subsequent deprotection of the σ-nitrobenzyl protective group, no adverse reaction was detected beyond the naturally occurring ATP mediated reaction.[81] This approach was also applied to several derivatives of cyclic adenosine

monophosphate (cAMP).[82] Derivatives of the photolabile protective group, σ-nitrobenzyl, are still used to this day due to their relative ease of synthesis in addition to being chemically compatible towards most typical biochemical experimental conditions. σ-nitrobenzyl is today commonly replaced with a (nitrophenyl)ethyl (NPE) moiety after it was revealed that the photoproduct from the σ-nitrobenzyl, a nitrosoaldehyde, was harmful in some biological contexts. The photoproduct of NPE decaging, a nitroso acetophenone, was deemed less likely to interfere since it is less reactive and came with an additional benefit of an increased rate of de-caging.[83] Various derivatives of the NPEs have been synthesized (**Scheme *1***, **b-f**) and implemented in biochemical studies as substrate cages. Incorporation of electron rich substituents on the nitrophenyl ring such as methoxy (-OMe) (**Scheme *1***, **c**) and methylenedioxy (**Scheme *1***, **d**) or replacing the ring altogether with a nitrodibenzofuranyl moiety (**Scheme *1***, **e**) induce a red shift the absorbance spectrum which is desirable considering that these compounds almost exclusively absorb high energy UV-light (> 300 nm).

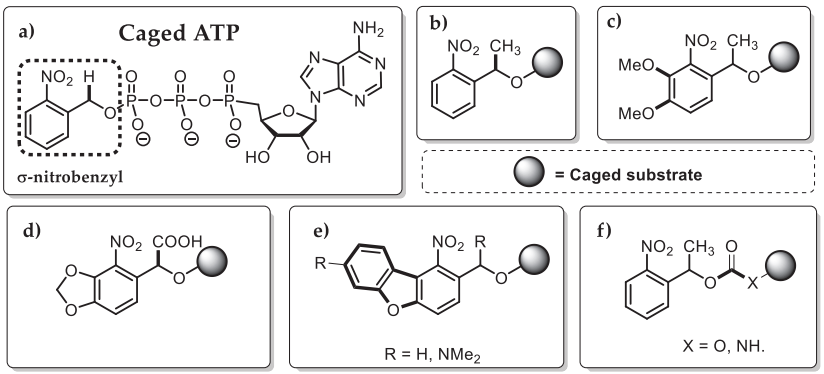

Scheme 1. a) The structure of Caged ATP. **b)** The generic structure of the NPE type photocage and **c)** to **f)** showing structural modifications to the NPE in order to fine tune the properties of the photocage.

It is important to note that these modifications comes with a trade-off: they result in a lower overall quantum efficiency of the reaction.[84] Additionally, replacing the methyl substituent between the substrate and the aromatic ring with a carboxylic acid (**Scheme *1***, d) increases the aqueous solubility with the compromise of a few additional synthetic steps.[85] The NPE type of photocage has been very successful for the caging of various O- and HN-nucleophiles and incorporation of carbonate or carbamide linkers have shown to increase the efficiency of uncaging by increasing the thermodynamic driving force of the reaction by the expulsion of CO_2 (**Scheme *1***, f).[86] Initially, photocages were used in studies where temporal resolution was not critical, and continuous light sources sufficed to activate the substrate gradually, as demonstrated for enzymes depending on inositol[87] and cADP-Ribose[88]. However, as researchers progressed towards more challenging systems, there was a growing necessity for optimizing the photocage quantum yield and decaging rate. The evolution of σ-nitrobenzyl and NPE photocages underscored the importance of careful design of the photocage for biochemical applications, highlighting the need to balance

various parameters for optimal performance. Subsequently, in the design of a photocage, several parameters must be considered.[19,89]

1) Photo-decaging rate
2) The absorption spectrum and extinction coefficient (λ)
3) Quantum yield (ϕ)
4) Stability and solubility

In time-resolved experiments, the process and associated mechanism of decaging is crucial, especially when the reaction under study is of rapid nature. The rate of decaging must be faster than the reaction being observed, or at least well-characterized and consistent, to ensure accurate timing. This allows for the selection of an appropriate time delay, preventing premature probing of the sample before the full effect of the pump laser is realized. Depending on the type of photocage, several steps might be required for the final decaging of the substrate following photoactivation. The NPE photocage demonstrates this particularly well, where a "caged proton" photocage releases its substrate (a proton) on a timescale much faster than other derivatives of NPEs releases its substrate (**Scheme 2**). The irreversible acidification is achieved due to the high acidity of the leaving group (pKa ~2) enabling efficient "pH-dives" close to pH 2.[90] The detailed mechanistic study of the decaging of the caged proton photocage revealed that the rate of decaging differs depending on experimental conditions such as the initial pH and the extent of pH change induced following the laser pulse.[91] Generally, the decaging rate is dependent on the property of the leaving group. A better leaving group will provide a greater thermodynamic driving force following excitation.

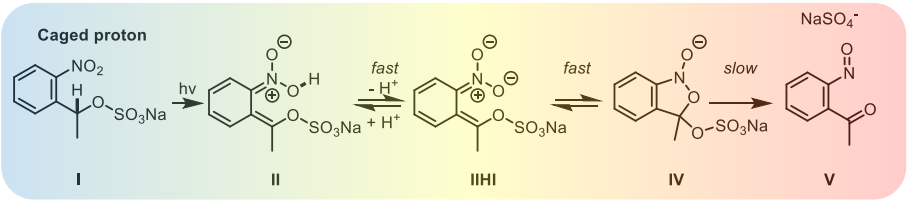

Scheme 2. The reaction mechanism of NPE based photocage **I** (caged proton) which upon photolysis results in the rapid release of a proton on a much faster time scale compared to NPE photocages where a nucleophile is otherwise released in the **IV** → **V** transition as opposed to the chemical proton released in the **II** → **III** transition.

The Grotthuss–Draper law intuitively explains the second parameter to consider, the absorbance of light, inherently tied to the absorbance spectrum and molar extinction coefficient of the photocage. Photocages normally requires light in the 200 – 400 nm range, as this energetic light is necessary to overcome the energy barriers associated with the decaging mechanism. Ideally, light with lower energy would almost always be favorable since this would reduce the risk of light mediated side reactions. This consideration is particularly important in the UV range below 300 nm, where proteins containing aromatic amino acids exhibit significant absorbance of light. The presence of chromophores or other light-absorbing substances in the system adds further complexity, often necessitating compromises to address these additional factors. The introduction of light into the sample

must be precisely controlled, both spatially and temporally, usually managed with a nanosecond pump-laser with a set wavelength. The selection of wavelength for the light activation is often not trivial. The sample thickness in the experiment can lead to non-uniform light absorbance throughout the sample and thus, a non-homogenous reaction initiation. This occurs because the optical density causes light to become more and more diluted as it traverses and is absorbed throughout the sample.[19] The intensity of light has caused much controversy, especially within the field of TR-SFX, where theoretical and practical aspects of chemistry collide. It is common that a much higher fluence of the laser pulse is used than what would be theoretically required based on the overall quantum efficiency of the process and absorbance properties of the sample. This has caused much debate whether certain observed effects, especially those on a very rapid time scale and when only minor changes are observed, can be solely attributed to the chemistry and not to secondary effects from the pump laser such as multiphoton effects or heat.[92–95] This is potentially more detrimental when the protein itself acts as the chromophore or has significant absorbance at the wavelength of irradiation. Conversely, when designing a photocage, the aim should be to ensure efficient light absorption and a high extinction coefficient. To counteract the consequences of a poorly absorbing photocage, the concentration can be increased to such an extent that essentially all photons that enter the sample will be absorbed (i.e., the optical density is much greater than 1) assuming that another important parameter is met, high aqueous solubility. Hence, the combination of low aqueous solubility and poor light absorbance is typically a challenge to resolve whereas if one parameter is lacking, one might compensate by increasing the other.

Upon photon absorption by a photocage, multiple outcomes are possible, influencing the overall quantum yield of decaging. This yield is determined by various factors, including the relaxation of the excited state, reversibility of the reaction and availability of other photochemical pathways not leading to the desired photoproduct. Quantum yields can surpass 1 (> 100 %) which at first glance might seem counterintuitive considering the second law of photochemistry, the Stark-Einstein law*. However, as demonstrated in the case of a nitric oxide (NO) photocage (**Scheme *3***) , the answer lies in the reaction mechanism where two equivalents of the substrate (NO) are produced with a ϕ_{350} ~1.6.[96]

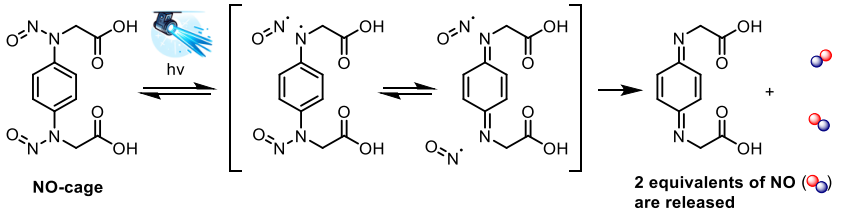

Scheme 3. The mechanism for the photolysis of a nitric oxide photocage upon illumination by 350 nm light to produce two molar equivalents of nitric oxide.

Hence, the quantum yield of the photocage correlates to the laser fluence requirements previously discussed. Furthermore, the stability of the photocage towards the experimental

* *Historically, it has not been a very successful strategy to dispute Einstein, and this is certainly not for a lack of trying.*

conditions is of utmost importance for a time-resolved measurements which will be a major topic of discussion later in this thesis.

1.5.2 CAGED OXYGEN

Working with substrates that are highly reactive can be a double-edged sword when incorporating them into photocages. A very reactive substrate typically transfers this reactivity to the photocage which has both pros and cons. The case study in this thesis, and major source of sleepless nights is exclusively attributed to oxygen photocages, which upon excitation releases molecular oxygen. Despite its position as a powerful oxidizing agent in the electrochemical series, molecular oxygen typically exhibits a rather sluggish kinetically nature in reactions at ambient temperatures. The full redox potential is typically only realized when the reaction is carried out as a concerted four-electron process, akin to various enzymatic oxidation reactions.[97] It should be noted that this kinetic sluggishness is responsible for the coexistence between most organic compounds and the oxygen rich environment necessary to sustain life as we know it, which could be argued has some merit to it. Bypassing the spin restriction is necessary to react with O_2 and is typically referred to as "activating" dioxygen which is achieved through three primary methods. Spin inversion to singlet oxygen via photosensitized reactions, by coordination of dioxygen to a metal complex or by the generation of oxygen radicals. In the context of producing a $^3O_2$ photocage, this rules out the first and third method as this no longer leaves oxygen in the ground state. A crude observation with regard to the release of small molecules in the gaseous state (CO, NO and O_2) is that these are commonly released from transition metal complexes, with some notable exceptions.[98] $^3O_2$ form complexes with various transition metals, as shown in **Figure *10***, either via coordination to one central metal ion or by acting as a bridging ligand between two metals.

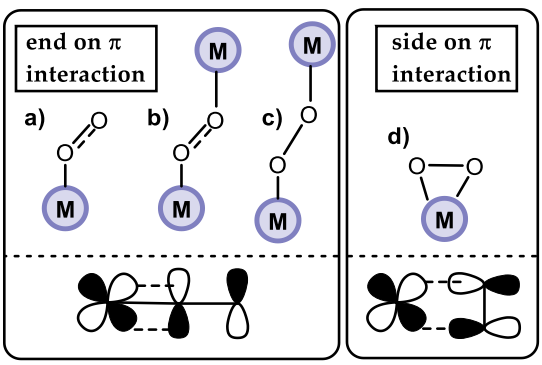

Figure 10. Some of the relevant different binding modes of molecular oxygen to transition metals**:** **a)** η^1-superoxo **b)** μ-superoxo **c)** μ-peroxo **d)** η^2 -superoxo. Shown is also the molecular orbital interaction between the HOMO of the metal and LUMO of oxygen.

When oxygen binds to a metal, the antibonding 2p* orbital of O_2 accepts an electron from the filled d-orbital of the metal which results in oxygen adapting the formal oxidation state of either a superoxide (O_2^-) or peroxide (O_2^{2-}). This change in electron distribution significantly

impacts the O–O bond length. Amongst the known dioxygen-metal complexes, several have shown to be photoresponsive and release oxygen in the triplet state. Such examples includes complexes based on iridium[99], synthetic heme (iron),[100] rhenium[101] and molybdenum[102]. However, these are not viable platforms for the development of biologically relevant photocages since these complexes are only soluble in organic solvents. A metal of particular interest is cobalt which shows a diverse range of interactions with oxygen whilst also being relatively stable at ambient temperatures. Cobalt complexes exhibits diverse reactivity towards molecular oxygen, this effect is evident in the varying O–O bond distances observed in different motifs. In μ-superoxo type cobalt complexes, the O–O distances range from 1.24 to 1.35 Å in contrast to μ-peroxo complexes that typically has longer O–O distances ranging between 1.30 to 1.48 Å.[103] Bridged μ-peroxo-μ-hydroxo (**Scheme *4***, complex **A1** - **A2**) and μ-peroxo-μ-amido (**Scheme *4***, complex **A3**) binuclear cobalt(III) type complexes were discovered to release molecular oxygen thermally, chemically, and photochemically in the 1970s.[104]

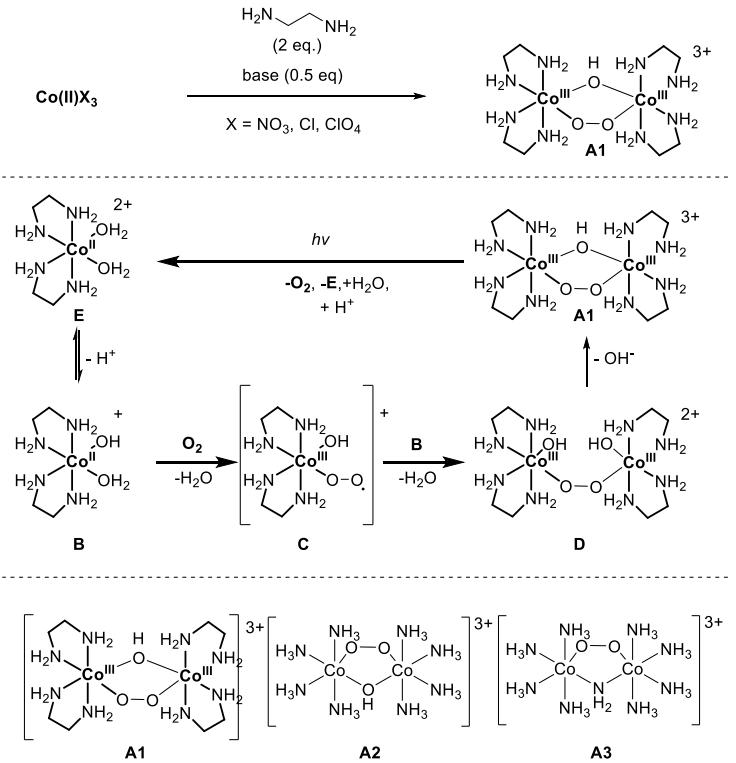

Scheme 4: Top) The proposed reaction mechanism for the formation of binuclear μ-hydroxo-μ-peroxo cobalt (III) complexes under basic conditions in the presence of excess oxygen in a protic solvent. **Bottom)** Early μ-peroxo-μ-hydroxo and μ-peroxo-μ-amido binuclear cobalt (III) type complexes discovered to release oxygen upon thermal or photochemical external stimuli.

Cobalt(III), with its electronic configuration of [Ar]3d^6, forms a variety of complexes, an overwhelming majority being octahedral with a low-spin electronic configuration.[105] This

conveniently means that most of these complexes are diamagnetic and can be characterized by conventional nuclear magnetic resonance (NMR) spectroscopy as opposed to more specialized techniques[†]. The mechanism (**Scheme *4***) under basic conditions is proposed to proceed via deprotonation of the ligand and subsequent oxygen ligation, resulting in an intermediate such as intermediate **C**. This could proceed to react with an additional equivalent of **B** to presumable form the binuclear oxygen-adduct **D** with an overall formal +2 charge. Upon coordination of the hydroxide ligand to both metal centers this yields the final complex **A1** with a formal charge of +3. The addition of 0.5 molar equivalents of a base is thought to significantly increase the reaction rate by favoring the formation of intermediate **B** but is not strictly needed for the reaction. The binuclear μ-hydroxo-μ-peroxo complex **A1** is photoresponsive and will upon UV-light irradiation irreversibly decompose to reform the initial species **E** and release molecular oxygen in the triplet state, representing the first example of a **caged oxygen** complex.

Isotopic labelling studies with $^{18}O_2$ has confirmed that it is indeed the O_2 originating from the peroxide bridge that is released upon photoexcitation. Furthermore, the photochemically released oxygen is thought to only comprise $^3O_2$ as no significant formation of $^1O_2$ has been detected experimentally.[104,106–110] Details regarding the precise nature of the intermediates following photolysis remains elusive but Co^{+3} have suggested to form but ultimately result in the formation of mononuclear Co^{+2} species. Both reduction and aquation can occur simultaneously, adding complexity to the photochemical behavior of these systems. The photorelease of oxygen is proposed to proceed by a concerted mechanism with a superoxide to cobalt(III) electron transfer from the excited state of the complex upon the excitation by light.[106] The mechanistic studies of these complexes are mainly based on optical absorbance spectroscopy. These compounds exhibit two moderately intense charge transfer bands near 360-450 nm resulting from a $\pi^*(O_2^{-2})$ ligand to metal charge transfer (LMCT) transition. This characteristic absorbance band disappear upon photodissociation of oxygen and opens a convenient window to track the photorelease dynamics of O_2 from complexes of this type.[111] A major limitation of these early ammonium and ethylenediamine based complexes was the limited solubility in aqueous medium. In addition to this, the quantum yields of the photochemical oxygen liberation were low (> 0.1 %). It is therefore not surprising that these compounds saw limited use as tools in biochemical studies and was considered more of a chemical curiosity amongst a few dedicated cobalt enthusiasts at the time.

More than two decades later, MacArthur and Einarsdóttir *et. al.* demonstrated that introduction of a bipyridine (bpy) ligand produced a compound with improved photophysical properties compared to their ethylenediamine counterparts. This (μ-hydroxo-μ-peroxo)bis[bis(bipyridyl)cobalt(III)] (HPBC) compound (caged oxygen) exhibits a significantly improved light mediated oxygen liberation efficiency compared to complexes like **A1**-**A3** with a photochemical quantum yield (ϕ_{355}) of ~ 0.04.[112]

[†] *At least from the perspective of an organic chemist.*

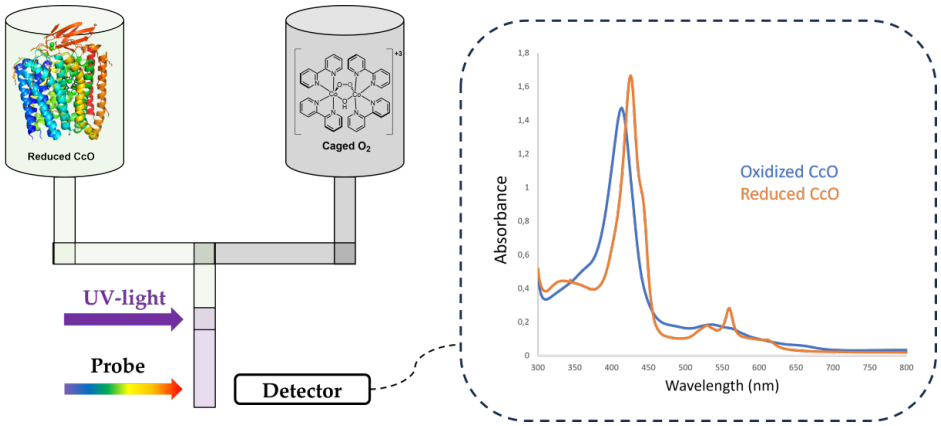

Figure 11. Time-resolved spectroscopic investigations into the mechanistic cycle of CcO by mixing reduced CcO with the HPBC caged oxygen photocage. Also shown is the absorbance spectrum for oxidized CcO (blue) and reduced CcO (orange).

Initially prepared as a perchlorate salt with limited aqueous solubility, a more soluble nitrate salt was prepared with significantly improved solubility; and allegedly a **~10 fold** increase in quantum efficiency‡.[113] Einarsdóttir *et. al.* subsequently demonstrated that a caged oxygen compound could upon photodissociation generate a sufficient concentration of oxygen to ligate to/react with: deoxy hemoglobin, the fully reduced bovine aa_3 and bacterial ba_3 type-CcO under experimental conditions suitable for UV/Vis spectroscopic studies.[112,114,115] Similar results could be achieved when the two-electron semireduced carbon monoxide bound (MVCO) ba_3 type-CcO was employed which in addition to the reaction with oxygen also demonstrated the equivalent reaction with nitric oxide by a ruthenium based photolabile NO carrier.[116] It is furthermore stated that under the reported experimental conditions§: the HPBC type photocages are stable and compatible with the biochemical reducing agents employed in the studies (sodium ascorbate + ruthenium hexamine,[114] dithiothreitol[113]). The undeniable successful implementation of caged oxygen complexes in spectroscopic studies gave rise to questions regarding the application towards more challenging systems. Although it would become apparent why a mixing approach (**Figure *11***) was employed in previous investigations of this system which is not clearly explained in the associated publications.

‡ *Although not impossible, it is definitely not common that the exchange of counterions significantly changes the quantum yield to this extent.*

§ *It should be noted that this is conveniently phrased. When this phrase is used, no further comments are made regarding the stability even slightly outside the scope of the experimental parameters.*

1.5.3 PHOTOCAGES IN TIME-RESOLVED X-RAY BASED STUDIES

I am sure that people around my generation (1994) will fondly remember the joy when a teacher, often a substitute teacher, entered the classroom equipped with the thick TV on wheels. I remember one of these days clearly when we were introduced to an educational TV-show, "once upon a time", where hemoglobin was reduced to a talking red ball with legs, arms and eyes. Visually, we could follow hemoglobins as they went to work in our bodies and I remember thinking, "if I could just see more things in the textbook this clearly, it would make things so much easier". With the emphasis on "seeing". Modern science must have heard my wish and responded with the development of modern time-resolved X-ray based methods for visualizing and understanding the chemistry of life.

Studying how proteins interact with substrates through X-rays to visualize the "substrate-structure-function" relationship is an emerging field of research. The field is still in its infancy, undoubtably with challenges to discover and overcome before establishing itself as a household name.[19,94] However, three pivotal studies have set things in motion by attacking some of the first challenges, paving the way for more research in this area. A 4-hydroxyphenacyl caged fluoroacetate (**Scheme 5**) was implemented in a time-resolved crystallographic experiment which demonstrated the successful decaging of the substrate and subsequent binding to *Rhodopseudomonas palustris* fluoroacetate dehalogenase (FAcD) upon which the natural catalytic reaction of the enzyme could be visualized.[117] FAcD has a slow catalytic turnover rate in the order of 10 seconds, likely a consequence of the strong nature of the C–F bond, the strongest bond in traditional organic chemistry.[118] This slow nature of catalysis of FAcD was exploited to probe a large amount of time points simultaneously by an innovative technical solution for laser activation and subsequent X-ray probing termed the "hit and return – HARE" method.[119] The devil is in the details. The success of this study can partially be attributed to a convenient red shift of the absorbance spectrum of the photocage when exposed to the experimental conditions. This is likely an effect from the pH (8.5) which is close to the expected pK_a for 4-hydroxyacetophenones (~8*). (*The addition of the fluoroacetate moiety is not expected to significantly change the pK_a**).

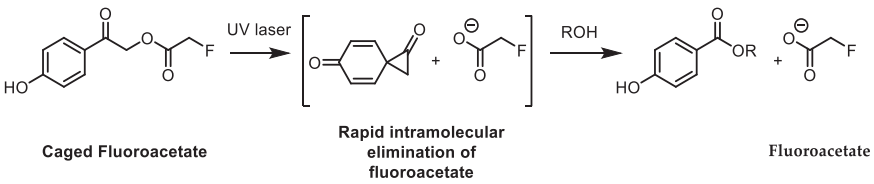

Scheme 5. Caged fluoroacetate and the associated mechanism for photoliberation of fluoroacetate. The rapid nature of the release of the substrate from the 4-hydroxyphenacyl type photocage stems from the formation of the bicyclic intermediate which is later hydrolyzed to form an ester.

This likely results in an equilibrium where more than 50 % of the caged fluoroacetate is expected to shift toward the deprotonated phenolate, which is known to result in a different absorbance spectrum.[120] This allowed for more efficient decaging utilizing light with a wavelength of 344 nm, well above the typical very narrow absorbance maximum for the 4-hydroxyphenacyl type photocage which has a strong spectral overlap with the absorbance

maximum (280 nm) for aromatic amino acids such as tryptophan and tyrosine. There will always be an additional time delay tied to the diffusion of the released substrate within any system employing a photocage. Caged fluoroacetate in the caged state was found to occupy a solvent channel in the enzyme prior to light activation. The extent to which a photocage diffuses into a protein crystal could significantly impact the time-delay between photoactivation and interaction with the substrate.

Prior validation of reaction initiation in crystals is critical but often a difficult challenge. Factors that are particularly relevant to consider are: the porosity of the crystal, size of the photocage and released substrate, temperature, accessibility within the protein structure and potential interactions with the protein.[119,121,122] It is not obvious what the direct consequences would have been for this study if the caged fluoroacetate did not access the solvent channel and instead would have needed to diffuse into the crystal following decaging. Hence, potential diffusion is important to consider in future studies for substrates where diffusion could be influencing the temporal resolution of the experiment. Furthermore, the experimental sample composition of a successful TF-SFX experiment should be noted. The protein concentration prior to crystallization into crystals with the following dimensions: 20x20x30 μm^3, was 0.5 mM and upon 1:1 dilution with 100 mM caged fluoroacetate gave the final 0.25 mM protein to 50 mM photocage and the authors have estimated this to represent 4-14 equivalents of photocage per active site.

The first reported TR-SFX study to successfully employ a photocage utilized caged NO (**Scheme 3**) to liberate nitric oxide in the presence of nitric oxide reductase, isolated from the fungus *Fusarium oxysporum* (P450nor).[123] The enzyme contains heme groups which enables the binding of NO to the heme. In its natural environment and in the presence of NADH, P450nor will reduce NO to form N_2O. The binding of NO and ligation to the heme was captured by SFX, 20 ms after UV laser excitation, and resolved to a resolution of 2.1 Å. This XFEL based TR-SFX study was conducted on a sample consisting of P450nor crystals (20-50 x 20-50 x 10 μm^3) which corresponds to a concentration of heme groups around 16 mM. The photocage concentration was 14 mM but since it can release two equivalents of NO it is effectively closer to 28 mM which results in a near 2:1 relationship between protein and photocage. The careful consideration to the various experimental parameters, and subsequent compromises made, were determining factors for the successful outcome of the experiment. Several key discoveries were made that are important to consider for future work. The laser fluence was reduced below what would theoretically be optimal when only considering the optical absorbance properties of the sample and the quantum yield of the photocage. A pulse energy of >1.4 nJ/μm^2 was found to result in a decrease in the absorbance spectrum of the heme in microcrystals of P450nor and pulse energies beyond 4 nJ/μm^2 lead to physical damage to the crystals. (It should be kept in mind that it is often difficult to compare laser fluences between different experiments). The laser fluence employed for the TR-SFX experiment generated a NO-bound structure with approximately 50 % occupancy, which is argued could have been higher if a higher laser power was used. However, it is not obvious that achieving 100 % occupancy would lead to any additional scientific insights. Additionally, the authors reason that photorelease of NO beyond its aqueous solubility by

increasing the laser fluence or by increasing the concentration of photocage could lead to other practical issues from bubble formation. This is something to consider for gaseous substrates or in general when the solubility of some component is expected to change upon photolysis, it is after all a dynamic system when photocages are involved.

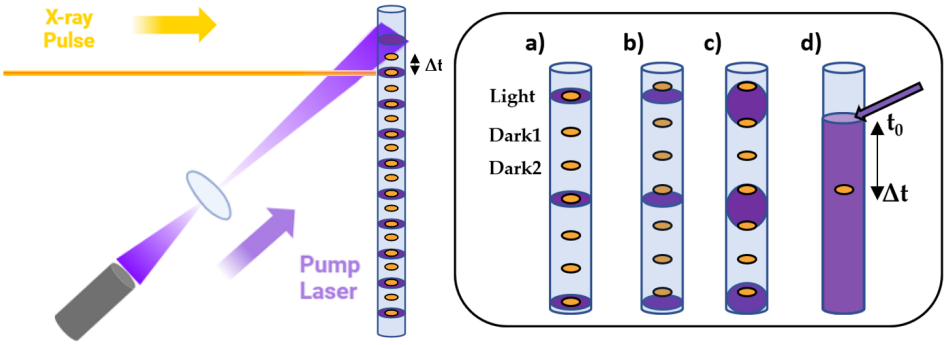

Figure 12. Different types of illumination schemes typically employed in TR-SFX, TR-WAXS and TR-SAXS experiments where the repetition rate of the X-ray and pump laser are synchronized to collect as much reliable data as possible. The alternating dark and light scheme provide access to both the active state and the reference dark state on a chemically identical sample which strengthens the reliability compared to running two separate dark and light measurements on different samples. Small differences in preparation could bias the interpretation. **a)** the most common illumination scheme used where the spacing and use of two dark probes increases the probability of obtaining a true dark reference. **b)** The illustration shows how if the pump laser and X-ray pulse is not timed properly, only dark states might be collected or only partially illuminated sample. **c)** This case where light and dark1 are both probed by the light pulse is unfortunately encountered sometimes. **d)** For long time-points in a flow-based experiment it becomes more difficult to align the laser and the X-ray probed area due to inherent inaccuracies associated with the flowrate and one might instead change the illumination method. Continuous illumination from a laser diode is a suitable alternative for some systems and enables essentially any time delay to be probed.

No further reaction was observed following ligation of NO, even in the presence of excess NADH which is required for the reaction to proceed further. This is attributed to an effect in in the crystalline phase that supposedly prevented efficient supply of NADH to the active site. Spectroscopic evidence is provided that suggest that the formation of the next intermediate for the reaction is slowed down by a factor of 20 in microcrystals. The X-ray probe following the laser excitation thus cannot capture this slow intermediate via TR-SFX viscous jet delivery and an alternative experimental setup would be required to resolve this. In this work, to demonstrate that the NO-ligation is indeed triggered by the light induced decaging, an alternating scheme of dark and light was employed during data collection. (**Figure *12***, illumination scheme **a**) This serves the purpose of eliminating the possibility of a dark reaction being operative and secondly, it enables one strength of TR-SFX to be exploited. The analysis is based on difference electron density maps and small differences

and associated occupancies can still be interpreted chemically.[124] The electron density from the dark data can be subtracted from the light data and the whatever is left will in theory be the electron density changes triggered by the light probe.[125] It was discovered during the analysis of the data from dark1 that this was contaminated with light, reminiscent of a **C** -type illumination scheme shown in **Figure *12***. The illuminated area is probed in both light and dark1 X-ray probes while "dark2" is still a proper dark, meaning it did not receive any activation by light. This can be caused by multiple experimental errors such as by a mischaracterized laser profile, wrong flowrate in correlation to the laser and X-ray probe frequency, or by severe inconsistency in the flow of the sample.

A third relevant study employed X-ray solution scattering, a complementary technique to crystallographic methods, where the interaction between proteins in solution and X-rays are explored. Time-resolved small- and wide-angle X-ray scattering (TR-SAXS/TR-WAXS) experiments allows access to the study of proteins that might be too challenging to crystalize whilst still providing valuable information about the structural dynamics of the system.[126,127] As with TR-SFX, the technique has proven successful for light responsive systems such as photosynthetic proteins and photoreceptors.[128,129] The first example of the implementation of a photocage in a time-resolved X-ray based study suitably employed the first ever described photocage, caged ATP (**Scheme *1*a**). The work showcased the photorelease of ATP and subsequent binding to the nucleotide-binding domains of bacterial lipid flippase MsbA. The ATP mediated dimerization was recorded in solution using time-resolved X-ray solution scattering (XSS).[130] To deliver the sample to the X-ray beam, most liquid scattering experiments employs thin glass or quartz capillaries. In this work, a 1 mm quartz capillary delivered the protein (0.5 mM) together with the caged ATP (1.5 mM) and utilized a 355 nm laser pulse to trigger the dimerization. The σ-nitrobenzyl photocages have very low absorbance at the wavelength of irradiation (430 $M^{-1}cm^{-1}$). This is stated to be advantageous since this will ensure that the light is evenly distributed throughout the sample and subsequently yield a uniform reaction initiation. This represents a situation where only around 14 % of the emitted light is absorbed by the sample, estimated by **Equation 6** to calculate the fraction of light absorbed. The authors estimated that the photolytic yield of ATP under the experimental conditions to be around ~0.95 mM based on a quantum yield of ~0.6 and the pump power used in the experiment.

$$Fraction\ of\ light\ (f) = 1 - 10^{-A} \quad (6)$$

Taken together, these three studies demonstrate that time resolved X-ray based studies of the structural dynamics of proteins with photocages are possible, although associated with many trials and tribulations.

1.6 KCSA – OR WAS IT KSCA? AN ADDITIONAL PROTEIN UNDER INVESTIGATION

I sat down in a meeting with my co-supervisor which typically started with a thorough summary of recent developments in the world of cricket. Quickly discussions followed regarding more relevant topics such as Covid-19 and other ongoing world events. Then, nearing the end of the almost two hours meeting I was asked regarding the possibility of implementing a photocage to quickly acidify a solution for a potential project. Over the course of my PhD, I was given a great amount of freedom to plan my own time and whenever I found it suitable, simply try something without telling my supervisor(s). Because really, wants to hear about expensive failures, and yes, I have to say there were more than I care to, or will admit. However, here I could for the first time with confidence say that this would be an easy task. I had already completed the synthesis of such a compound based on a gut feeling that it might come in handy.

Ion channels constitute a crucial component of cellular membranes, playing a vital role in a diverse range of biological processes. They act as gatekeepers and control the flow of ions across membranes, an essential part of neuronal transmission, muscle contraction, and the regulation of heartbeats.[131] Various channels exists for selective transportation of sodium, chloride, calcium and potassium.[60] The K-channel streptomyces A (KcsA), was the first potassium ion channel to be structurally elucidated by X-ray crystallography,[132] which was later awarded with the Nobel prize in chemistry in 2003. KcsA exists as a tetramer, each monomer being 17.6 kDa, and is often used as a model system due to its relative simplicity compared to other K^+-channels. The importance of understanding the structure and function relationship for this class of proteins stems from their implication in several disease and disorders.[133] KscA consists of only two of the otherwise six transmembrane domains compared to related eukaryotic potassium channels. The two domains present contains the important pore region, in which the selectivity filter and activation gate is located. These motifs have been of large interest for many scientific studies.[132] KscA stands out from other K^+- channels by being pH-gated instead of being regulated by changes in membrane potential, so called voltage-dependent. The conformational change of KcsA is regulated by the cytoplasmic pH and will at levels below pH 4 have an increased probability for adopting an open conformation and closed conformation above this pH.[134] Various mechanism for explaining the pH gating has been proposed and at what site in the channel this occurs has yet to be experimentally proven to a satisfactory degree.[134]

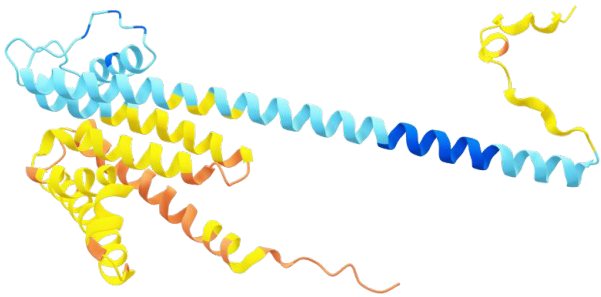

Figure 13. The structure of the monomer of KscA from Streptomyces as predicted by Alphafold.[135]

The structural changes in the channel upon opening and closing are considered to be in the size range where it is not necessary to achieve atomic resolution, instead alternative techniques such as SAXS and WAXS can be used. Initially, it was thought impossible to resolve site specific structural dynamics in proteins by SAXS/WAXS. Low signal to noise as a consequence of protein overlap with other signals was rapidly addressed by various technical advances.[136] Improvements in the interpretation of SAXS and WAXS data with 3D models has further enabled more and more complicated structural dynamics to be resolved by these techniques.[137] The work presented in this thesis will showcase the implementation of a photocage to rapidly acidify a solution of KcsA and the observed structural changes by time resolved X-ray solution scattering.

1.7 LOW MOLECULAR WEIGTH ORGANOGELATORS AND OXYGEN?

I repeatedly asked myself the question, how did I end up here, as I found myself in a bit of a conundrum trying to explain how organogels and structural biology logically ties together in a PhD thesis in organic chemistry. They don't. But they could, you just have to use your imagination. I have to admit that I don't find gels particularly interesting by themselves… However, I was curious about what access to a semi-solid material could bring, especially when combined with my actual scientific interest, which is in the design and implementation of photocages in order to address scientific problems. So, please bear with me when I must give a short introduction to the upside-down world of "gels".

1.7.1 GEL DEFINITIONS: A NECESSARY EVIL

"It is easier to conclude that you have a gel than it is to define what it actually is." – Henrik Sunden.

The definition of a gel is a sensitive topic in material chemistry. The American delicacy from the 1960-70s "Jell-O" and various other household commodities such as hair gel might come to mind. These are gels, but they are arguably very different with regards to their properties. One is sturdy and mostly retains its shape, to the delight of young children observing the jiggy dance as Jell-O made its way to the dinner table. Others are soft and depending on the type of hair gel might even cause some debate whether it should even be allowed to fall

under this classification. It is more practical to define gel forming materials as; compounds (gelators) that form a matrix which immobilizes a liquid, ideally constituting less than 1 % of the total mass of the solvent and gelator combined.[138] This should generate a gel-like material exhibiting solid-like behavior derived mainly from the gelator as opposed from the solvent. The property of the formed gel depends on the nature of the matrix that forms upon gelation. Gels derived from polymerization of monomers can cross-link and covalently lock in and encapsulate the solvent-gelator interactions. This typically results in permanent gels that cannot be regenerated. Much interest has been given to a specific class of gelators, the low molecular weight gelators (LMWG), due to their unique ability to self-assembly into one-dimensional supramolecular structures. The formed structures can then cross-link by various supramolecular interactions such as intertwining, branching or by forming insoluble structures, thus capturing solvent and driving the gelation process.

This self-assembly is driven by typical intermolecular interactions such as π-interactions, hydrogen-bonding and Van der Waals interactions.[139] In order to facilitate the gel driving interactions, some form of activation is required and the reason for this will vary depending on the type of gelator. Common activation routes for gelation involves, heating/cooling, pH changes or sonication. Gels obtained from LMWGs are often stiff of nature while breaking under relatively low physical strain, reverting back to a liquid. One of the many challenges in this field is the design and prediction of molecules that can efficiently form a gel. As an indication of how difficult this is, many modern gelators are still serendipitously discovered as opposed to predicted based on computer models or chemical intuition. Although, there has been significant advances in the field of rational design of gelators in recent years.[138,140,141] The strength or stiffness of a gel based on a LMWG depends on the equilibrium between the network built within the matrix and dissolved gelator still in solution. In order to assess the ability of a gelator to form a gel the minimum gelation concentration (MGC) is often referred to which is a benchmark for gelation efficiency. This is commonly investigated by a rather crude and often criticized method, the inverted vial test (**Figure *14***).

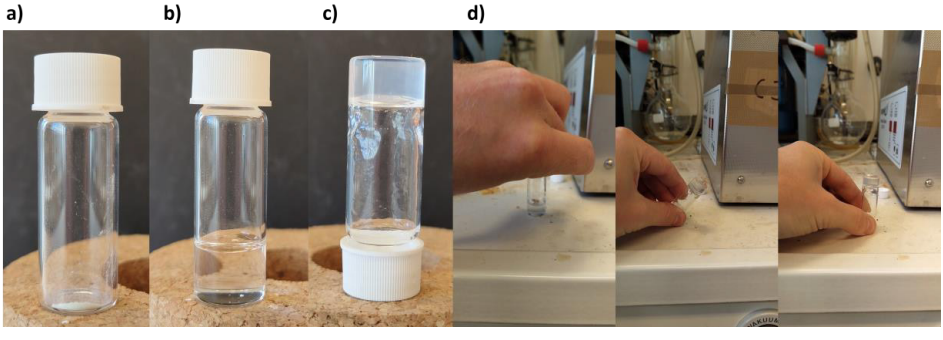

Figure 14. An overview of the inverted vial test showing **a)** An OTHO organogelator in a 4 ml glass vial typically used for the inverted vial test. **b)** The addition of solvent and subsequent solvation of the OTHO. **c)** The result of a successful inverted vial test where after heating and subsequent cooling, the dissolved OTHO has formed a gel capable of supporting its own weight and successfully completing the inverted vial test. **d)** The inverted vial test in action.

This crude evaluation passes the definition of a gel if lack of flow is observed in an upside-down vial following gelation. The critique is often associated to the lack of further rheological characterization and the lack of standardization associated with the inverted vial test.[142] Rheology is the study of how matter flow (or in this case, does not flow) and is a common method for characterizing the properties of gels. It measures the property of a material to resist deformation under stress. Based on the performance it can be helpful to define a gel as "weak" or "strong" based on the intensity of interactions where strong gels are more solid-like and weak gels are less well defined and could even include traits more resembling viscoelastic liquids. The elasticity, quantified by the shear modulus (G), vary between weak and strong gels.[141] This is typically divided into two components: the storage modulus (G') and the loss modulus (G''), where the storage modulus (G') represents the elasticity and the loss modulus (G'') is related to viscosity. A higher G' value suggests a more elastic gel and a high G'' value is indicative of a more viscous gel more likely to flow under stress.

1.7.2 THE OXOTRIPHENYLHEXANOATE (OTHO) GELATOR

The serendipitous discovery of a vial that had spontaneously formed a gel, was a pivotal moment that led to focused research on a specific class of molecules known as the oxotriphenylhexanoate (OTHO) gelators. The synthesis of gelators can be a time-consuming and lengthy process, involving multiple steps to produce the desired target in order to investigate its properties. However, OTHO gelator (**Scheme *6***, top) stand out due to their relative ease of synthesis, which involves a multicomponent reaction that efficiently creates a compound of high molecular complexity in a single step. The OTHO framework is versatile, supporting various substitutions at different sites without losing its effective gelation properties.[143–145] The OTHO features a 1,6-ketoester with three strategically positioned aromatic rings which are suggested to mediate the important π-interactions for gelation. The synthesis of OTHOs involves the formal conjugate addition of unsaturated aldehydes to chalcones mediated by a N-heterocyclic carbene (NHC) dialkyl imidazolium ionic liquid (**Scheme *6***). The mechanism shown in **Scheme *6*** is proposed to proceed via the following steps.

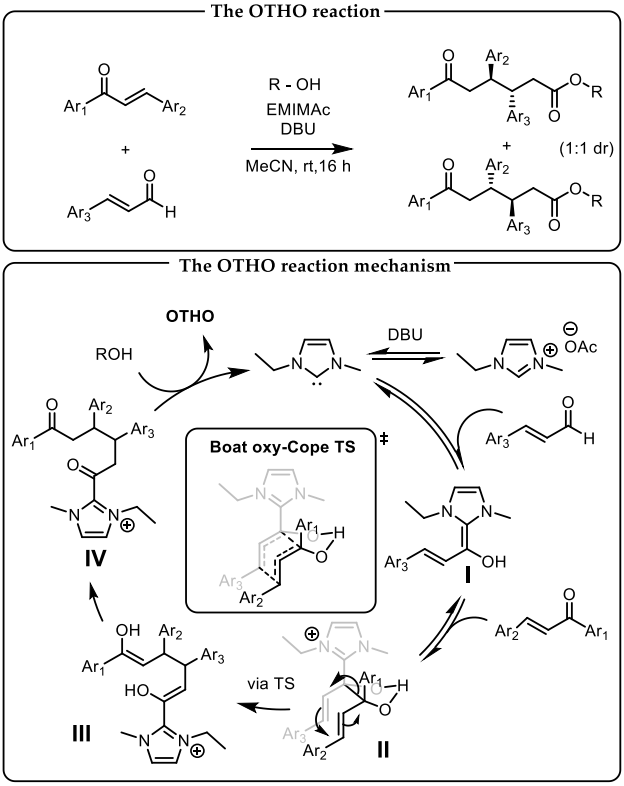

Scheme 6. Top) The multicomponent OTHO forming reaction. **Bottom)** The proposed reaction mechanism for the OTHO forming reaction.

Deprotonation of the NHC pre-catalyst by a base such as 1,8-Diazabicyclo(5.4.0)undec-7-ene (DBU) generates the free carbene that performs a 1,2-addition to the unsaturated aldehyde. Following proton transfer, Breslow intermediate **II** is formed and undergoes an oxy-Cope rearrangement reaction to yield **III**. This reaction can typically proceed via two transitions states (TS) which will lead to different diastereomeric outcomes, where the chair-type TS will generate a syn-configuration and the boat-type TS will generate an anti-configuration in the final product. The OTHO precursors have stereoelectronic properties that optimize the required orbital overlaps of the double bonds in the boat type conformation as opposed to the chair, leading to exclusively anti-configuration between the Ar_2 and Ar_3 aromatic rings. This was confirmed with X-ray crystallography of several OTHO derivatives and was also shown to be important for the gel formation properties. Following the oxy-Cope rearrangement intermediate **III** is formed which upon tautomerization proceeds to form intermediate **IV** that will be released in the presence of a primary alcohol to yield the desired OTHO and regenerating the free carbene.[146,147]

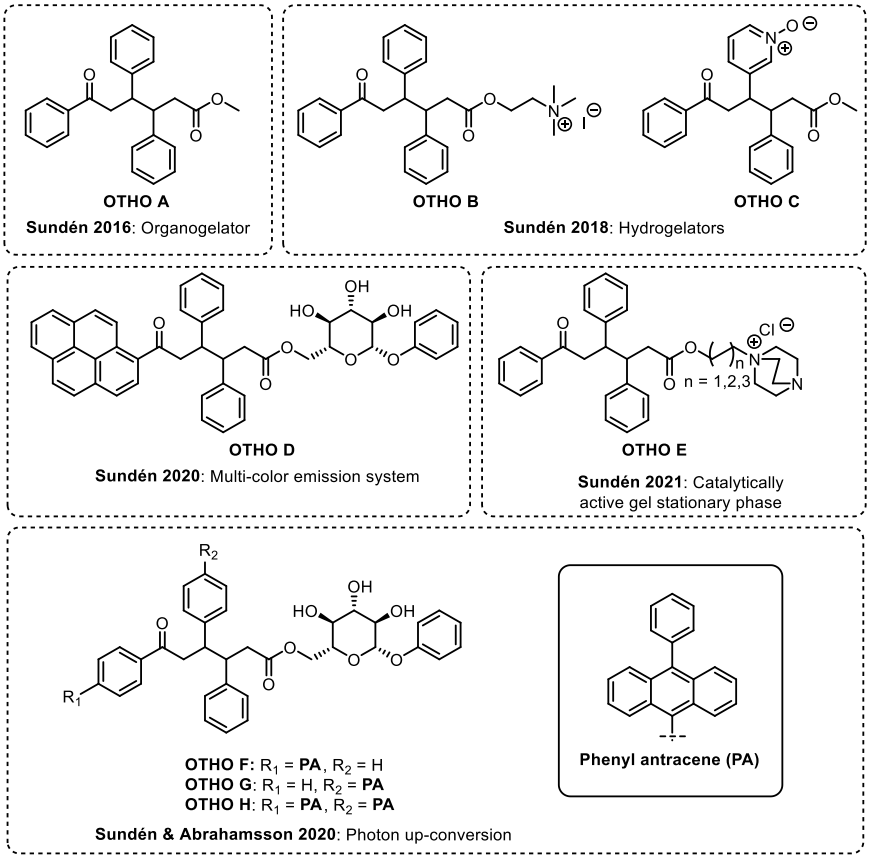

Scheme 7. Recent applications of OTHOs in material science. OTHO **A** is the simplest OTHO which served as a starting point for further diversification in subsequent studies.

The adaptability of the OTHO framework and ease of synthesis has facilitated the development of a range compounds for diverse applications in the field of material science. Notable examples are shown in **Scheme 7** with hydrogel derivatives (OTHO **B** and **C)**,[148] multi-color emission in the gel phase (OTHO **D)**,[149] light mediated gel writing and erasing,[150] as a chromatographic stationary phase with catalytic activity (OTHO **E)**,[151] photon up-conversion OTHO **F-H**,[152] some of these structures are shown in in **Scheme 7**. Furthermore, chemists with a keen eye for motifs that can bind oxygen would certainly pay extra attention to OTHOs such as **F-H**, due to the presence of a phenyl-anthracene (**PA**), a moiety that is known to reversibly bind and release oxygen in the singlet state.

2. RESULTS AND DISCUSSION

"We did this not because it was easy – but because we thought it would be easy". Upon joining the Oxidase project, I initially worried about what I would do for the final years of my PhD. The project seems simple and straightforward; mix a photolabile oxygen cage with a protein, blast it with a laser and collect several different time-points to visualize the oxygen reduction mechanism at an atomic resolution to make a molecular movie. Simple enough. Did we succeed in this endeavor? ***No****, absolutely not, at least not in the way we intended to. Do I think it is achievable?* ***Absolutely****, or at least probably! If at first you don't succeed; try, try and try again. Most good stories contain a phase of adversity and challenges, which is eventually overcome by the protagonist followed by an: "and they lived happily ever after" ending. Is this such as story? Is it even a good story? We have progressed the story through the initial few chapters, containing numerous failures and character developing moments. Will there be a happy ending for TR-SFX with photocages in the end? Only time can tell.*

2.1 PAPER I: EVALUATION AND DEVELOPMENT OF OXYGEN PHOTOCAGES FOR TIME-RESOLVED X-RAY STRUCTURAL STUDIES

Paper I aims to address some of the numerous challenges associated with the utilization of oxygen photocages to study oxygen dependent enzymes such as CcO. We aimed to expand the scope of oxygen photocages from time-resolved absorbance spectroscopy to TR-SFX. This necessitated the validation of a homogenous reaction initiation in reduced microcrystals of CcO following spatiotemporal release of molecular oxygen by a single laser flash. Our work demonstrates that HPBC type photocages can release supersaturated levels of molecular oxygen upon excitation of a single laser pulse. This allowed the validation that a homogenous reaction initiation can be achieved in microcrystals of reduced CcO with an oxygen photocage.

2.1.1 HOUSTON, WE HAVE A PROBLEM!

Our journey began with the synthesis of caged oxygen compound **HPBC 1**, which was synthesized as the nitrate salt according to a literature procedure (**Figure *15*a**), resulting in the binuclear cobalt complex with three nitrate counterions.[113] This resulted in the target compound in the form of a brown powder as opposed to the described black crystalline solid. Following optimization of the reaction conditions, a more reliable protocol was developed which consistently resulted in high purity product (consult the supplementary information associated with **Paper I** for more details). We verified by absorbance spectroscopy that photolysis of an aqueous solution containing **HPBC 1** resulted in the formation of molecular oxygen, evident by the disappearance of the characteristic LMCT at 400 nm and visible bubble formation (**Figure *15*b**).[113] Initially, **HPBC 1** was described and isolated as a perchlorate salt with limited aqueous solubility and a lower quantum yield for

light induced oxygen release. The significant discrepancy in reported quantum yields raised questions since such a large difference is unlikely to arise by simply changing counterions.

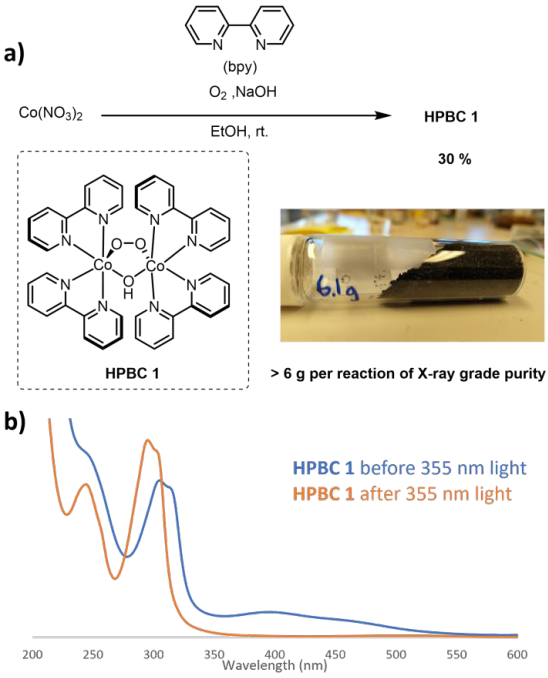

Figure 15. a) Synthesis of **HPBC 1**. Reaction conditions: bpy (2.0 eq.), NaOH (0.5 eq.) and O_2.

To confirm whether or not this was correct, we synthesized the perchlorate (PF_6) in addition to the tetrafluoroborate (BF_4) derivative of **HPBC 1** by the addition of salts containing the respective counterion which resulted in precipitation of the target compounds. All three salts of **HPBC 1** shared identical absorbance spectrums and photolytic properties when exposed to UV-light. If there was a difference in quantum yield this should have been apparent and we thus concluded that one of the reported quantum yields must be incorrect. This prompted us to reinvestigate the quantum yield for **HPBC 1** by chemical actinometry which revealed that the original report for the perchlorate derivative was correct, with a quantum yield of ~0.04 at 355 nm.

Next, we turned our attention into validating that we could replicate the oxygen mediated turnover of reduced CcO upon photolysis of **HPBC 1**. A more severe issue was discovered at this stage when attempting to reproduce results from a previous study of **HPBC 1** and CcO.[114] It stated that "a spectrum taken 1 min after mixing a solution of the cobalt complex with the reduced unliganded enzyme" does not result in premature oxidation of CcO or deterioration of the caged oxygen compound **HPBC 1**. That is, the caged oxygen compound does not react with the enzyme or its reducing agents prior to light activation. However, when we replicated this experiment, we observed a rapid deterioration of **HPBC 1**. Typically, CcO is produced in the reduced state via two methods: by treatment with excess sodium ascorbate (NaAsc) together with a mediator, or by treatment of excess sodium

dithionite (NaDt). We exposed **HPBC 1** to equimolar amounts of both reductants, which resulted in complete decomposition within a few seconds for NaDt and minutes for NaAsc (**Figure *16***). This presented a significant challenge; under these conditions it would not be possible to pre-mix the photocage with the reduced CcO. The consequences of this for a potential SFX based experiments were severe and would necessitate a sophisticated sample delivery system that can accommodate a very rapid mixing under anaerobic conditions. It should be noted that there has been significant development towards mix and inject systems that can achieve mixing resolutions in the range of seconds in the last few years.[153,154] However, it is still relatively new and is not something that is routinely available at XFELs and synchrotrons which would make an already complicated experiment more difficult. Initial testing with developing a 3D-printed LCP mixing device for in-house testing further discouraged pursuing a mixing strategy. To circumvent the redox incompatibilities between the photocage and reducing agents, we decided to investigate if it was possible to stabilize the caged oxygen compound.

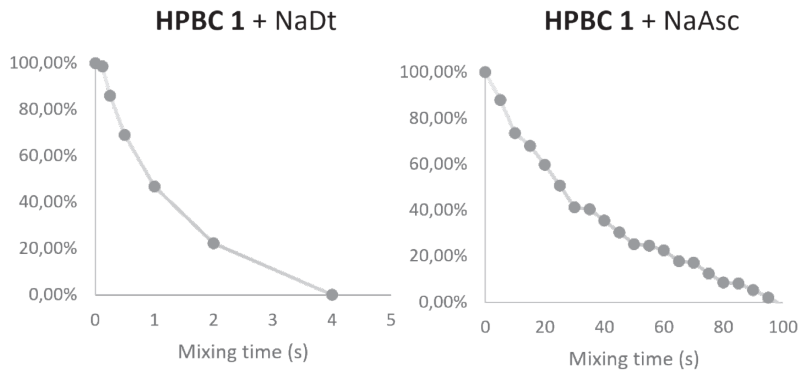

Figure 16. Mixing of caged oxygen **HPBC 1** (5 mM) with 5 mM NaDt (left) and 5 mM NaAsc + phenazine methosulfate (1.5 μM, mediator) (right) showing the degradation of **HPBC 1** over time based on the disappearance of the 400 nm absorbance peak, followed by UV/vis spectroscopy. The measurement was performed under flow conditions by rapidly mixing the individual components in a 0.3 mm quarts capillary in a custom 3D printed flow cell.

2.1.2 SYNTHESIS OF CAGED OXYGEN PHOTOCAGES

We rationalized that by employing more electron donating ligands this would increase the electron density around the cobalt atoms and make the complex less prone towards chemical reduction. In addition to investigating more electron donating ligands, we also explored a variety of different ligands in order to gain a better understanding of HPBC type photocages. Our investigation soon revealed that the synthetic procedure for HPBC compounds, while straightforward, was extremely sensitive to minor structural changes to the bipyridine ligand. For a more in-depth discussion of ligands that did not yield HPBC compounds, see **Paper 1** and its accompanying supplementary material. It was consistently observed that the formation of any precipitate during the synthesis generally precludes the successful formation of an HPBC-type complex. Furthermore, as opposed to **HPBC 1** which

is easily produced in large amounts, any structural modification decreases the tendency to crystallize and demands tedious purification by slow vapor diffusion. In the end, HPBC compounds **2-7**, shown in **Scheme** *8* were synthesized and we proceeded to investigate the spectroscopic, photolytic and redox properties. Detailed information regarding the synthesis, purification and characterization of novel HPBC compounds can be found in the supplementary information for **Paper I**. Crystal structures were obtained for **HPBC 1**, **2**, **4**, ,**6** and **7**. Additionally the photoproduct of **HPBC 1**, **3 and 6** were also obtained and can be found in **Paper I** and the associated supplementary information.

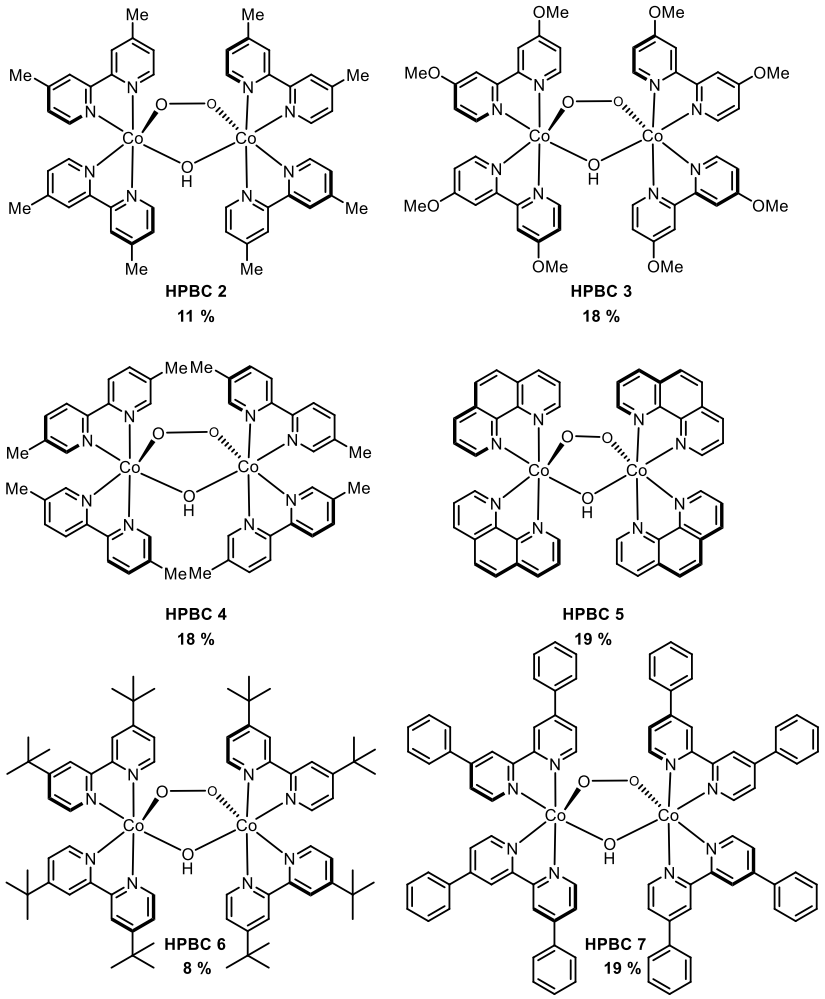

Scheme 8: Successfully synthesized and characterized HPBC compounds **2-7** and the yield of isolation following slow vapor diffusion purification. All compounds were isolated as the nitrate salt except for HPBC **6** which was isolated as the hexafluorophosphate (PF_6) salt.

The absorbance spectrum for HPBC compounds **1-7** confirmed the presence of the characteristic $\pi^*(O_2^{-2})$ LMCT transition at 400 nm which disappeared upon light irradiation.

The formation of equimolar amounts of molecular oxygen was also confirmed independently using a fluorescence oxygen sensor (Ocean optics, NeoFox using the patch-based FOXY formulation), shown in **Figure 17**.

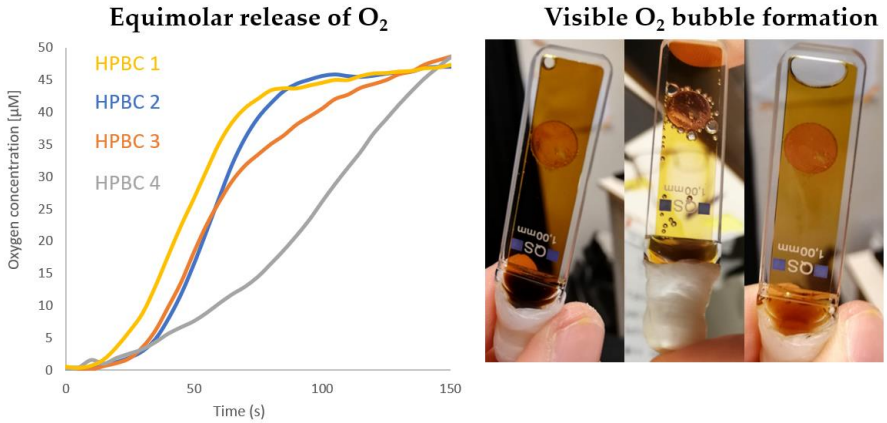

Figure 17. The release of molecular oxygen determined by a fluorescent oxygen sensor for **HPBC 1-4** (50 µM). **HPBC 5** exhibited premature degradation during preparation at room temperature which prevented the detection of equimolar concentrations of oxygen and was excluded. The image on the right shows the sequence of illuminating **HPBC 1** (5 mM) with 385 nm LEDs in a sealed cuvette, showing the evolution of oxygen gas. Additionally, **HPBC 6** and **7** were not sufficiently soluble in aqueous solution for this experiment.

The quantum yield for the oxygen liberation was determined by chemical actinometry for several wavelengths and the results are summarized in **Table 1**. The redox stability was investigated by cyclic voltammetry and by mixing with the relevant biochemical reducing agents in a 1:1 molar ratio in a flow cell. Based on the results summarized in **Table 1**, it becomes apparent our initial hypothesis: that a HPBC complex based on a more electron donating ligand should be more resilient towards reduction, indeed hold true. **HPBC 3**, with methoxy (-OMe) substituents in the para-position of the bipyridine rings, shows a significant improved stability towards NaDt and NaAsc + PMS (Table 1, Entry 3). Surprisingly, HPBC **2** showed that similar improvements in stability was achievable with a methyl group (Table 1, Entry 2). **HPBC 4** with a methyl substituent in the meta-position is only marginally more stable than unsubstituted **HPBC 1** (Table 1, Entry 4). Phenanthroline derivative **HPBC 5** has the least electron donating ligand which is reflected in the observed redox stability towards reductants with the shortest half-life (Table 1, Entry 5). It was also observed that a solution of **HPBC 5** would deteriorate at an appreciable rate even at room temperature, restricting its potential use as a viable photocage. **HPBC 6** (PF_6 -salt) and **7** ($-NO_3$ salt) were almost completely insoluble in aqueous solution (> 50 µM) which also precludes its use in biochemical studies. The peak anodic current obtained from the cyclic voltammetry also agrees well with the obtained mixing data. A rather unfortunate observation is that the stability towards reduction seems to also correlate with a decrease in the quantum yield for the light induced oxygen release, which was lower for all HPBC compounds that were tested across all wavelengths.

Table 1. Relevant data for HPBC compounds **1-7** from **Paper I**. Determined half-lives of HPBC (5 mM) mixed with NaAsc (5 mM) + Phenazine methosulphate (PMS) (1.5 μM) and NaDt (5 mM). The peak anodic current was measured for HPBC **1-7** (150 μM) with cyclic voltammetry in MeCN (NBu_4PF_6: 0.05 M) with a sweep rate of 100 mV/s. Values are reported vs Ag/AgCl reference electrode with a working electrode consisting of glassy carbon and a platinum counter electrode.

Entry	**HPBC**	$T_{1/2}$ (NaAsc + PMS)	$T_{1/2}$ (NaDT)	Quantum yield (φ) in water	Quantum yield(φ) in MeCN	Peak anodic current[f] (V)
1	(**1**) - bpy	25 s	~0.8 s	0.04[b] 0.06[c] **0.04[d]** 0.03[e]	0.07[b] 0.19[c] 0.19[d] 0.13[e]	-0,23 V
2	(**2**) – 4Me	19 min	20 s	0.02[b] 0.02[c] **0.02[d]** >0.01[e]	0.05[b] 0.08[c] 0.08[e]	-0,34 V
3	(**3**) – 4OMe	21 min	13 s	0.02[b] 0.02[c] **0.02[d]** >0.01[e]	0.06[b] 0.10 [c] 0.08 [e]	-0,33 V
4	(**4**) – 5Me	1 min	2 s	0.02[b] 0.02[c] **0.03[d]** 0.01[e]	0.07[b] 0.08 [c] 0.12[e]	-0,21 V
5	(**5**) – Phen	7 s	~0.7 s	n.d[f]	n.d[f]	-0,17 V
6	(**6**) – 4dtbbpy	n.d.[a]	n.d.[a]	n.d[g]	0.02[b] 0.04 [c] 0.04 [e]	-0,35 V
7	(**7**) – 4Ph	n.d.[a]	n.d.[a]	n.d[g]	0.03[b] 0.03 [c] 0.03 [e]	-0,27 V

[a]Not determined due to poor aqueous solubility. [b]Using 302 nm monochromatic light. [c]Using 334 nm monochromatic light. [d]Using 355 nm monochromatic light. [e]Using 392 nm monochromatic light. [f]Observed significant decomposition in solution at room temperature. [g]Not soluble. [h]Measured in MeCN. [I]Refers to the first reduction peak in the voltammogram. dtbbpy = 4,4 -Di-tert-butyl-2,2 -dipyridyl.

It would be an understatement to say that the results were underwhelming. An improvement with regard to the stability was achieved but it comes at the cost of a lower quantum yield of O_2 release. Furthermore, the improvements in redox stability in HPBC **2** and **3** were not sufficient to continue with a mixing-free approach with CcO. Early screenings of **HPBC 1** compatibility towards biochemical reductants had shown that very mild reducing agents such as thiol-based glutathione and tris(2-carboxyethyl)phosphine (TCEP) did not cause any measurable deterioration. This prompted another question, could we find less reductive conditions to reduce the enzyme. Following an extensive screening it was found that a large excess of dithiothreitol (DTT) produced CcO in the fully reduced state. Incubation with **HPBC 1** (1 mM) and DTT (4 mM) showed only minor degradation, similar to those observed by prolonged storage at room temperature, by UV/Vis and NMR (**Paper I**, supplementary figure **S5**, **S6**). This prompted a compromise to be made. DTT can reduce the protein but the reduction is significantly slower than conventional methods, typically occurring within 20 minutes as opposed to sub-second. However, this would allow us to pursue a mixing free experimental setup for TR-SFX studies.

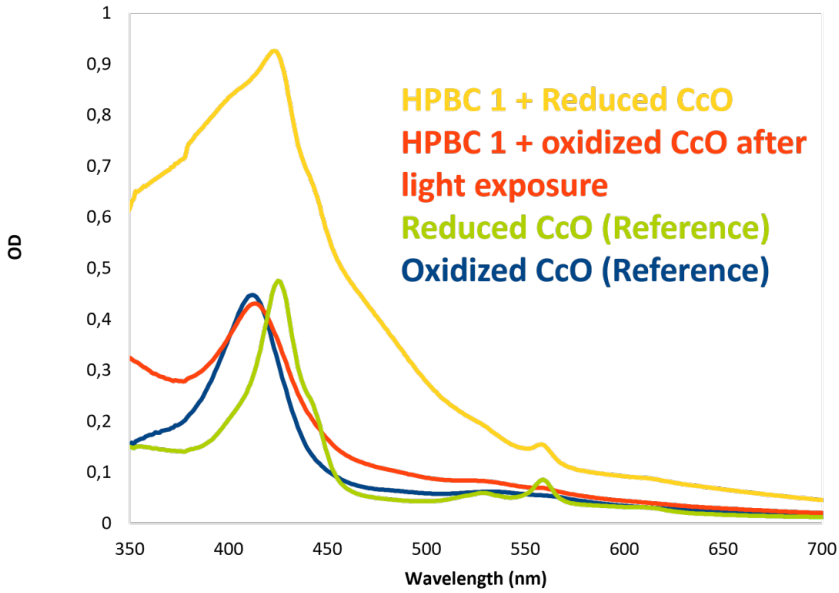

Figure 18. Absorbance spectrums showing the oxidized spectrum of CcO (blue), the reduced spectrum (green), **HPBC 1** and reduced CcO mixed after 1 h (yellow) and the same sample after 385 nm light exposure (red). This showed that the DTT reduced CcO can be turned over in the presence of oxygen.

Incubating DTT reduced CcO with **HPBC 1** in an airtight cuvette for one hour followed by exposure of UV-light showed the expected absorbance changes associated with the oxidation of reduced CcO (**Figure 18**, yellow to red, compared against green to blue; note that yellow contains the absorbance contribution from **HPBC 1**).

2.1.3 SPECTROSCOPIC VALIDATION OF THE REACTION BETWEEN CAGED O_2 AND REDUCED CCO

After a significant effort to establish conditions where reduced CcO and the caged oxygen photocage could be premixed, we carried on validating that a homogenous reaction initiation can be achieved at concentrations and conditions relevant to a SFX experiment. We hesitantly decided to continue to employ **HPBC 1** for further studies due to concerns regarding the diminished quantum yield for the more stable **HPBC 2** and **3**. We were able to demonstrate that concentration exceeding oxygen saturation (>2 mM) could be achieved upon excitation of a solution of **HPBC 1** in a 0.3 mm quartz capillary (**Figure *19***). This was crucial to validate since a crystalline sample is non-homogeneous and microcrystals of CcO is expected to have a local CcO concentration around 2.4 mM. Hence, a high local concentration of released oxygen is a prerequisite to enable TR-SFX.

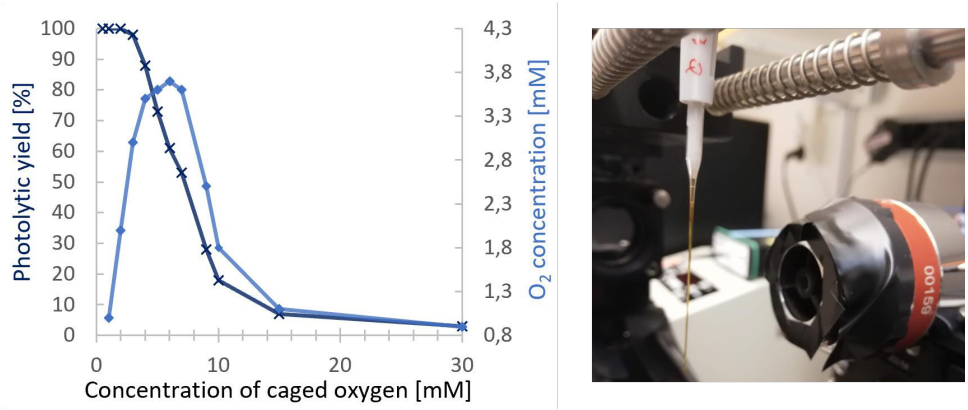

Figure 19. Left) Yield of O_2 upon a single 355 nm laser pulse (~1 J/cm2, 5 ns pulse) showing the percentage yield (dark blue) and the molar yield (blue) of released oxygen. **Right)** Close up on the capillary containing **HPBC 1** prior to light illumination.

Aqueous solutions of **HPBC 1** ranging 0.5 mM to 30 mM were exposed to a single laser pulse (355 nm) and the yield of released oxygen was determined by the disappearance of the 400 nm peak in the absorbance spectrum. At concentrations below 2 mM, full photolytic release of O_2 was achieved. The maximum molar yield of O_2 was achieved at a concentration of 4 mM where a rather impressive **>3.5 mM** concentration of O_2 was reached following a single laser pulse. It is important to note that there is a diminished yield upon increasing the concentration of **HPBC 1** beyond 3 mM due to limited light penetration at higher optical densities of the sample. Satisfied with the yield of oxygen release the next challenge was to verify that a homogenous reaction initiation can occur with sufficient temporal resolution at concentrations relevant for crystallographic studies. Most previous spectroscopic studies employed a higher ratio of oxygen to protein, something that would be completely unrealistic to achieve for SFX due to the dense/concentrated nature of crystals. Therefore, we initially wanted to demonstrate that the reaction could be initiated in an aqueous solution at high protein concentrations. This would address the question if a sufficient spatiotemporal resolution was achievable at higher protein concentrations which

are required for further TR-SFX studies. It was a great relief to observe oxidation of CcO upon exposing a sample consisting of reduced CcO (120 μM), DTT (4 mM) and **HPBC 1** (2.5 mM) to a single laser pulse (355 nm, ~1.5 mJ/pulse at the sample position measured with a power meter). The most exciting part of this experiment was fine tuning the laser due to the poor quantum yield of **HPBC 1**, which necessitated very high laser fluence to be used. The laser spot size had to be optimized to achieve a narrow beam to focus the available light, while making sure that the focal point was sufficiently far away from the quartz capillary as to avoid accidental laser cutting of the capillary and sample, illustrated in **Figure *20***.

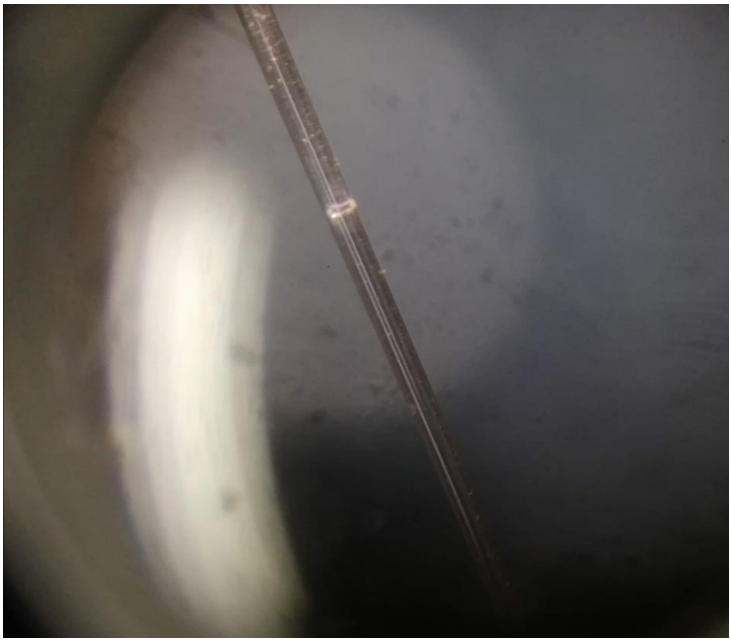

Figure 20. Accidental "laser cutting" of the capillary following a slight misalignment of the laser in order to achieve sufficient power to initiate the reaction between **HPBC 1** and CcO. The trick here is to achieve what is in Swedish referred to as a "lagom" spotsize and laser fluence ratio which is a unique Swedish expression referring to just the right amount.

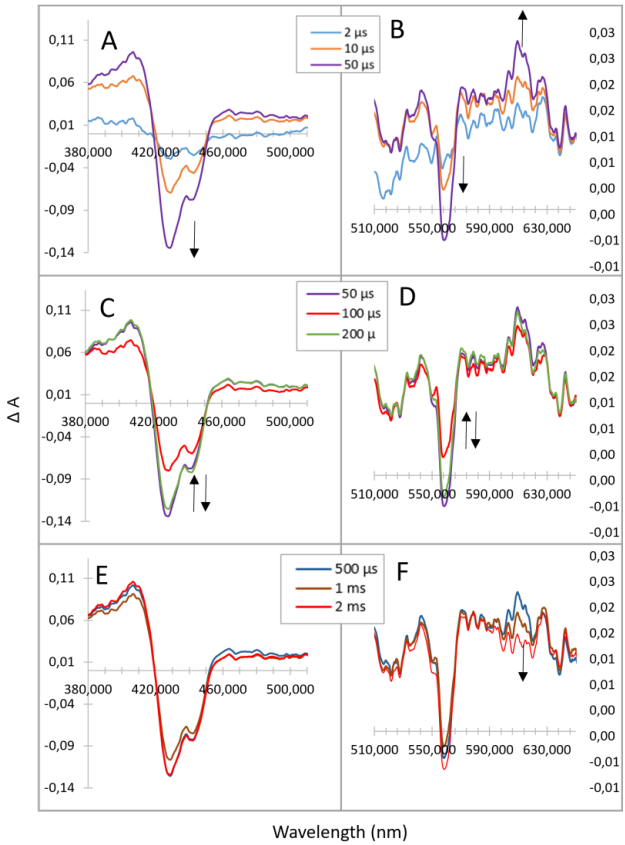

Figure 21. TR-optical absorbance difference spectrums of DTT (4 mM), reduced CcO (120 µM, pH 8) and **HPBC 1** (2.5 mM) 2, 10, 50, 100, 200, 500 µs, 1 and 2 ms after a 355 nm laser pulse. The spectral contribution of HPBC 1 has been removed and the reduced protein + **HPBC 1** was used as the blank to obtain the difference spectrums. Characteristics spectral features of the intermediate P_R are evident at the 50 µs time point. (Figure is taken from **Paper I** with the permission from the authors).

This was achieved in a sufficient population of the enzyme to distinguish between various reaction intermediates for CcO. As a highlight, a high population of the short-lived oxo-intermediate $\mathbf{P_R}$ could be resolved with a time delay (**Figure *21***, 10 - 50 µs, **A** - **B**) consistent with the current mechanistic paradigm for CcO. After this time the $\mathbf{P_R}$ state will transition into the **F-**state which is apparent in **Figure *21*D** from the re-reduction and subsequent oxidation of heme b, which is evident from the increase and then decrease of the negative peak at 560 nm, associated with heme b. The formation of the oxidized enzyme from the **F**-state is then seen as the peak at 610 nm slowly decays in the following milliseconds (**Figure *21***, **F**). This was an important validation; the reaction could be triggered with sufficient temporal resolution at high concentrations (**Figure *21***). For an in-dept discussion of relevant intermediates and time-points see **Paper I**. It should also be emphasized that it is imperative to only use fresh DTT for these experiments since it is sensitive to air and solutions of DTT

quickly oxidize and lose reducing potency. To mitigate the oxygen leakage and compensate for the slow reduction of CcO, we incorporated an oxygen scrub mixture into our system. This consisted of glucose oxidase, catalase, and glucose, which stepwise will consume oxygen and prevented samples from oxidizing prematurely whilst not interfering notably with the kinetics of the measurement. The oxygen scavenger system proved to be very useful for the next step, which was to initiate the reaction in microcrystals of reduced CcO. To put the difficulty of this next task into context, please consider the following trivia: Protein purification requires **40 L** of media each week to produce about 30 mg of purified protein. An XFEL experiment for CcO typically consumes about 4-6 ml of crystal slurry. Spectroscopists typically avoid using a liquid cubic phase (LCP) as a medium for time-resolved absorbance spectroscopy measurements for a very good reason. The reason being that LCP is quite similar to the viscosity and turbidity of Vaseline which makes the practical handling of the sample quite difficult. The sample needed to perform the validation was very precious which prompted us to utilize the crystals that were of least interest for upcoming XFEL experiments. This was a mistake in hindsight since the crystals used were slightly smaller (~5-6 μm) than those actually used for time resolved data collection at XFELs later on (typically ~15 μm) since the size of the crystals will affect the diffusion of various substrates in the sample which should be kept in mind.

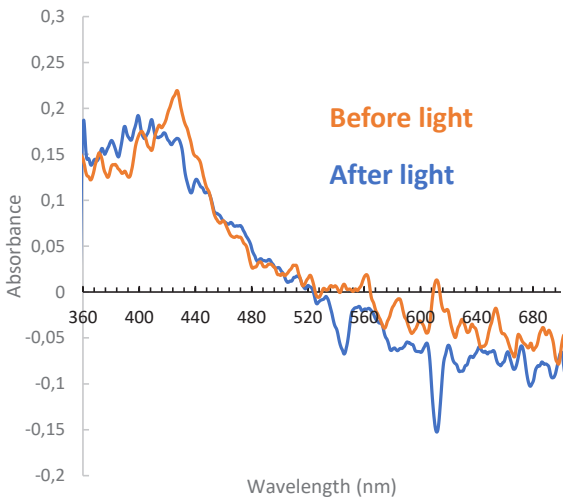

Figure 22. Reduced microcrystals of CcO (50-60 μM) in LCP (orange). Also present in the sample was DTT (15 mM) and **HPBC 1** (2.5 mM). 1 ms after exposure to a 355 nm laser pulse (blue), showing the oxidation of the reduced enzyme, evident by the shift in the soret peak maximum from 427 nm towards 412 nm. The spectral contribution from **HPBC 1** has been removed for clarity.

However, microcrystals of reduced CcO treated with the oxygen scrub system were mixed with **HPBC 1** and loaded into a 0.3 mm quartz capillary and exposed to a 355 nm laser pulse. This resulted in spectral signals consistent with oxidation of the reduced enzyme. However, due to the turbidity of the sample and the additional complications of competing absorbance from **HPBC 1**, and various other components in the sample, only the signal from the soret

peak (around 410 nm) shift is observable in our experiment (**Figure 22**). DTT reduced microcrystals of CcO are oxidized by oxygen released by **HPBC 1** following excitation with a 355 nm laser. This was the final piece of the puzzle in terms of validating that it is possible to oxidize microcrystals of CcO with oxygen produced from a caged oxygen compound. It should be emphasized that we were able to demonstrate that it is possible, but definitely not easy. Premature oxidation of the crystalline sample was more problematic than for the previous solution-based experiments. This we partially attributed to the pH which is 5.3 for the crystalline CcO sample as opposed to ~7.6 at which the solution-based spectroscopy was performed at. Thus, the DTT mediated reduction of the crystalline sample was significantly slower than in solution. Furthermore, it was not always behaving consistently and the rate of reduction varied significantly. The exact reason for this is still not known but one component is definitely depending on crystal size. The consequences of this will be discussed in greater details in **Paper II**.

The development of the more redox stable HPBC compounds did eventually prove to be worthwhile for a side project (unfortunately outside the scope of this thesis) in which we investigated an artificial intermediate in the CcO reaction cycle, the carbon monoxide bound mixed valence (MVCO) state. This necessitated a prolonged incubation with an oxygen photocage where even a small amount of prematurely released oxygen could not be tolerated. Initial efforts to scavenge the oxygen released from **HPBC 1** were unsuccessful. However, upon incubation with **HPBC 3**, the sensitive MVCO state was intact for around one hour which enabled the reaction initiation by a laser pulse to release oxygen to form the **P**$_{M}$ intermediate (**Figure 23**). In an experiment, exposing MVCO and **HPBC 3** to a laser pulse allowed observation of the **P**$_{M}$ state for approximately 30 seconds, a duration not previously documented in the literature. The increase in absorbance in the difference spectrum at 610 nm is indicative of the formation of **P**$_{M}$.

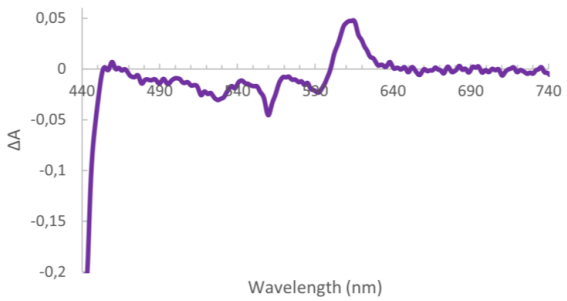

Figure 23. Difference spectrum of MVCO (120 μM) and **HPBC 3** (3 mM), following a single laser pulse (355 nm). The negative feature at 560 nm is a result of a slight over-reduction of the enzyme during preparation which is oxidized upon oxygen liberation. The spectral contribution of the caged oxygen compound has been removed for clarity. This experiment was performed in solution and the blank reference is MVCO + **HPBC 3**. The spectral characteristics shown are characteristic for the **P**$_{M}$ intermediate which shows an extended lifetime due to the lack of further electron to progress the reaction cycle.

Efforts are underway to translate these findings into a TR-SFX based experiment. An initial attempt was made at MAX IV but failed due to difficulties in attaining a pure MVCO state in the crystals in addition to an improvised laser illumination setup. The aim is to potentially observe the first oxo-intermediate in the reaction cycle, the $\mathbf{P_M}$ state. Unlike the conventional four-electron reduced enzyme, MVCO (a two-electron artificial intermediate) gets trapped in the PM state without progressing further.

2.2 PAPER II – TR-SFX OF CYTOCHROME C OXIDASE WITH AN OXYGEN PHOTOCAGE

Time resolved Blobbology (TR-BloBy) – The detailed study of various shapes and forms of blobs as any resemblance of sanity is slowly lost as a function of time.

In **Paper II** the structural dynamics of *ba*$_3$-type cytochrome c oxidase following the photoliberation of molecular oxygen from a caged oxygen photocage was investigated. This work built on the foundation from the reaction initiation methodology that was developed in **Paper I**. **Paper II** is based on the collective effort of our group in the past five years during numerous XFEL and synchrotron experiments. A significant challenge was to ensure the compatibility of the photocage with the microcrystal's chemical environment to avoid premature oxidation under the experimental conditions. Our findings include structural changes within 10 ms following oxygen release. We also report on the high-resolution structure of the enzyme in its resting state, highlighting a chloride ligand at the active site and in the vicinity of the BNC, verified by anomalous X-ray diffraction. This work advances our goal of employing time-resolved crystallography for detailed studies of oxygen dependent enzymes with the use of photocages.

This work builds upon previous TR-SFX experiments, mainly from photodissociation studies on the reduced CO-bound CcO in addition to the first and subsequent static room temperature SFX structures of oxidized *ba*$_3$-type CcO.[155–157] The next logical step was to pursue the reaction between the reduced enzyme and its native substrate, molecular oxygen. This was recently attempted by another group by mixing reduced *aa*$_3$-type CcO crystals with an oxygen saturated buffer in a SFX experiment. Eight seconds after mixing, the authors claim to observe the $\mathbf{P_R}$ state. The authors suggest that the lifetime of this typically microsecond lifetime intermediate is extended in the crystalline phase. In addition to electron density features in the active site reminiscent of two oxygen-type species, there is a transient water that only shows upon mixing with oxygen.[158] Furthermore, the steady-state reaction between oxygen and reduced CcO was investigated by another group employing cryo-electron microscopy. The authors claim to identify intermediates in the reaction cycle and propose a peroxide ligand in the oxidized form of the enzyme and molecular oxygen in the intermediate **P**-state.[159] Although, it is unclear how the temporal resolution in the experiment would allow for any significant populations of these intermediates under the timescale of such an experiment. This controversy is one of many in CcO structural studies. It should be emphasized that this is likely due to the inherent difficulty associated with the interpretation of crystallographic electron difference density. However, one should not be

overly critical, these are highly complex systems to study even when investigating "simple" light triggered systems. Initially, the oxidized enzymes structure was thought to contain a single oxygen species in the BNC,[160] later hypothesized as a peroxide.[161] Our group previously suggested a single oxygen species such as a water or a hydroxide in the *ba*$_3$-type CcO.[162] Amusingly enough, we subsequently disprove ourselves later on.

The Noodleman group proposed that this discrepancy in reported ligands to the BNC could be attributed to multiple conformations of a single oxygen atom at energetically very similar positions. This could be observed as an elongated electron density, which would be indistinguishable from a single oxygen species with different occupancies at resolutions around 2 Å.[163] Unphased by the challenges encountered in previous work, we set out to discover our very own unique set of problems. Taken together our work highlights the difficulty of incorporating substrate based photocages in TR-SFX studies and the numerous variables that needs to be kept in mind. Our first challenge that needed to be resolved was to demonstrate that the reaction could be initiated in microcrystals of CcO, which was addressed in **Paper I**. In a study by Rousseau et al. where reduced CcO and O_2 were mixed by a rapid mixing jet, they claim to observe an oxo-intermediate from the reaction cycle eight seconds after mixing. They reason that the reaction is slowed down by several orders of magnitude under their experimental conditions.[158] Under our conditions, we do not observe this phenomena, although it should be pointed out that there are many technical challenges with time-resolved absorbance spectroscopy measurements on crystalline samples, especially microcrystals in LCP. Spectroscopic validations can only prove so much and the only way forward was to employ a caged oxygen compound to initiate the reaction between reduced microcrystals of *ba*$_3$-type CcO and oxygen in a real life SFX experiment. More detailed information about sample preparation, data analysis, and other relevant experimental parameters can be found in the manuscript and supplementary information for **Paper II**.

2.2.1 TR-SFX STUDIES OF CCO AT SWISFELL 2021

The end goal of this project was to collect TR-SFX data as reduced CcO is oxidized by oxygen released by an oxygen photocage. The initial XFEL experiment (leaving out two failed experiments at the European XFEL where no data could be salvaged resulting from numerous technical issues) took place at SwissFEL in 2021. For a clearer data interpretation, we collected static reference structures for the oxidized and DTT reduced enzyme which were resolved to a resolution of 1.7 and 1.8 Å respectively. The oxidized structure (**Figure 24a**) was of significantly improved resolution than earlier reports.[162] It was now evident that the electron density in the BNC of the oxidized structure could not be simply described by a single oxygen species, as previously suggested. Anomalous diffraction later confirmed the identity of this ligand as a chloride ion (**Figure 24, b-c**). A more surprising finding was the presence of a second chloride in the vicinity of the active site where protons are though to enter the BNC. Although surprising, it was not hard to rationalize considering that the crystallization conditions contains 1.4 M NaCl and previous studies have suggested that a chloride can ligate Cu_B.[164,165]

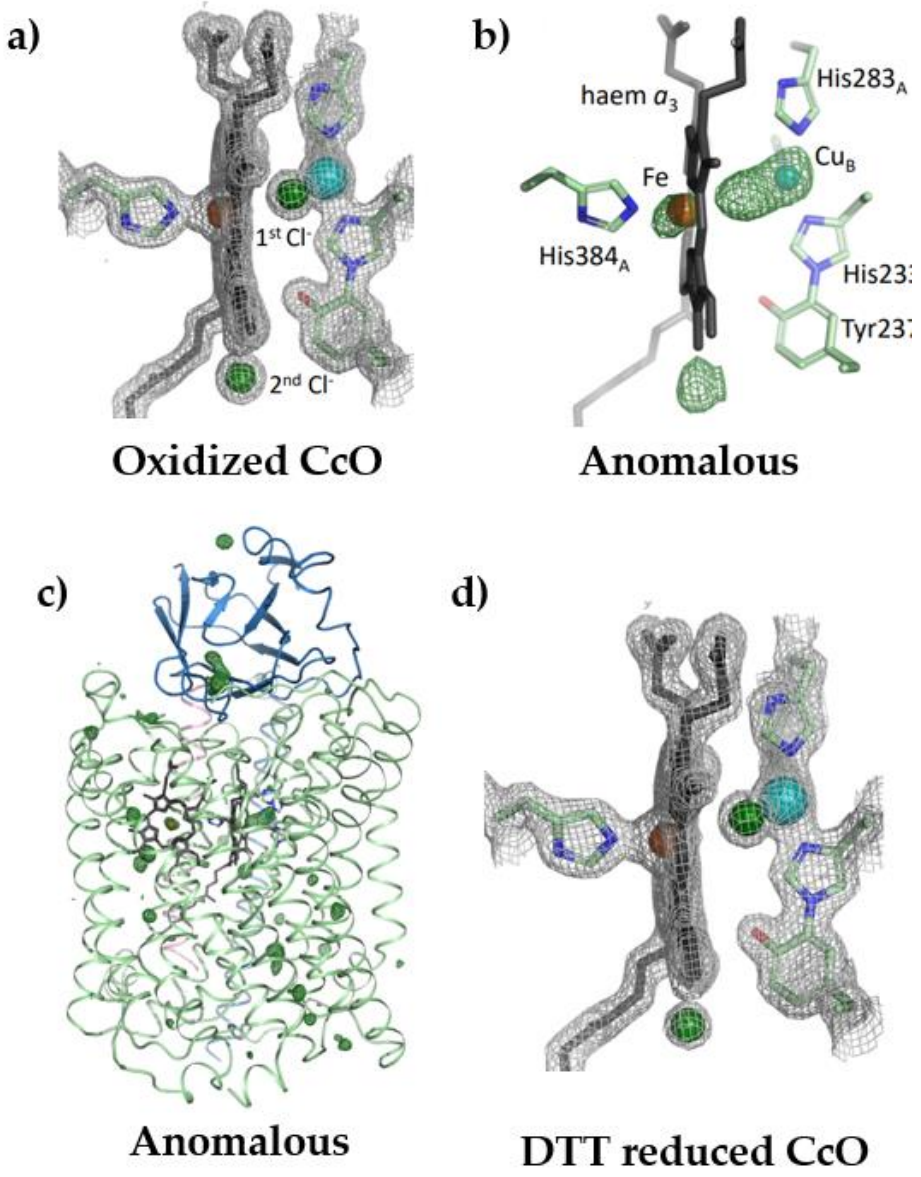

Figure 24. a) Refined $2F_{obs}$-F_{calc} electron density map for the BNC for CcO in the oxidized state. This SFX structure was resolved to a resolution of 1.7 Å. **b)** F_{obs}(hkl)-F_{obs}(-h-k-l) Bijvoet difference Fourier electron density map of oxidized CcO revealing a difference anomalous signal in the BNC on Cu_B and heme a_3, and two chloride ions. **c)** A long-distance overview of the anomalous map for oxidized CcO. **d)** Refined $2F_{obs}$-F_{calc} electron density map for the BNC for DTT reduced CcO at a resolution of 1.8 Å.

The DTT reduced structure (**Figure *24*d**) also contained additional electron density in the BNC which could not be explained by ligation by a single oxygen species. This is most certainly also a chloride considering that it is of similar intensity and occupies the same position as the chloride in the oxidized structure, but this has not been confirmed by anomalous diffraction. This was unexpected considering the overwhelming CcO literature supporting an empty BNC in the reduced state of the enzyme.[65,166] It is thus expected that the enzyme was not reduced to 100 % by treatment with DTT under these conditions in crystals as opposed to solution where full reduction seems to occur, at least as far as the absorbance spectroscopy can prove. A more detailed discussion regarding the extent of the reduction by DTT in crystals is found in the manuscript for **Paper II**. In addition to this there is also a thorough discussion relating to other structural changes that arise upon DTT reduction which are outside the scope of this thesis where the time-dependent changes are in the spotlight.

TR-SFX data of DTT reduced CcO together with the oxygen photocage **HPBC 1** upon exposure to a 355 nm laser pulse with the following time-delays; 100 μs, 1 ms, 10 ms and 30 ms was collected. For the 100 μs and 1 ms data an alternating cycle of light, dark1 and dark2 (**Figure *12***, collection scheme A) data collection scheme was used. The same was not possible for the following 10 and 30 ms time points due to technical problems related to the experimental setup on site. To collect the 10 and 30 ms time point, the laser was offset and the jet was illuminated upstream of the X-rays, which prevented the alternating dark/light data accusation cycle (**Figure *12***, collection scheme D). As a consequence of this, no internal dark reference was collected for the 10 and 30 ms time points from the same sample. In hindsight, the sensible thing to do** would have been to collect half light and dark on the same sample reservoir for reasons that will become apparent later.

The 100 μs and 1 ms time points shows no significant difference in the F_o-F_o compared to the internal dark references (Extended data figure 4 in the supplementary information for **Paper III**). This means that no observable change occurred following the laser activation and subsequent release of oxygen. The 10 ms time point showed striking differences compared to the non-illuminated reference consisting of caged oxygen **HPBC 1** and DTT reduced CcO (**Figure *25*, left**) This was initially thought to be a very convincing time-resolved signal, showing strong electron density differences at the BNC, and near the proton channel that decreases upon liberation of oxygen. In the 30 ms time point, the density in the BNC is again present and the strong negative density in the BNC shows a reduction in intensity (**Figure *25***). The interpretation at that time was that the shorter time points simply did not allow for sufficient time for oxygen diffusion following release from the photocage. The chemical interpretation of the BNC in the 10 ms time point was that we possibly captured the activated oxidized state of the enzyme, after reaching the end point of the chemical reduction of oxygen. The subsequent 30 ms time point showed increased density in the BNC, which we attributed to a potentially slower rebinding of the chloride ion (**Figure *25***).

** *It is worth noting that XFEL experiments are chaotic of nature. Too often, strategic decisions regarding data collection and details of an experiments have to be made in the middle of the night as was the case with this experiment.*

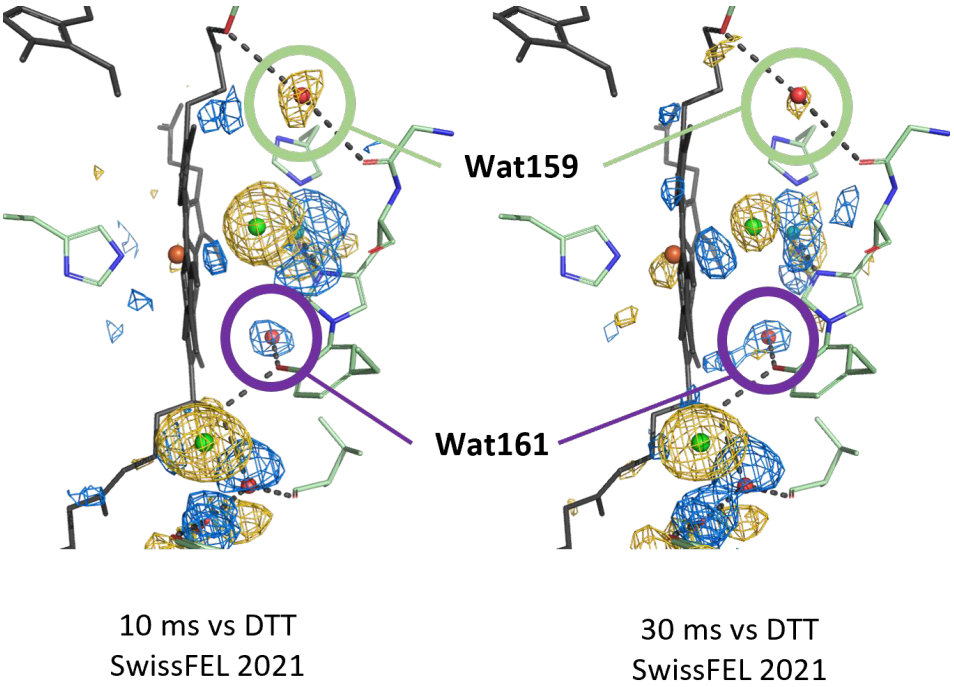

Figure 25. Left) F_{obs}(DTT reduced CcO + photocage + light) - F_{obs}(DTT reduced CcO) isomorphous difference Fourier electron density map showing electron density changes at the BNC 10 ms after light activation of the photocage. **Right)** F_{obs}(DTT reduced CcO + photocage + light) - F_{obs}(DTT reduced CcO) isomorphous difference Fourier electron density map showing electron density changes at the BNC 30 ms after light activation of the photocage. Maps are contoured at ± 3.2 σ (where σ is the root mean square electron density in the unit cell) with gold positive density and blue negative density.

The well-ordered chloride in the proposed proton transfer pathway to the BNC was an interesting discovery that could have implications related to the proton transfer mechanism. In order to supply protons for the oxygen reduction process, the protons need to reach the BNC. This is thought to occur via the K-channel analogue via proton transfer mediated by several protonatable amino acids and structurally conserved waters in this region of the protein, shown in **Figure *26***. This network of hydrogen bonds connects protonatable residues from the outside of the protein to the BNC with the longest distance of 4 Å between Tyr_{248} and Thr_{312} where a conformational change is proposed to mediate efficient proton transfer between these residues.[167]

Proposed proton transfer connectivity to the BNC via the K-channel analogue

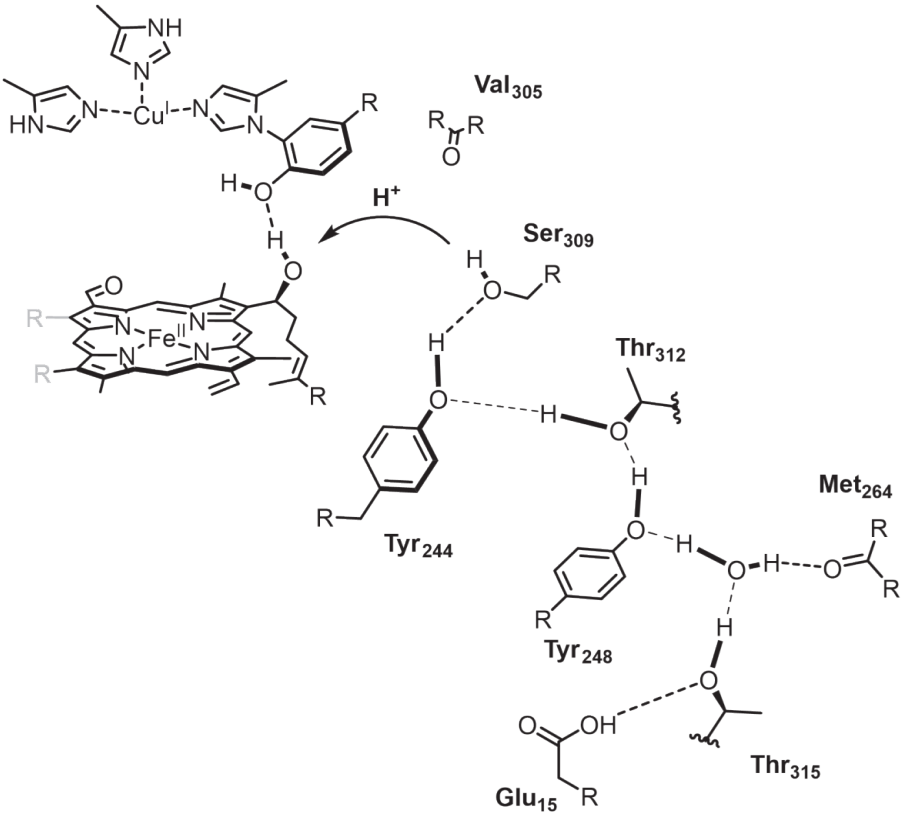

Figure 26. The proposed proton transfer route to the BNC via the K-channel analogue mediated by a network of protonatable amino acids and structurally conserved waters within the channel.

The chloride is found in a position that likely disrupts the network illustrated in **Figure 27**, which might prevent efficient proton transfer to the BNC. The water which is typically able to make efficient hydrogen bond interactions with residues connected to the BNC instead occupies a position slightly further away from the BNC. The chloride would not be able to efficiently support a hydrogen bonding interaction with the hydrogen of the farnesyl oxygen facing out from the BNC, potentially breaking the network required for efficient proton transfer. Considering the high concentration of chloride ions in the crystallization conditions, it is a fair to question whether this could be a "naturally occurring" effect in the enzyme. The host system for the enzyme, *Thermus thermophilus*, was originally discovered around a thermal vent in salt-water.[168] One can speculate that if chloride occupying this position was detrimental to its function, then nature perhaps would have found a way to circumvent it. Considering the prevalence and importance of chloride in biological systems

it would be strange if it had a directly poisonous effect on the enzyme.[169] We reason that any species capable of adopting and blocking this position could perhaps be related to a mechanism for preventing back leakage of protons from the BNC. During conditions of repeating turnover of the enzyme one could speculate that something reminiscent of this type of rebinding/reorganization would not have time to occur prior to the initiation of the next reaction cycle. Then, upon stagnation of the reaction, the coordination of an endogenous ligand could break the proton connectivity in the network. Such an active/inactive network of hydrogen bonding could be reminiscent of the active and inactive $\mathbf{O_H}$ and **O** states of CcO. Although, it is not clear at this time if this is correlated or just a coincidence.

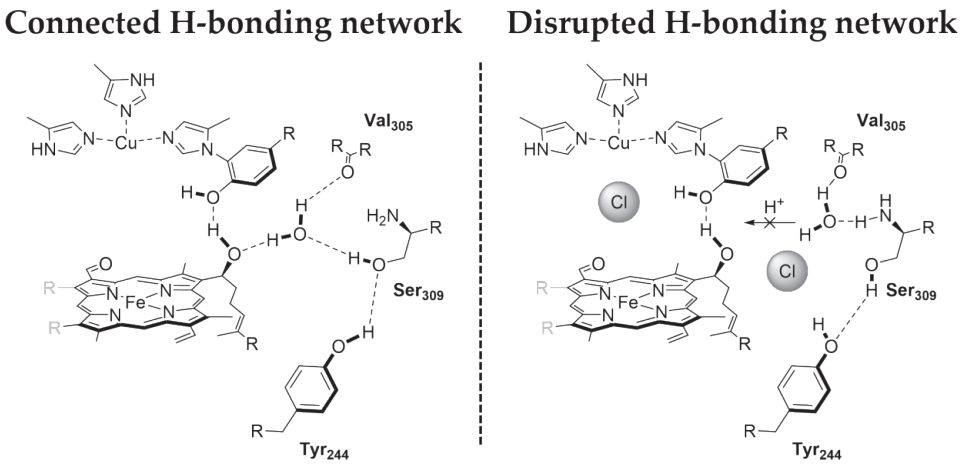

Figure 27. Left) *Reduced CcO*: The proposed proton transfer pathway in the reduced state of the enzyme which has a connected network of hydrogen bonds to the BNC. This is mediated by a conserved water molecule in a strategic position near the BNC. **Right)** *Oxidized CcO:* The chloride in the channel potentially disrupts the proton transfer channel in the oxidized resting state of the enzyme.

2.2.2 TR-SFX STUDIES OF CCO AT LCLS 2022

Since the data collected at this time did not contain any active intermediates in the catalytic reaction, we conducted another XFEL experiment at LCLS with the goal to capture time points between 1 and 10 ms, we decided on ~ 3.3 ms. A reference structures for the reduced enzyme was recollected employing a more efficient reductant, dithiobutylamine (DTBA) which is an analogue of DTT with similar redox potential but is more efficient at low pH due to a decreased pKa compared to DTT (**Figure *28*, right**).[170] This was promoted by the previous observation of residual electron density for the DTT reduced structure in the BNC reminiscent of a chloride (**Figure *28*, left**). The decreased reduction efficiency of DTT at pH 5.3 was suspected to not generate full population of the reduced state in the previous experiment and instead DTBA was used. Additionally, for the LCLS experiment we had improved the crystal spectroscopy setup significantly which allowed us to confirm that the expected reduced state had been achieved prior to data collection (Extended data figure 2J in

the supplementary information for **Paper II**). The structure of the DTBA reduced CcO was resolved to a resolution of 2.3 Å, which showed a mostly empty BNC, again suggesting that the DTT reduced structure was likely not fully reduced as previously thought.

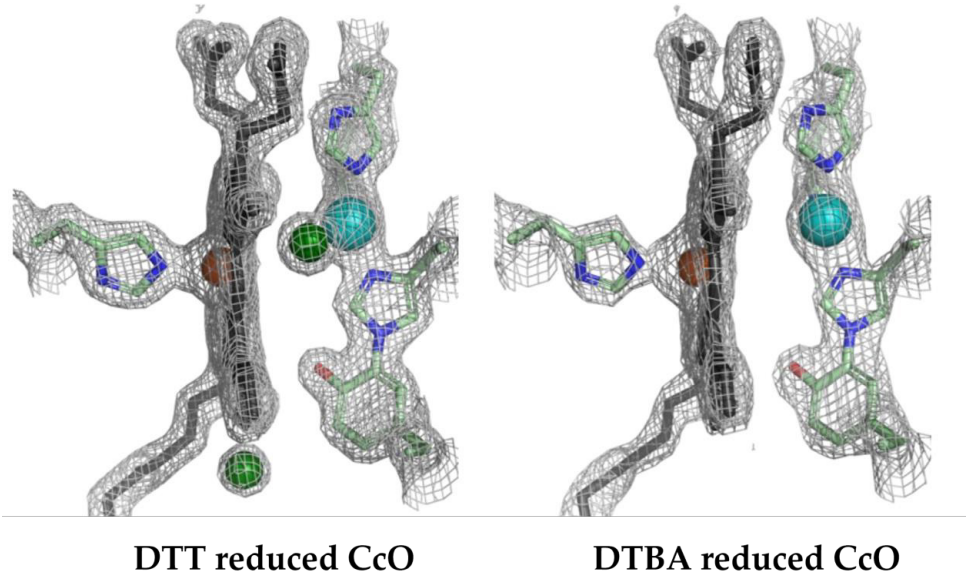

Figure 28. Left) Refined $2F_{obs}$-F_{calc} electron density map for the BNC for DTT reduced CcO at a resolution of 1.8 Å collected at SwissFEL 2021. **Right)** Refined $2F_{obs}$-F_{calc} electron density map for the BNC for DTBA reduced CcO at a resolution of around 2.3 Å showing an empty active site collected at LCLS 2022.

The full extent of the differences in the DTT reduction kinetics in microcrystals were not fully realized at the time prior to the first SFX experiment at SwissFEL 2021. The previous spectroscopic validations in **Paper I** had utilized crystals of smaller dimensions (~6 μm) that likely reduced more rapidly than those employed in the SFX study at SwissFEL (~15 μm). This resulted in the starting state for the time resolved studies to be an equilibrium between reduced and oxidized CcO that was more shifted towards the oxidized side than expected. This is evident by the difference map from DTT reduced CcO against the DTT reduced CcO with photocaged added (**Figure *29*, right**). A difference map calculated by subtracting oxidized CcO from DTT reduced CcO showed differences indicating that it is indeed reduced to a certain extent upon treatment with DTT as expected (**Figure *29*, left**). However, it was evident that the DTT reduced reference and the DTT reduced CcO with photocage added were not identical which would have been the ideal scenario since that would have meant that there were no changes upon addition of the photocage to the dark state of the enzyme.

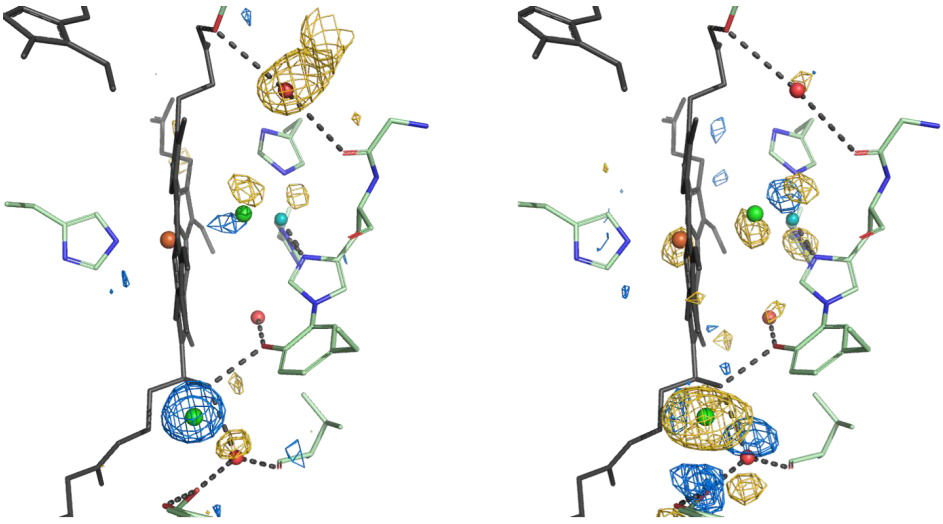

Figure 29. Left) F_{obs}(DTT reduced CcO) - F_{obs}(Oxidized CcO) isomorphous difference Fourier electron density map showing the changes in electron density upon reduction by DTT. **Right)** F_{obs}(DTT reduced CcO+ photocage) - F_{obs}(DTT reduced CcO) isomorphous difference Fourier electron density map showing electron density changes at the BNC when the photocage is added to microcrystals and the enzyme slowly turns-over due to the slow leakage of oxygen from **HPBC 1**. Maps are contoured at ± 3.2 σ with gold positive density and blue negative density.

Similar time-resolved experiments were attempted at LCLS, initially attempting to reproduce the 10 ms and 30 ms time points obtained at SwissFEL 2021 and also to obtain shorter time points around 3.3 ms. There were several technical issues with the laser illumination setup which resulted in a comedically large laser spotsize which we compensated for by running the laser at the maximum power setting. Initial difference maps did not show any significant time-resolved signals when comparing the combined dark data versus the light, but the importance of separating these were not realized until much later which will be addressed in the future perspective part of the thesis.

2.2.3 TR-SFX STUDIES OF CCO AT SWISFELL 2023

The confirmation that the fully reduced state most likely should have an empty BNC upon achieving complete reduction prompted the question regarding the extent of reduction of the sample used in the time-resolved data from SwissFEL 2021. Digging into the logbook from the 2021 experiment revealed that the 10 ms data is derived from a sample that was delayed by approximately 2 hours in between preparation and collection on the sample compared to the average of other samples. This would typically not be a problem but the fact that we were unable to collect the data with an alternating dark/light collection scheme made things more complicated. The consequence of this is that we have no internal reference for the 10 ms data. Since this sample was incubated with the reductant for a longer time, we

cannot rule out that some of the observed differences could be derived from a more reduced enzyme. A more reduced sample would also show the disappearance of the density associated with the chloride which is the most prominent difference in the 10 ms time point. Therefore, we aimed to replicate this in the subsequent SwissFEL TR-SFX experiment in 2023.

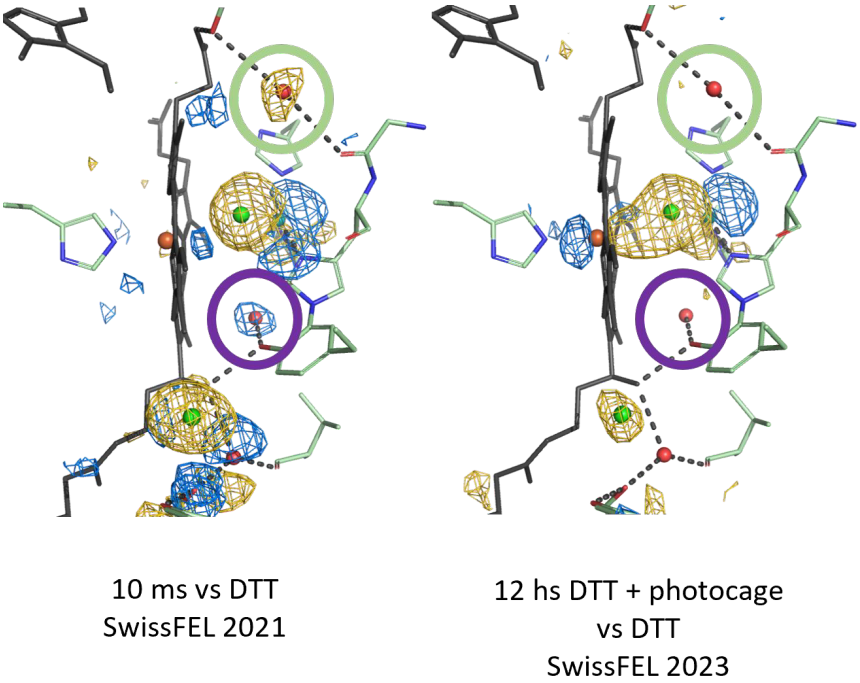

Figure 30. **Left)** F_{obs}(DTT reduced CcO + photocage) - F_{obs}(DTT reduced CcO) isomorphous difference Fourier electron density map showing electron density changes at the BNC 10 ms after light activation of the photocage. **Right)** F_{obs}(DTT reduced CcO + photocage after 12 h incubation) - F_{obs}(DTT reduced CcO from the 2023 SwissFEL experiment) isomorphous difference Fourier electron density map showing electron density changes at the BNC. Note that this is not a time-resolved structure as opposed to the 10 ms map. Both maps are contoured at ± 3.2 σ with gold positive density and blue negative density.

In addition to collecting a new oxidized reference structure and DTT/DTBA reduced references, we also collected data on a sample where DTT reduced CcO + caged oxygen **HPBC 1** were incubated for 12 h prior to data collection. The same sample in the same reservoir was used to collect the static structure of DTT + caged oxygen **HPBC 1** shortly after the addition of the photocage and then again 12 hours later. The obtained difference maps support the hypothesis that parts of the observed difference signals in the 2021 SwissFEL data (10 ms and 30 ms time points) could be attributed to the sample achieving a higher degree of reduction prior to data collection. Both difference maps; the 10 ms and the 12 h DTT + photocage incubated sample, show the loss of the BNC chloride ligand (**Figure *30***). This was obviously a bit disappointing since it meant that the strongest features observed in the difference maps for the 10 ms was not a true time resolved signal as originally thought.

Furthermore, since the one large difference between the 10 and 30 ms time points is related to the density associated with the chlorides it is not clear that the 10 ms and 30 ms time point are chemically distinguishable.

2.2.4 INTREPETATION OF COMPLICATED DATA – WHERE DOES THIS LEAVE US?

Following numerous control experiments, a more systematic approach was required in order to separate the changes in electron density that arise from the changes in reduction level and the potential signals from enzymatic turnover following the UV-pulse. In the manuscript for **Paper II** there is a more through discussions about the results of a polder electron density map quantification. Upon closer examination, two regions in the vicinity of the active site suggests that there is still evidence for some enzymatic turnover during the 10 ms time point collected at SwissFEL 2021. The first region (green circle in **Figure *30***) is poorly resolved in most structures which could be interpretated as either a disordered water molecule or even a chain of water molecules. In the DTBA reduced structure of CcO this region has more electron density, suggesting that the reduced state has a higher population of this somewhat poorly resolved species, in **Paper II** we refer to this as **Wat159**. Hence, one change in the electron density in the 10 ms difference map is not consistent with the sample being more reduced over time. In the 10 ms difference map this feature becomes weaker (difference density minimum = -4.5 σ for Δt = 10 ms, and -3.6 σ for Δt = 30 ms) following the UV-pulse. This suggests that there might be a smaller population of the reduced enzyme being turned over following the oxygen release from the laser activation.

There is one additional piece of evidence that suggests a time resolved signal in the 10 ms difference map. In the DTBA and DTT reduced reference structures there is no significant electron density in the region within hydrogen bonding distance to the crossed-linked tyrosine in the BNC. In the 10 ms difference map there is a negative feature (purple circle, **Figure *30***) which means that there is a feature that arises upon light illumination and liberation of oxygen. In **Paper II** this is interpreted as a water that is referred to as **Wat161** (with difference density maxima = 4.9 σ for Δt = 10 ms). This is a further indication that there is another population of the enzyme within the observed electron density that in not a function of either the oxidized or the reduced enzyme alone. Considering that both these new densities are close to the BNC they are very interesting as they could be involved in the actual proton pumping chemistry, although we did not manage to capture these features live. Arguably, a 10 ms time delay is too long to observe any active reaction intermediates from the reaction cycle. It is therefore more likely that what is observed in the 10 ms structure is an activated state of the enzyme.

It should be mentioned that the density shown in the purple circle associated to **Wat161** in **Figure *30*** has been previously observed in the mixing SFX study between CcO and an oxygenated buffer by the Rousseau group eight seconds after mixing where an intermediate structure was proposed at a 2.5 Å resolution.[158] Due to the position in appropriate hydrogen bond distance to the cross-linked redox active tyrosine, it is likely that this water is involved in the redox reaction to reduce oxygen to water by mediating efficient proton transfer

connectivity in addition to perhaps modulating the pKa of the tyrosine by hydrogen bond interactions. The second transient feature of the difference maps obtained is the elongated density observed in the green circle in **Figure 30**, modelled as **Wat 159,** is in close proximity to a nearby glycine residue. A water in this region has been observed in previous time-resolved SFX studies of CcO during conditions of CO-dislocation.[157]

Additionally, attempts were made at SwissFEL 2023 to reproduce previous the time-resolved signals but the experiment suffered from multiple technical and chemical complications. Inconsistency in the reduction kinetics in the sample which made it difficult to reliably reproducibly the correct starting state of the enzyme in conjunction with the fact that our starting state is a steady state equilibrium between the oxidized and reduced enzyme with varying proportions evolving over time, further complicates things as it makes it difficult to reproduce the exact same sample consistently. Additionally, we encountered issues with contamination from unknown ligands in the BNC, which potentially hindered the enzymes activity by blocking the turnover process after oxygen release or alternatively affected the reduction level of the enzyme. In addition to this we experienced issues with running the sample jet which did not provide a stable flow, impacting any temporal resolution of the experiment since the flowrate inherently influences the relative interactions between the laser and X-ray probe.

It is apparent at this stage that the results ended up being more nuanced than what was initially though upon being woken up in the middle of the night on the fourth night of a five day long continuous beamtime. Woken up to observe a clear light induced large structural change in the difference map on the big screen. Since that night the changes that we can associate to a potential effect of the photo-released oxygen has decreased with each refinement and subsequent control experiment. Still, at the end of the day there are remaining differences in the electron density that are best explained by a small population of the enzyme being turned over by oxygen following laser activation.

Our work highlights the numerous challenges that TR-SFX faces with regard to substrate-based proteins. Some are of technical nature, as advances in rapid mixing could have allowed for the use of a more potent reducing agent whilst not giving it sufficient time to completely degrade the photocage. Others are inherent to the system of study, such as CcO which proved to us that the fact that an enzyme has been studied over multiple decades does not mean that it does not still have aces up its sleeves. The remaining difference signals for the 10 ms time point from SwissFEL 2021 after subtracting the changes associated with the higher degree of reduction and subsequent loss in the chloride densities suggests that a sub-population of the enzyme likely did react upon release of oxygen. This suggests the presence of transient water species which reorganize at different redox states of the enzyme during the catalytic cycle to potentially facilitate efficient proton transfer in the enzyme. We were able to conclude the presence of chlorides in the BNC and in the close vicinity of the BNC in the oxidized state in the enzyme and provide a framework for future TR-SFX studies with oxygen photocages. Since then, we have accumulated further evidence of TR-SFX enzymatic turnover with this protocol which is briefly summarized in the future perspective section of this thesis.

2.3 PAPER III – SINGLET OXYGEN GELS

The work summarized in **Paper III** relates to a slightly different type of caged compound. It is fair to say that it is still a photocage since the chemical payload can indeed be liberated by light excitation. However, the end products in this work are not typical photocages that one might employ for time-resolved biochemical studies. There is no obvious reason for why this type of functionalized gel could not be used for such studies later on, where the photocage is covalently attached to a gel. "Hydrogels" are already incorporated into many crystallography experiments, comprising the viscous matrix used for sample delivery and crystallization.[171,172] We decided to pitch in by providing the first example of a gel capable of releasing the substrate, in a spatiotemporal manor by external stimuli. One might be tempted to hope at this point in this thesis that we would solve the problems associated with oxygen photocages in **Paper I** and **Paper II**, by providing a new compound able to bind and release oxygen. Unfortunately, no. The nature of oxygen in the triplet ground state as previously discussed severely limits the options to bind and release it in a controlled way. The same cannot be said for its more energetic cousin, singlet oxygen. $^1O_2$ exhibits versatile chemical reactivity towards many motifs in organic chemistry and one particular reaction caught our eye. The reversible [4+2] cycloaddition to acenes. We envisioned that by incorporating such a $^1O_2$ binding motif in a LMWG it would produce a novel functional material. The question that might arise is; why is it desirable to release singlet oxygen from a stationary material? The necessity of such material is motivated since these materials are being pursued in cancer research related to PDT. Many strategies have been pursued to release singlet oxygen from a stationary material derived from gold nanorods[173], covalent organic polymers,[52,174] and nanoparticles[53]. There, the organic endoperoxide is exposed to high temperatures or strong IR irradiation to trigger the release of $^1O_2$. Recent effort has also looked into the *in situ* modification of organic endoperoxides to release $^1O_2$ under biologically relevant conditions and temperatures by chemical[54] and biochemical trigger[55]. Although our materials are far from direct implementation towards application such as PDT, we provide an important proof of concept for the feasibility of utilizing a gel for the direct spatiotemporal release of $^1O_2$ by external stimuli.

2.3.1 SYNTHESIS OF GELATORS TO BIND AND RELEASE SINGLET OXYGEN

The rationale behind the selection of the OTHO framework was mainly due to its synthetic versatility, in addition to the presence of an internal OTHO expert in-house. We envisioned that numerous compounds would need to be tested and evaluated prior to finding compounds with suitable properties as both gelators and efficient releasers of $^1O_2$. The multicomponent OTHO reaction (**Scheme 9b**) thus served as real workhorse in **Paper III**.

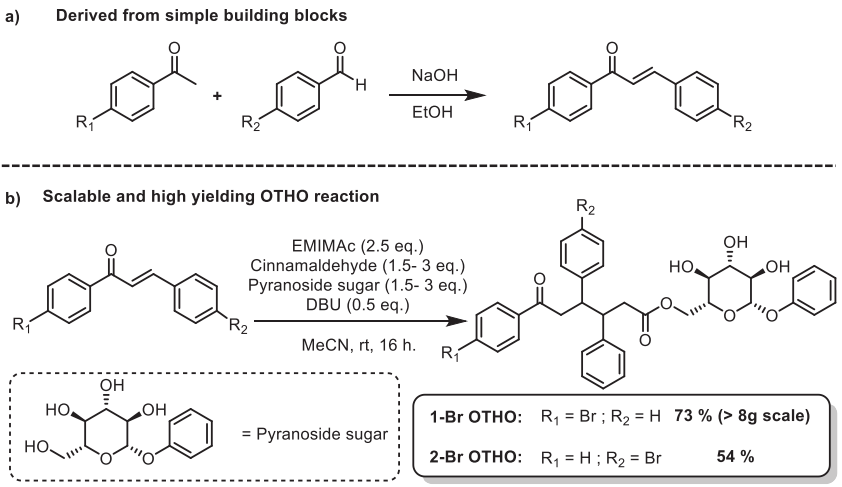

Scheme 9. a) Condensation reaction to form various chalcones to be used in the subsequent OTHO reaction. **b)** The OTHO reaction yielding the two brominated OTHOs.

The starting materials for the OTHO reaction are easily accessed via a conventional condensation reaction between any aromatic aldehyde and acetophenone as shown in ***Scheme 9*a**. This provided easy access to chalcones that could be used directly in the OTHO forming reaction which provided access to brominated **1-Br** and **2-Br** OTHOs (***Scheme 9*b**). The oxygen carrier motif could be easily introduced via conventional palladium cross coupling chemistry from the brominated OTHOs. We selected phenyl substituted anthracenes as the oxygen carrier motif for two main reasons. One is the high yield of singlet oxygen release and two; the tunability over the oxygen release rate upon chemical modification of the phenyl substituent. This was envisioned to allow for two distinct modes of activation for $^1O_2$ release. Mode one would rely on photochemical excitation and subsequent release upon UV-light irradiation. The second mode would be tailored to allow for a thermally induced release at temperatures relevant for biochemical applications. Phenyl and pyridine substituents on the anthracene were anticipated to allow for photochemical activation and a phenylacetylene substituent was expected to be suitable for thermal activation. A more thorough examination of the reasoning behind the selection of the oxygen carrier motif and the various activation methods employed in this study can be found in the manuscript for **Paper III**. Synthesis of these OTHOs were relatively straight forward. **OTHO 1** and **3** were accessed through synthesis of the corresponding boronic ester OTHO by a Miyaura Borylation and subsequent palladium coupling with brominated anthracene (***Scheme 10***).

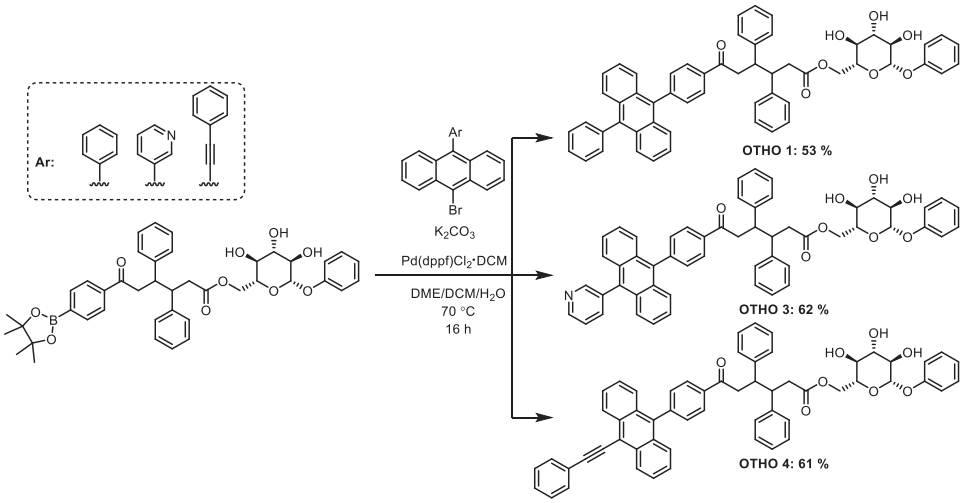

Scheme 10. Final Suzuki coupling to yield target OTHOs 1, 3 and 4.

Phenyl acetylene substituted **OTHO 4** was accessed by iodination of 9-bromoanthracene followed by a Sonogashira cross coupling to yield the phenylacetylene substituted bromoanthracene. This was coupled with **1-Br-OTHO** via a typical Suzuki cross coupling to yield **OTHO 4**. OTHOs **2** and **5** were synthesized at a later stage for reasons that will become evident later via **2-Br-OTHO** by a similar procedure but utilizing a boronic ester anthracene coupling partner and a brominated OTHO precursor (**Scheme *11***).

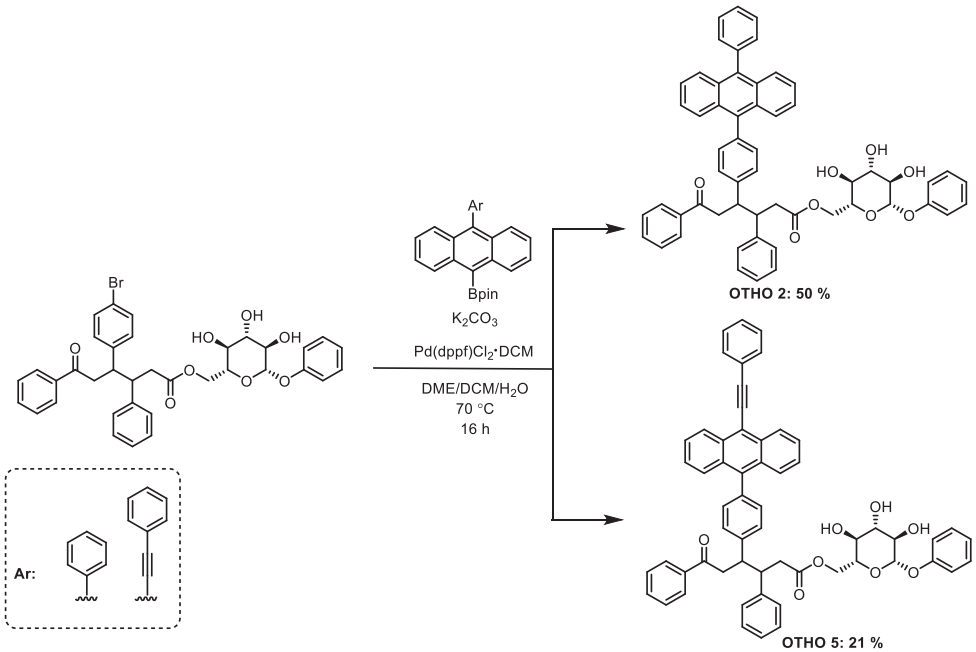

Scheme 11. Final Suzuki coupling to yield target OTHOs **2** and **5**.

Following the synthesis of **OTHOs 1-5,** the corresponding endoperoxides were synthesized via a [4+2] cycloaddition between the anthracene OTHOs **1**-**5** and photochemically generated singlet oxygen. This resulted in excellent yields (78 – 95 %) of the corresponding endoperoxide OTHOs **1-O₂** - **5-O₂** following a quick filtration through silica to remove the remaining photosensitizer and evaporation of the solvent (**Scheme *12***).

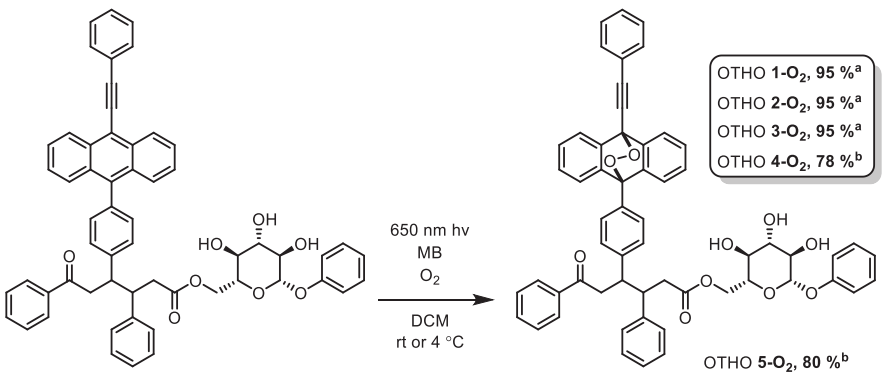

Scheme 12. Synthesis of the final endoperoxide OTHOs **1-O₂** to **5-O₂** from OTHOs **1**-**5** by treatment of methylene blue (MB), red light illumination and oxygen gas sparging. The synthesis of **OTHO 5-O₂** is shown as an example. [a]Synthesis was carried out at room temperature. [b]Reaction mixture was cooled to 4 °C with a cold finger submerged into the reaction mixture.

2.3.2 INVESTIGATION OF THE GELATION PROPERTIES

Our initial efforts were directed towards OTHOs with the oxygen carrier motif attached to the -Ar_1 position and thus the gelation investigation was initiated with OTHOs **1**,**3** and **4**. The inverted vial test was used as to confirm if the crude definition of a gel could be satisfied. A range of solvents were investigated but the best gelation was achieved with toluene which was used to determine the minimum gelation concentrations (MGC). **OTHO 1** and **1-O_2** efficiently formed gels at 1 mg/ml in toluene (Table 2, Entry 1). Furthermore, the gels obtained were completely transparent which is important for efficient penetration of light for photoactivation. *m*-Pyridine substituted **OTHO 3** showed an interesting property in toluene. The endoperoxide **3-O_2** was able to form a gel at 1.4 mg/ml concentration but the precursor anthracene did not form a gel even at concentration exceeding 10 mg/ml. (Table 2, Entry 3) We imagine that this peculiar property potentially could be exploited to destabilize the gel matrix by transitioning from the endoperoxide to the anthracene.

Table 2. Gelation properties for **OTHOs 1-5** and **1-O_2** – **5-O_2** in toluene. For more information regarding the gelation in other solvents, see Table 1 in the manuscript for **Paper III**.

Entry	OTHO	Toluene (5 mg/ml)	Minimum gelation concentration[a] (mg/ml)
1	**1**	**G**	1
	1-O_2	**G**	1
2	**2**	**G**	1
	2-O_2	**G**	1.4
3	**3**	P	P
	3-O_2	**G**	1.4
4	**4**	**G**	10
	4-O_2	**G**	2.2
5	**5**	**G**	2
	5-O_2	**G**	2.8

G = Gel, **P** = Precipitate. Minimum required gelation concentration was determined by the inverted vial test where the concentration was decreased until the gel could no longer support its own weight in toluene.

Phenylacetylene substituted **OTHO 4** suffered from inconsistent gelation. Sometimes a gel could be obtained at 10 mg/ml and sometimes not, seemingly depending on the weather that day. The corresponding endoperoxide **OTHO 4-O_2** did provide facile gelation at 2.2 mg/ml (Table 2, Entry 4). The MGC for **OTHO 4** was deemed too high. Therefore, we sought to improve the gelation properties of **OTHO 4**. The OTHO framework fortunately provides several chemical handles for the incorporation of the anthracene. The -Ar_1 and -Ar_2 positions being the most easily accessible, we opted to attach the oxygen-binding motif on the -Ar_2

position to assess its effect on gelation. Hence, **OTHOs 2** and **5** were synthesized and their gelation properties were investigated. First, **OTHO 2** was evaluated which caused some concerns since there was no obvious improvement in gelation properties compared to **OTHO 1**. However, we reasoned that any potential difference might not be apparent since **OTHO 1** was already a potent gelator. Fortunately, we decided to still pursue the synthesis of **OTHO 5** only based on the general crude observation that **OTHO 2** seemed to form gels a bit faster than **OTHO 1**. This resulted in a five-fold decrease in the MGC for **OTHO 5** although the corresponding endoperoxide **OTHO 5-O$_2$** exhibited a slight increase in MGC compared to **4-O$_2$**, increasing from 2.2 mg/ml to 2.8 mg/ml (Table 2, Entry 5). The rheological properties of **OTHO 5** and **5-O$_2$** were investigated in greater detail by dynamic shear oscillation where the storage modulus (G′) and loss modulus (G″) were obtained as a function of the strain and frequency. Frequency sweeps revealed that the gels were mostly independent in the high frequency domain and less so in the lower region. **OTHO 5-O$_2$** showed less frequency independent characteristics compared to **5**, which suggests that in **OTHO 5-O$_2$**, the endoperoxide does destabilize the gel matrix to some extent compared to **OTHO 5**. A more thorough discussion of the rheological properties can be found in the manuscript for **Paper III**.

2.3.3 SPATIOTEMPORAL RELEASE OF SINGLET OXYGEN

Satisfied that we would be able to convince a material chemist that we at least satisfy the minimum criteria for achieving a gel type material, we investigated the oxygen release properties of the OTHO endoperoxides. The thermolytic properties of the OTHOs were found to correlate well with the corresponding diaryl substituted anthracenes, suggesting that the OTHO framework does not affect the oxygen carriers release properties. All endoperoxides were found to release $^1O_2$ and reform the corresponding anthracene OTHO upon heating to 90 °C in toluene and by UV light irradiation at 270 nm. The thermolytic and photochemical half-lives ($t_{1/2}$) were measured and are summarized in **Table 3**. Phenyl substituted **1-O$_2$** and **2-O$_2$** proved to have a thermal half-life close to the corresponding 9,10-diphenyl anthracene with $t_{1/2}$ of 9.5 h at 90 °C in toluene (**Table 3**, Entry 1-2). At 40 °C it showed only minor conversion following more than one week of heating and essentially no conversion was observed at 20 °C **(Table 3**, Entry 1-2). This satisfies the conditions for the photochemical activation which requires the endoperoxide to be stable unless triggered by photochemical stimuli. Pyridine substituted **3-O$_2$** also satisfies this condition but has a shorter thermal and photochemical $t_{1/2}$ than **1-O$_2$** and **2-O$_2$**, around 6 h at 90 °C in toluene (**Table 3**, Entry 3). **OTHO 4-O$_2$** and **5-O$_2$** were confirmed to satisfy the conditions for thermal activation. At biologically relevant temperatures (40 °C) we observe a thermal $t_{1/2}$ of 1.5 h (**Table 3**, Entry 4-5).

Table 3. Thermolysis and photolysis of 1-O_2 to **5-O_2** in toluene to form the corresponding anthracene OTHOs 1-5 as illustrated in the scheme below.

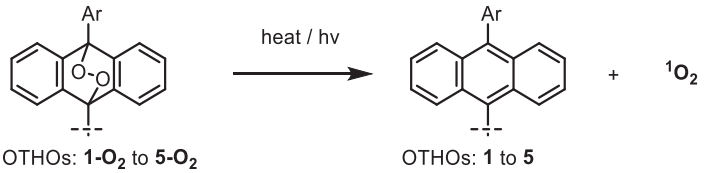

Entry	OTHOs	$t_{1/2}$[a] 90 °C	$t_{1/2}$[b] 40 °C	$t_{1/2}$[c] 270 nm
1	**1-O_2**	9.5 h 8 h[175]	> 1 week	~6 min
2	**2-O_2**	9.5 h 8 h[175]	> 1 week	~6 min
3	**3-O_2**	6 h 5 h[176]	> 1 week	~2.5 min
4	**4-O_2**	~5 min	1.5 h 5 h[177]	~1.5 min
5	**5-O_2**	~5 min	1.5 h 5 h[177]	~1.5 min

[a]Thermolytic half-life for endoperoxides **1-O_2** - **5-O_2** at 90 °C in toluene (~ 25 μM). Note that the reference values obtained from literature for OTHO **1**,**2** and **3** is taken from symmetrically aryl-substituted compounds. [b]Thermolytic half-life at 40 °C in toluene (~ 25 μM). [c]Photochemical half-life for **1-O_2** - **5-O_2** upon exposure to 270 nm light over several minutes (~ 25 μM).

Satisfied that both modes of activations had been realized, we carried on investigating the release in the gel phase since this work would be of little interest unless similar results could also be achieved in the gel phase. One potential point of failure we realized was if the gels would lose their structural integrity upon heating. If the temperature required to achieve efficient thermolysis of the endoperoxide exceeded the gels thermal tolerance, it would prevent the thermal activation mode completely. Thus, a gel comprised of **5-O_2** (5 mg/ml in toluene) was heated to 40 °C over several hours and the thermolysis was measured over time. In between each measurement we ensured that the gels structural integrity was maintained by completing the inverted vial test (**Figure *31*b**). Furthermore, it was possible to capture $^1O_2$ in the gel phase by gelating a solution of **OTHO 5-O_2** with a catalytic amount of MB and then exposing the gel to red light over 2 h, which shows the disappearance of the anthracene absorbance upon the formation of the endoperoxide (**Figure *31*a**). Full conversion back to **OTHO 5** was achieved after several hours and the measured thermal $t_{1/2}$ was similar to the $t_{1/2}$ measured in solution at the same temperature, suggesting that thermal properties are similar in the gel state.

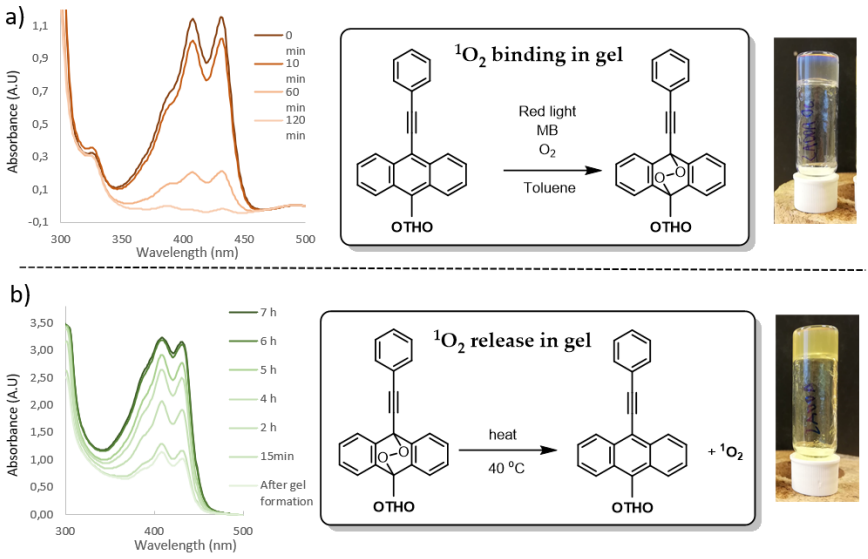

Figure 31. a) Absorbance spectrum showing the formation of OTHO **5-O₂** inside a gel matrix in the presence of methylene blue (MB) and red-light following saturation of the solution with oxygen gas and subsequent gelation. **b)** Thermolysis of OTHO **5-O₂** in the gel phase resulting in formation of OTHO **5** and release of **$^1O_2$**, the formation of **5** can be followed by the increase in the absorbance spectrum with peaks at 400 nm appearing as the anthracene is reformed.

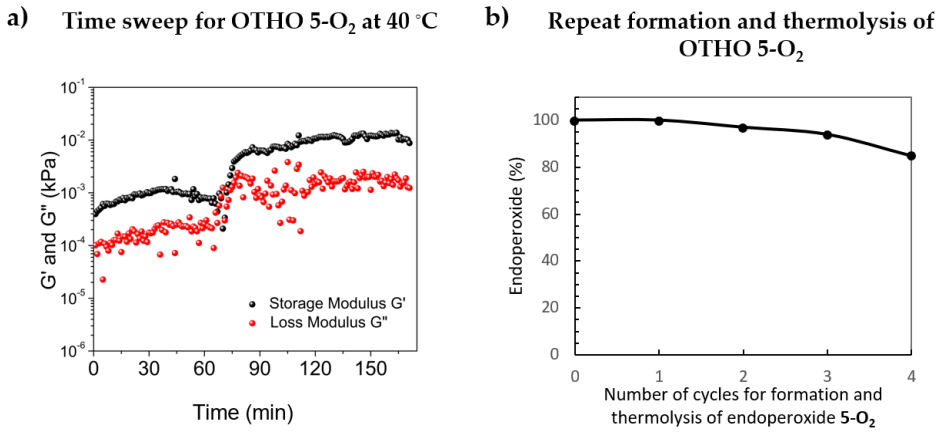

Figure 32. a) Rheology showing the time-sweep measurement of OTHO **5-O₂** as it was heated to 40 °C for over two hours. Shown is an increase in gel stiffness as it is heated which is indicative of transitioning from the endoperoxide to the anthracene OTHO. **b)** The repeat thermolysis and formation of OTHO **5-O₂** in toluene showing minor degradation upon several cycles. Measurement was performed in toluene and the thermolysis was carried out at 90 °C as opposed to 40 °C to save time.

The structural integrity was maintained throughout the full duration of the experiment. In order to investigate this in more detail we measured the rheological properties of the gel

during the thermolysis of OTHO **5-O₂** to **5** at 40 °C over 2 h. An increase in gel strength was observed as the gel was heated for over two hours, consistent with what would be expected for gels of more similar character to OTHO **5** (**Figure 32a**). It should still be pointed out that the absolute value for the strain sweep could also be affected to some degree by evaporation of solvent under the measurement due to the long experimental time. We also found that following full thermolysis of **5-O₂** to **5**, it was possible to reform the endoperoxide and repeat this four times without experiencing significant degradation of the OTHO (**Figure 32b**). Only about 20 % deterioration was observed upon four cycles which is consistent with a high yield of singlet oxygen release as opposed to degradation associated with O-O bond cleavage which results in formation of side products. In situ formation of **OTHO 5-O₂** was also investigated with fluorescent microscopy to visualize the spatial selectivity of $^1O_2$ binding.

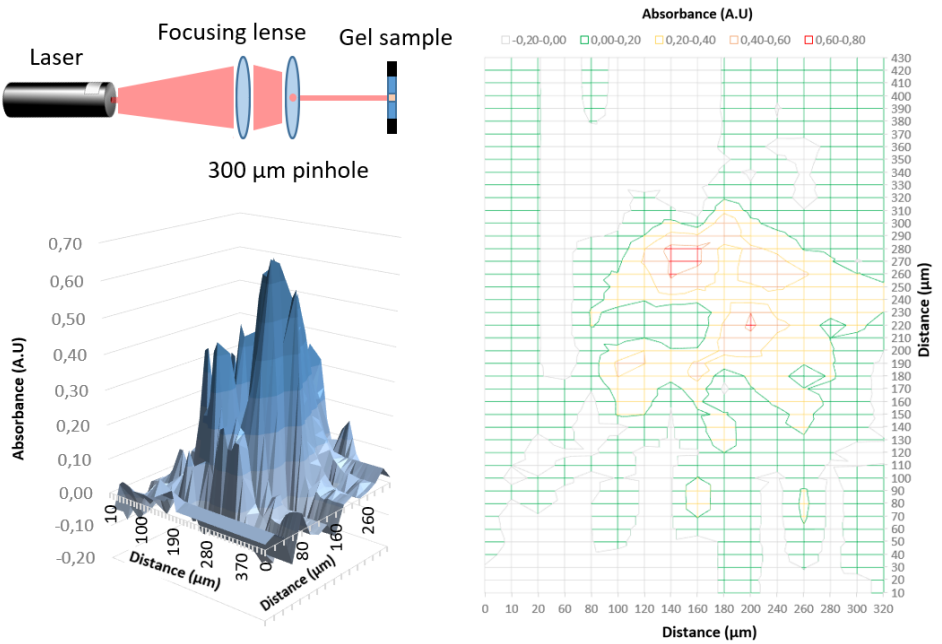

Figure 33. 2D-topogical map obtained by measuring the difference in absorbance before and after UV-light illumination of a gel of **2-O₂** (5 mg/ml in toluene).

A solution of **OTHO 5** (5 mg/ml) was saturated with oxygen gas and then gelated. Fluorescent microscopy was then used to monitor the fluorescence of anthracene as it decreased with formation of the endoperoxide following illumination with red light. The decrease in fluorescence was consistent with the time of irradiation (**Figure S36** in the supplementary information for **Paper III**). In order to investigate the spatial release of $^1O_2$ in the gel phase by photochemical stimuli we illuminated a gel consisting of **OTHO 2-O₂** with 320 nm light. Only the section of the gel that was illuminated shows significant release of $^1O_2$, judged by the increase in absorbance in the illuminated area. Furthermore, no detectible diffusion was observed within the gel matrix, suggesting that the gel is stationary under the

timescale and experimental conditions of the measurement. This is evident by the topological map obtained by scanning the illuminated area and measuring the absorbance before and after UV illumination (**Figure *33***). This is a very important feature for materials used in chemical writing applications and highlights the advantage of a covalently linked oxygen carrier to the gelator as opposed to an additive to the gel which will experience significant diffusion over time.

Taken together our work demonstrates the first spatiotemporal catch and release of $^1O_2$ in a gel matrix and both thermal and photochemical activation were demonstrated. Efforts are ongoing to develop hydrogels which are more biologically relevant which have similar properties to the gelators developed in this work.

2.4 PAPER IV – SOLUTION SCATTERING OF KCSA

The main finding of **Paper IV** is that a structural rearrangement can be induced by photochemically decreasing the pH with a photocaged acid in the presence of the pH responsive ion channel KcsA. This was observed with X-ray scattering studies at ESRF in three separate experiments between 2021 – 2023. In **Paper IV** we employ the photocaged acid "caged proton" to rapidly induce a pH dive which triggers a conformational change in KcsA.

2.4.1 PREPARATIONS FOR TR-XSS STUDIES OF KCSA

The ultimate objective of this project was to perform TR-XSS on KcsA to track structural changes following the decrease in pH by a photocage. The first step towards facilitating this was to synthesize the proton photocage and to verify that a sufficient decrease in pH was achievable upon light illumination under feasible experimental conditions. The first hurdle was to synthesize a sufficient amount of the photocage for testing. Previous synthetic protocols required anion exchange[90] and we decided to work around this. We found that it was possible to simply precipitate the alkylammonium intermediate to form the desired sodium salt. However, this suffered from very low yields.

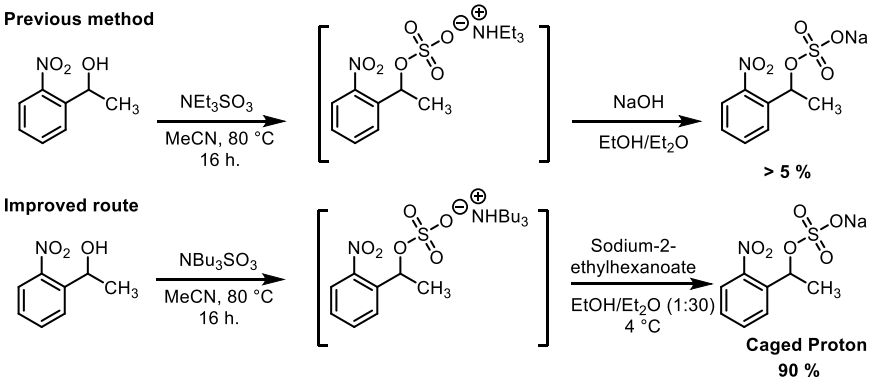

Scheme 13. Previous and current synthetic route for the gram scale production of the caged proton photocage.

This was salvaged by using a more efficient sulphonating reagent that had been shown to be more efficiently replaced via precipitation by a sodium ethyl hexanoate salt.[178] This improved the yield to 90 % (**Scheme *13***) and produced gram scale quantities without the need for any column chromatography. We could confirm that a solution of caged proton was acidified following illumination from a 385 nm LED by simply measuring the pH before and after with a pH meter. One challenge with this project was that we would have to design and bring our own illumination setup and associated delivery system to the first two synchrotron experiments. The absorbance of NPE type photocages is almost exclusively restricted to the UV region with only very minor absorbance above 400 nm. Due to the lack of readily available UV sources that could provide sufficient fluence at this wavelength, we hesitantly decided to employ several LEDs with a wavelength of 385 nm. We reasoned that since the NPE type photocage still does absorb light in this region and has a decent quantum yield (0.47 at 350 nm) a sufficient decrease in pH should still be achievable even when illuminated at a suboptimal wavelength given that sufficient light fluence was available.

Substantial efforts were directed toward optimizing the KcsA sample composition to minimize the buffering capacity of the solution since excessive buffering capacity would decrease the efficiency of the photoacid. We decided to start with a pH of 5.8 as this was close to the estimated pH where the conformational change was expected to occur. In addition to this, the presence of His-tags potentially adds an inherent buffering capacity to the protein itself. Hence, by starting at a pH closer to the pKa of histidine we expected the potential protonation of the His-tag to be less problematic. With the sample composition dialed in, we turned our attention to validating that the pH cage could provide the required decrease in pH under experimentally relevant flow conditions. Technical details about the X-ray pulse, flowrate and light have to be kept in mind for these types of experiments. The repetition rate of the X-ray beam and the pulse duration will influence the required flowrate as the sample needs to be replenished between each pulse as to avoid potential radiation damage to the sample. This sets a minimum required flowrate at which the light probe needs to activate the photocage, especially when suboptimal continuous LEDs are utilized as opposed to a high fluence pulsed laser.

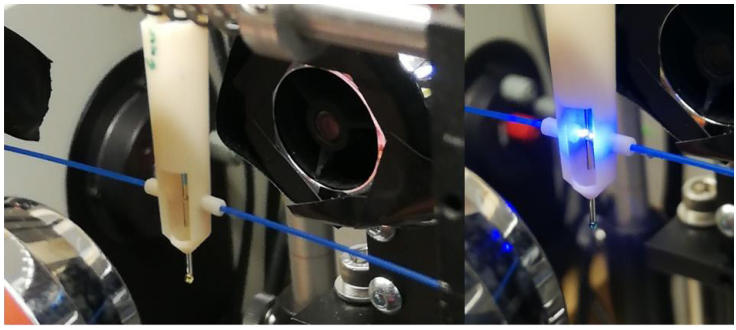

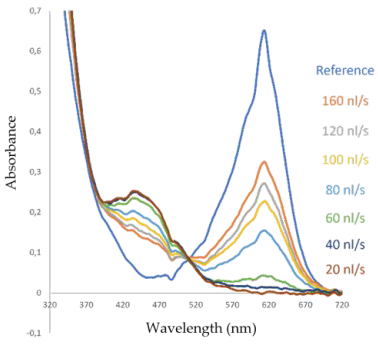

Flowrate (nl/s)	Estimated pH after light illumination
Reference	10
160	~ 5.2
120	~ 4.9
100	~ 4.7
80	~ 4.2
60	~ 3.5
40	~ 3.0
20	> 3.0

Figure 34. Top) The illumination setup for the validation of photoinduced decrease in pH upon photolysis of the pH cage. Note the color of the drop of sample that is coming out from the end of the capillary. The left image has a droplet with yellow color following illumination of the sample which shows that it is now acidic. The right image has a blue droplet which was captured just when the illumination was started and shows that the pH is > 6 (pH was 10) prior to illumination. **Bottom)** Photolysis of caged proton (25 mM) under flow conditions in the presence of bromocresol green (300 μM) to visualize and estimate the change in pH upon photolysis in a 600 μm capillary illuminated by two 385 nm LEDs (1000mA x 2).

Our 3D-printed custom build flow-cell system was used since we had previous experience with bringing this experimental setup to synchrotron facilities.[156] Bromocresol green, a pH indicator which is typically used between pH 3.5 – 6, was used to visualize the pH change and also act as a "proton buffering substitute" instead of the protein as it could be used in concentrations that somewhat resembling what would be used later on. The pH change could be estimated based on the relative ratio between the absorbance at 620 nm and 450 nm with an isosbestic point at 510 nm in the absorbance spectrum for bromocresol green.[179] Since the conformational change in KcsA will consume protons, we reasoned that using the pH indicator at similar concentration to the protein would mimic the buffering of the protein in the real-life experiment to some extent. Upon flowing a sample comprised of caged proton (25 mM) and bromocresol green (300 μM) in a 0.7 mm quartz capillary at different flowrates we could estimate the change in pH as a function of the flowrate (**Figure 34**). Two 385 nm LEDs (1000 mA x 2) coupled through fiber optic cables was used for the illumination which is shown in **Figure 34**. This confirmed to us that a sufficient pH decrease was possible under experimentally relevant conditions. Although a rough estimate since the true

buffering capacity was not known, it gave us a ballpark estimate for the pH change following photolysis of the photocage.

2.4.2 VALIDATION OF REACTION INITIATION OF KCSA WITH CAGED PROTON

After confirming the feasibility of inducing a sufficient pH dive upon photolysis of the photocage, a preliminary proof-of-concept X-ray solution scattering experiment was conducted at the ID02 beamline at ESRF in May 2021. The purpose of this experiment was to verify that different signals could be observed for KcsA at different pH levels, relevant to the pH mediated structural change, and that the same change could be induced by photolysis of the photocage. We collected X-ray solution scattering data at pH 4.7, 7.2 and 8.9, confirming the anticipated pH-dependent scattering profile variation for KcsA at different pH levels. More importantly, we could replicate similar results when utilizing the proton photocage (100 mM) upon by illumination with 385 nm LEDs under flow conditions (30 nl/s) (**Figure 35**).

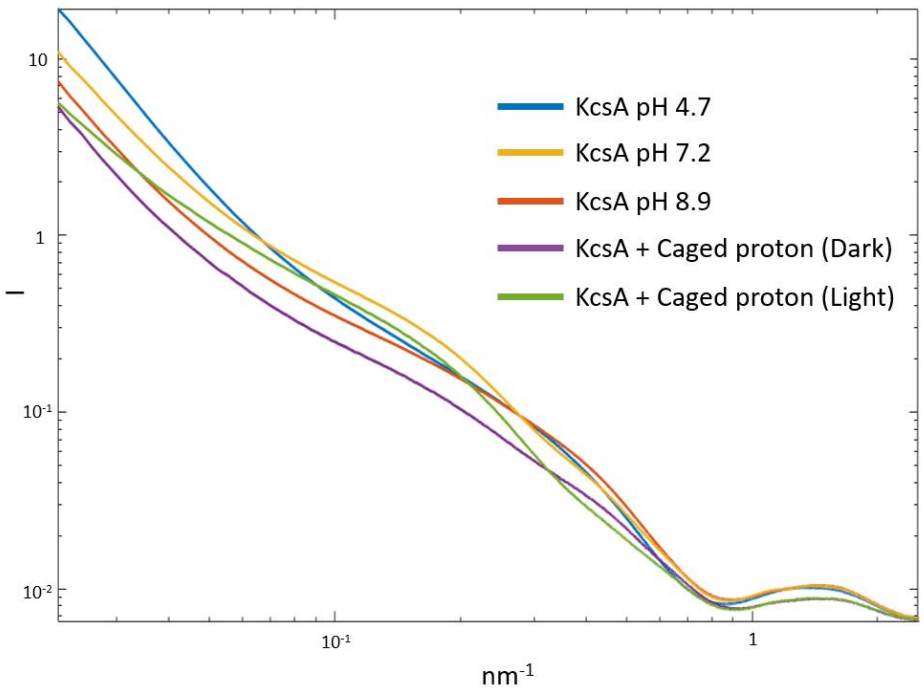

Figure 35. Absolute scattering curve for KcsA (16 mg/ml) at pH 4.7 (blue), KcsA at pH 7.2 (yellow), KcsA at pH 8.9 (red) and KcsA + Caged proton (100 mM) before (purple) and after (green) light illumination with 385 nm LEDs (50 mA x 4, 600 μm fiber optic cables) in a 600 μM quartz capillary at 30 nl/s. Note that this is a crude comparison and no refinements of the data has been done and is just here to illustrate what our initial hit looked like and no scientific conclusions have been from the curves.

The decrease in pH and subsequent reaction initiation was induced by upstream photolysis of the photoacid. Different protein batches were used for these experiments due to difficulties in obtaining sufficient amounts of protein, which resulted in variation in the data due to slight deviations in concentration. This is evident in **Figure 35** but the take home message from this experiment was simply that we needed to repeat this and improve our experimental setup and sample preparation for the next experiment, but the preliminary data we obtained was promising. An experienced solution scattering scientist will likely glance at the right image in **Figure 36** and proclaim – that might get a bit hot. Indeed, heat can influence solution scattering experiments and thus a control experiment are typically conducted to isolate the desired effect and exclude other variables that might interfere.[129] We could at least confirm that the signal observed could not be replicated by illumination of the photocage or KscA independently. An IR-laser could have confirmed that the effect was not due to the combined effect of KcsA together with caged proton, which is a fair point of criticism, but as far as a first try validation experiment goes, we were satisfied with the outcome.

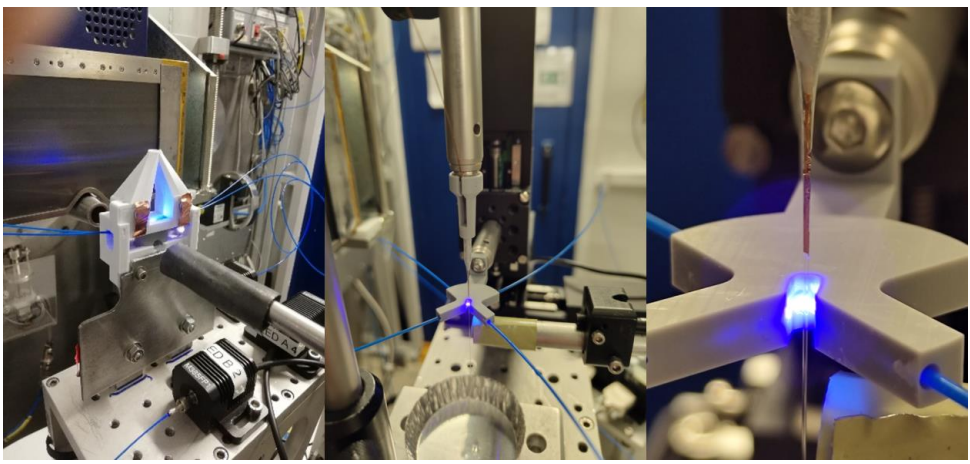

Figure 36. Experimental setup for the X-ray scattering experiments. **Left)** Setup for the first KscA SAXS experiment at ESRF (ID02) during May 2021. **Middle)** and **right)** Setup for the second X-ray scattering experiment at ESRF (ID02) during May 2023. For these experiments a 0.6 mm quartz capillary was used to deliver the sample to the X-ray beam. The photocaged proton was released by upstream illumination as shown above.

There were other complications during the experiments, as is often the case. Significant precipitation was observed following illumination for a prolonged time, which could be due to either precipitation of the photoproduct of the photocage or by some other component in the sample. This was problematic since scattering experiments are highly sensitive to minor changes in sample composition. In order to circumvent this in the following repeat experiment at the ID02 beamline at ESRF in May 2023, the sample position on the capillary was changed frequently but still lead to variance in the data between collections.

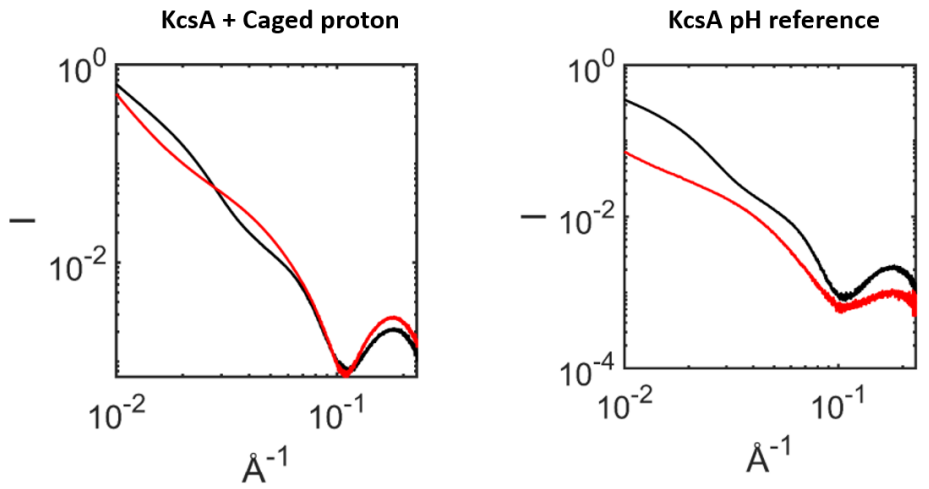

Figure 37. X-ray scattering curve from KcsA. Note the double hump characteristics for the curve associated with light activation and the low pH KcsA reference. **Left)** KcsA with caged proton at pH 5.8 before illumination (black) and after light illumination (red). **Right)** KcsA at pH 6.5 (black) and pH 3.7 (red). Variations in protein concentration is apparent here which prevented proper normalization of the two curves.

Again, small variations in the sample composition led to difficulties in normalizing data which we aimed to improve for the final time-resolved experiment. Despite these challenges, the clear effect observed following the pH cage photolysis (**Figure 37**) was promising and motivated us to continue our work towards a genuine time-resolved experiment.

2.4.3 TR-XSS OF KCSA AND CAGED PROTON

Third time is the charm. Time-resolved XSS data was collected at the dedicated time-resolved beamline ID09 at ESRF during July 2023. The advantage of this particular beamline is the utilization of a high-speed X-ray chopper which provides unprecedented short X-ray pulses down to 50 picoseconds.[180,181] To minimize sample consumption and allow for more comprehensive data collection in this experiment, we opted for a thinner capillary of 0.3 mm diameter, compared to the 0.6 mm capillaries used previously. The reaction was initiated by a 355 nm pulsed nanosecond laser and several time points were probed between a few microseconds to hundreds of milliseconds. Three different pulse intensities: 0.1 mJ/pulse (0.27 mJ/mm^2), 1.4 mJ/pulse (3.8 mJ/mm^2), and 2.9 mJ/pulse (7.9 mJ/mm^2) were focused to a beam profile measuring approximately 1.1 × 0.3 mm (W×H). A flowrate of 30 nl/s was used to ensure that the sample position was not illuminated more than once by the pump laser prior to the X-ray probe. We estimated that under our experimental conditions, with a quantum yield of 0.5 for the photocage at 355 nm, that the three different pH levels theoretically induced were: pH 3.5, pH 2.4 and pH 2.1 respectively for the different power settings, starting from a pH of 5.8. These final pH levels are likely not achieved considering the unknown buffering capacity of the sample due to the presence of His-tags, remaining protonatable buffer components and various protonatable residues in the protein.

Interestingly, the observed heat signals following the UV-pulse showed an interesting temporal feature. Two components could be extracted, one following the direct heating from the pulsed laser and one that evolved over time which we attributed to heat associated with the release mechanism of the photocage or from perhaps protonation of some buffer component. This can be observed upon recording a dataset with only the caged proton and buffer at different laser intensities at different time points (**Figure 38a**). With this in hand we could subtract the heating signal from the difference curves for the time-resolved data which is shown in **Figure 38b**.

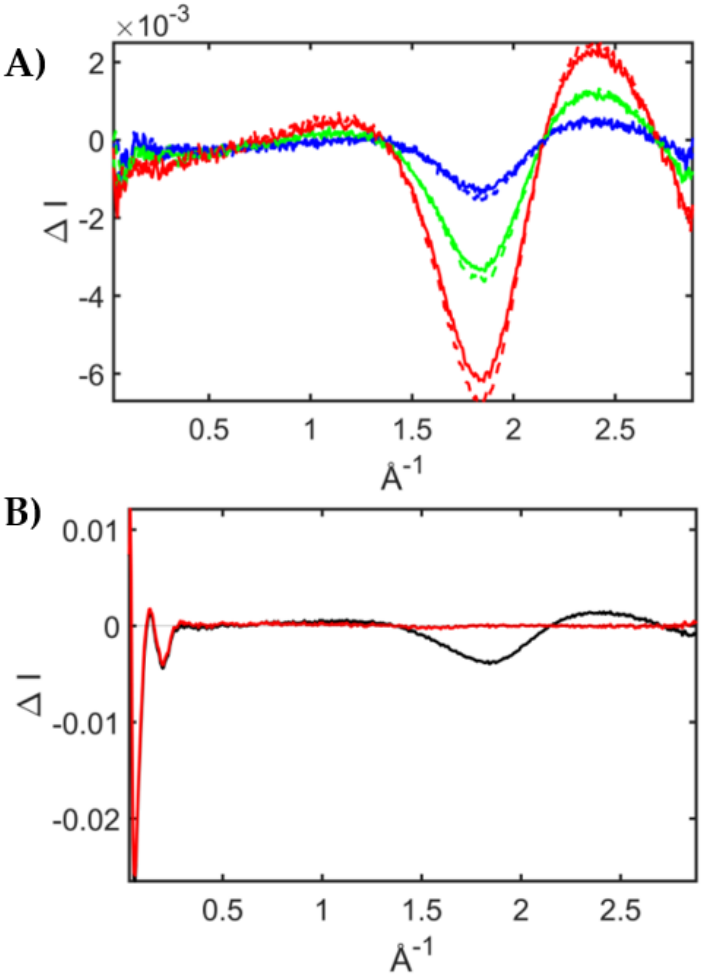

Figure 38. Left) Heating effect from caged proton upon photolysis from a 355 nm laser pulse at different intensities: 0.27 mJ/mm² (blue), 3.8 mJ/mm² (green) and 7.9 mJ/mm² (red). **Right)** Removal of the heat signal from one time-resolved datapoint where KscA and caged proton are exposed to a laser pulse.

The obtained TR-XSS data (**Figure 39**) shows an evolution over time where the amplitude of the difference scattering increases with the laser fluence. The positioning of the peaks in the scattering signal shows differences for the different laser fluences which is inherently tied to the magnitude of the induced pH change but this might change upon more careful analysis of the data. This indicates that there might be different structural paths for the conformational change available occurring at different pH levels. It could also be that the conformational change is achieved at different rates at different pH levels.

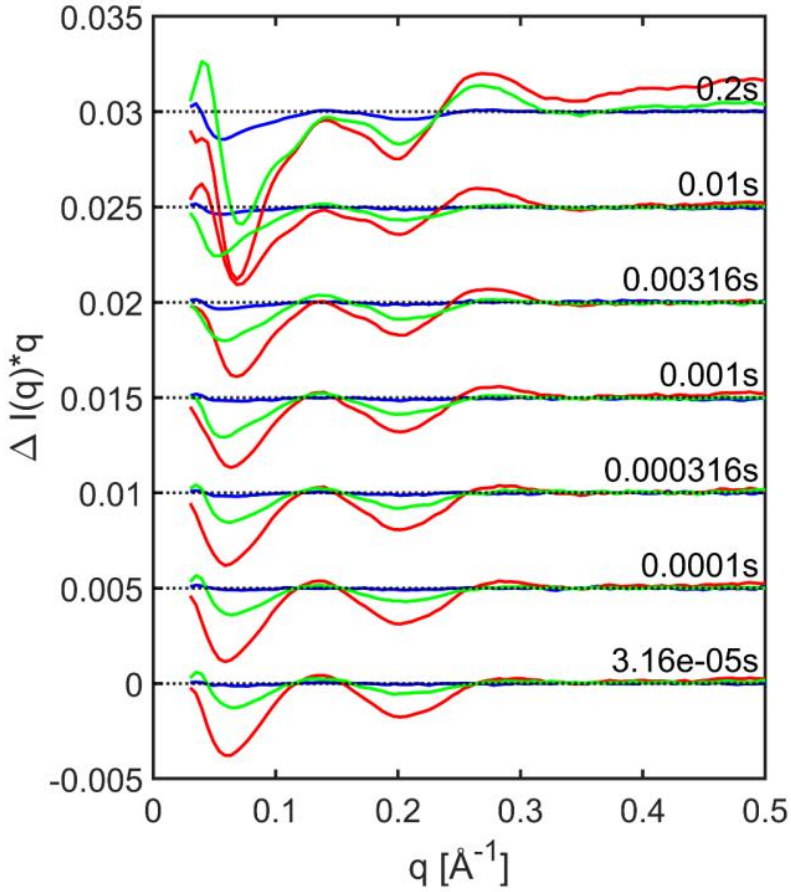

Figure 39. TR-XSS difference scattering curve data ranging 30μs to 200 ms following the photoactivation of caged proton and subsequent initiation of the reaction. The estimated pH levels are pH 3.5 (blue), pH 2.4 (green) and pH 2.1(red) but as mentioned above, these will likely be slightly higher than this in reality.

Efforts are ongoing with employing molecular dynamics simulations to elucidate which structural movements can be associated with our time-resolved data and to build 3D-models to visualize this. It is amazing how a 3D model can be derived from these "simple" 2D plots. Taken together, we show with impressive temporal resolution that a conformational change can be induced in KscA upon acidification with a photocage. Our results provide valuable

insight for further implementation of photocages for structural studies with substrate dependent systems by TR-XSS.

2.5 PAPER I – IV: SUMMARY AND CONCLUDING REMARKS

In **Paper I** we verify that an oxygen photocage can be used to initiate the reaction between CcO and oxygen which was subsequently implemented in **Paper II**. Furthermore, in **Paper I** we investigated a series of HPBC oxygen photocages and evaluate them as candidates for the use in time resolved studies of oxygen dependent enzymes. In **Paper II** we report the results from several TR-SFX experiments at XFELs employing an oxygen photocage to study structural changes following the release of oxygen. We discuss the various difficulties associated with the use of photocages in TR-SFX studies with CcO and provide crystallographic evidence of enzymatic turnover 10 ms following oxygen release. In **Paper III** we explore low molecular weight organogelators as a medium for the spatiotemporal release of singlet oxygen. We demonstrate this by synthesizing various OTHO derivatives that can bind and release $^1O_2$ upon external stimuli by light and heat in the gel phase and in solution. In **Paper IV** we study the structural dynamics of KcsA with X-ray scattering by inducing a pH decrease by photolysis of a photocage that releases protons. We show that upon light illumination KcsA undergoes a conformational change when caged proton is photolysed.

Taken together the work presented in this thesis shows the potential and difficulties with incorporating photocages in time resolved X-ray studies of substrate dependent proteins. The implementation of photocages for TR-SFX experiments has proven a significant challenge due to the complexity associated with these experiments, especially with the case of CcO. It has become clear that a perfect TR-SFX experiment with substrate photocages is perhaps not achievable any time soon. It is a very young field and more work and examples are needed before a final verdict can be made regarding the future prospects of the field. A more promising avenue for time resolved X-ray studies with photocages at this time is X-ray scattering experiments. The main reason for why TR-XSS is better suited at this time is because it is a simpler system for study. One has to learn how to walk before one can learn how to run is a suitable analogy. The complex nature of crystals and the sheer number of unknown variables in these experiments could benefit greatly from structural information that can be accessed by scattering studies which could be translated into TR-SFX experiments, building on that foundation.

This project has received funding from the European Research Council (ERC) under the European Union's Horizon 2020 research and innovation program under grant agreement No 789030.

3. FUTURE PERSPECTIVES AND LATE ADDITIONS

3.1 TR-SFX STUDIES WITH PHOTOCAGES

Considering the enormous effort that was made to improve the properties of the HPBC type photocage, and the minor improvements that were achieved, it is unlikely that continuing along this route will be fruitful. Rather than focusing on structural modification of the HPBC photocage, more creative and technically demanding reaction initiation setups could circumvent some of the aforementioned problems. By employing a rapid mixing strategy in an SFX experiment as opposed to incubating the HPBC photocage with the protein this would be more likely to yield a less oxygen contaminated starting state for the reaction. Other strategies were pursued in subsequent SFX experiments at LCLS in 2022/2023 and at SwissFEL in 2023. New crystallization conditions for CcO were developed where the pH was increased to pH 8 as opposed to 5.3. This we reasoned would result in more favorable reduction kinetics in crystals. This was semi-successful but a double-edged sword. As expected, the DTT and DTBA mediated reduction of CcO was significantly accelerated in crystals by shifting the equilibrium towards the active deprotonated state of the reductants. Although no significant degradation had been observed upon prolonged incubation between DTT or DTBA at neutral or slightly basic conditions with the HPBC photocages. Exposure to the crystal conditions at pH 8 which contains HEPES resulted in a prominent degradation of the photocage when DTBA was used as the reductant in the presence of HEPES. Attempts to utilize the more redox resilient oxygen photocage **HPBC 3** were made at SwissFEL in 2023 but did not lead to any visible difference signal at this time, possibly due to the lower quantum yield of the photocage.

Upon further refinements and careful examination of data collected during the 2022 LCLS TR-SFX experiment there is further evidence of enzymatic turnover following light induced release of oxygen. Here, an alternating collection scheme of light, dark1 and dark2 and was used. Initially, no significant signal was observed upon calculating a difference map between the combined darks and light at an approximately 3.3 ms time delay. However, upon separation of the dark1 and dark2, the difference electron density signals associated with Wat159 and Wat161 from **Paper II** could be reproduced (**Figure *40***). In this experiment, DTBA was used as the reductant instead of DTT and the experiment was conducted with microcrystals of CcO at pH 5.3. Although this signal is weak when calculating the difference map against the internal dark, a difference is observed upon when comparing the light, dark1 and dark2 against the DTBA reference (**Figure *40***). We are hopeful that further refinements will produce a more convincing difference map with the internal F_{obs}(light)-F_{obs}(dark) at a later state. Again, note that the difference density signal associated with the BNC ligand is likely not a time-resolved signal but arising from premature oxidation of the enzyme upon addition of the photocage as previously discussed in where the chloride in the BNC is again present in a sub-population of the enzyme. This leads to negative density

when calculating the difference map against the DTBA reference as this structure is mostly empty in the BNC. The reason behind the difference between dark 1 and dark 2 is likely due to the extremely large laser spot size and high intensity that was utilized to compensate for the size of the laser beam. This was a last resort solution[††] resulting from problems at the beamline which forced us to use a backup system that was not completely suitable for our experimental setup. We resorted to using a razorblade to attempt to reduce the light contamination but this was partially successful at best. As a consequence, it is fair to question whether any significant time resolution was achieved and likely an illumination scheme resembling **C** in **Figure *12*** was occurring. Furthermore, although the laser power was high (> 200 μJ/pulse) the spotsize was in the order of >700 μm, which likely lead to suboptimal photocage activation at best.

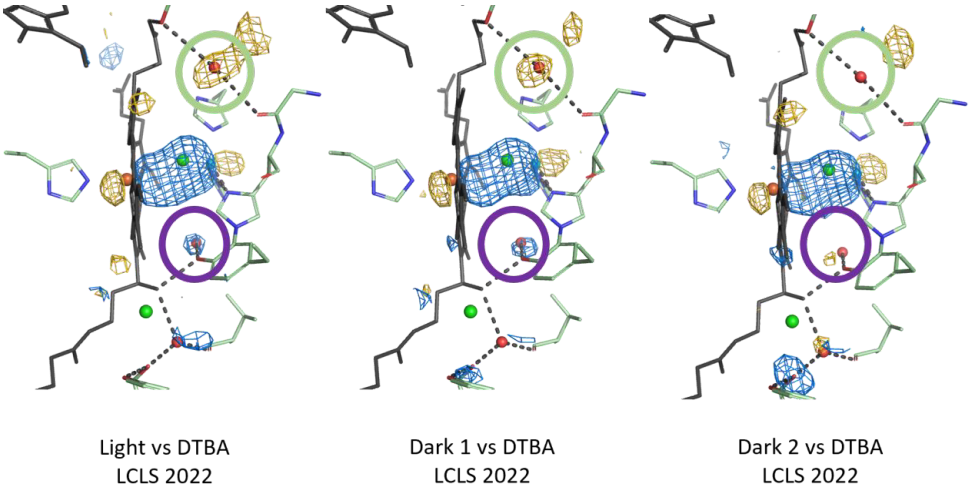

Figure 40. **Left)** F_{obs}(DTBA reduced CcO + photocage 3.3 ms after light activation) - F_{obs}(DTBA reduced CcO) isomorphous difference Fourier electron density map. **Middle)** F_{obs}(DTBA reduced CcO + photocage dark 1) - F_{obs}(DTBA reduced CcO) isomorphous difference Fourier electron density map. **Right)** F_{obs}(DTBA reduced CcO + photocage dark 2) - F_{obs}(DTBA reduced CcO) isomorphous difference Fourier electron density map. Maps are contoured at ± 3.2 σ with gold positive density and blue negative density.

In addition to this, TR-SFX experiments conducted at LCLS in February 2024 seems to contain similar small differences in the electron density upon photolysis of **HPBC 1** with DTT reduced CcO at pH 8. The advantage of this experiment compared to the previous time-resolved experiment from **Paper II** is that an internal dark reference was collected which was a major source of uncertainty in **Paper II**. Although proper refinements and further analysis is required this is most likely the strongest candidate to achieve a proper Fobs(light)-Fobs(dark) difference map with an internal dark. As might have become apparent, this is something that we have put quite some effort into.

[††] In our group this type of MacGyver quick fix is referred to as a "mickey-mouse solution" and should only be criticized upon failure to resolve the problem. My motto is "it is not stupid if it works".

Always leave the reader wanting for more is a common advice to novice writers. And as I cannot pretend to be anything beyond just that, I must adhere to this advice. One additional TR-SFX experiment with CcO and a photocage has been attempted on two occasions, the details of which unfortunately does not fit in this already long thesis. But the preliminary results obtained at LCLS in February 2024 deserves to be mentioned. DTBA reduced CcO was mixed with the previously mentioned nitric oxide photocage, **Caged NO** (**Scheme 3**), and TR-SFX data was collected 30 ms following excitation from a 355 nm laser (~40 μJ/pulse, ~70 μm spotsize). Describing the collection of sufficient images to generate a difference map a close call would be an understatement as the XFEL beam going on and off during the final hours of a five-day experiment when these data were collected. In the end, a less than optimal number of images could be collected but the initial map calculated on site shows the characteristics presence of an elongated density in the BNC, with a bent geometry, as would be expected from ligation of a nitric oxide species to the heme. We hope to report the details and associated maps regarding this experiment soon.

3.2 TOWARDS DEVELOPING SINGLET OXYGEN RELEASING HYDROGELS

Substantial work has been directed towards producing hydrogel equivalents of the endoperoxide OTHOs produced in **Paper III** and sadly there is still a long way to go. Initially, we envisioned that hydrogel OTHOs would be achievable upon simple introduction of a sufficiently polar functionality which has been previously demonstrated for structurally related OTHOs.[148] However, the presence of the oxygen binding motif in **OTHOs 1-5** and **1-O$_2$** - **5-O$_2$** likely interfere with the required intermolecular interactions which are required for gelation to occur in water. Amongst the numerous failed attempts synthesizing and gelatin various OTHOs with polar functionalities such as N-oxides and quaternary ammonium salts, none formed gels in aqueous solution and most remained mostly insoluble. Intrigued by the high aqueous solubility of the proton photocage from **Paper IV** we recognized the possibility of introducing several sulphate groups on the glucoside sugar already present in the OTHO framework. This did result in several OTHO hydrogels with MGCs in the range between 5 – 20 mg/ml. Unfortunately, upon formation of the corresponding endoperoxide the hydrogelation property were lost which we suspect is due to an increase in solubility. Efforts are still ongoing to modify **2-PA-Sulphate OTHO** and **Sulphate OTHO 2** shown in **Scheme 14** into endoperoxide hydrogelators by fine-tuning of the aqueous solubility but much work remains to be done. Gelation is a frustrating property to fine tune and I am not convinced that rational design beats dumb luck.

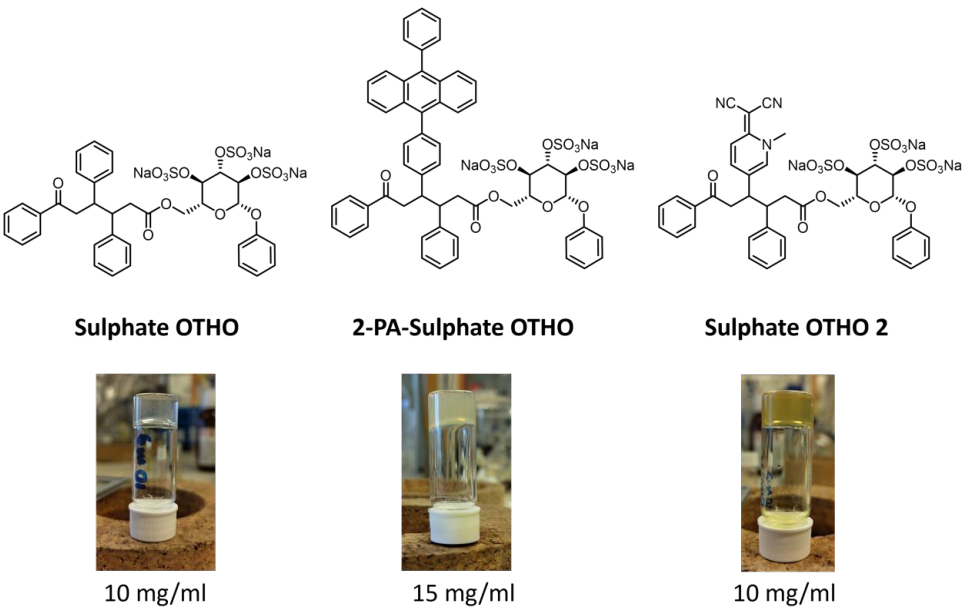

Scheme 14. Synthesized OTHO hydrogelators and their corresponding MGC in water. It should be noted that **Sulphate OTHO** can form a gel also at 5 mg/ml but less consistently.

3.3 FURTHER IMPLEMENTATION OF PHOTOCAGES IN TR-XSS STUIDES

The pursuit of further biologically relevant photocages seems like a logical endeavor in the field of time-resolved structural biology. As I might have hinted at before, combining photocages and crystallography is very complicated. The same is true for solution scattering experiments at least by only considering the experimental data collection, they are simpler by orders of magnitude. We are currently pursuing the synthesis of several novel caged biomolecules that initially will be implemented in TR-XSS studies building on the foundation established in **Paper IV**. My work has focused on optimizing and synthesizing photocage derivatives of octopamine, tyramine and acetyl choline. Photocages of octopamine and tyramine have been synthesized, each with the photocage attached to different positions, either by attachment at the phenol or amine. This was done to ensure that the caged – dark state – would be less likely to show activity towards the final biological target as it is not clear at this stage which functionality of the biomolecule is most essential for our future target. The work that has been done so far involves the synthesis and characterization of caged tyramine and octopamine and one acetylcholine derivative which remains to be turned into a photocage if it exhibits activity towards the biological target. The relevant compounds are shown in **Scheme 15**.

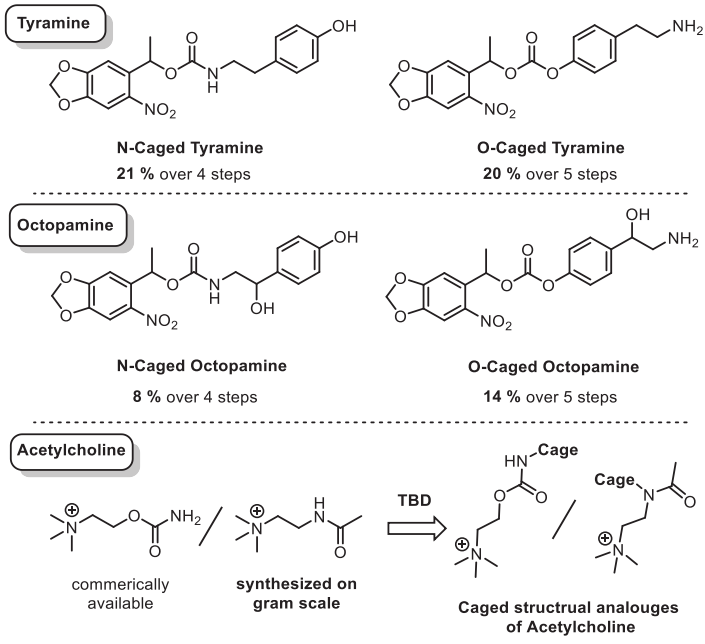

Scheme 15. Structures of caged octopamine and caged tyramine. Also shown is the structure of two structural analogues of acetylcholine (not shown), a caged acetylcholine is not feasible due to the lack of a functional group for the anchoring of the photocage.

4. REFERENCES

[1] T. W. Lyons, C. T. Reinhard, N. J. Planavsky, *Nature* **2014**, *506*, 307–315.

[2] M. P. Johnson, *Essays Biochem.* **2016**, *60*, 255–273.

[3] M. Wikström, K. Krab, V. Sharma, *Chem. Rev.* **2018**, *118*, 2469–2490.

[4] P. E. M. Siegbahn, M. R. A. Blomberg, *Biochim. Biophys. Acta - Bioenerg.* **2007**, *1767*, 1143–1156.

[5] M. Wikström, M. I. Verkhovsky, *Biochim. Biophys. Acta - Bioenerg.* **2007**, *1767*, 1200–1214.

[6] J. C. Maxwell, *Philos. Trans. R. Soc. London* **1865**, *155*, 459–512.

[7] A. Albini, *Photochemistry: Past, Present, Future*, Springer-Verlag, Berlin Heidelberg, **2016**.

[8] M. Montalti, A. Credi, L. Prodi, M. Teresa Gandolfi, in *Handb. Photochem. Third Ed.* (Ed.: Boca Raton), Taylor & Francis Group, LLC, FL, **2006**, pp. 601–616.

[9] K. Stranius, K. Börjesson, *Sci. Rep.* **2017**, *7*, 41145.

[10] N. R. Zaccai, I. N. Serdyuk, J. Zaccai, in *Methods Mol. Biophys.*, Cambridge University Press, **2017**, pp. 456–485.

[11] A. A. Kermani, A. A. Kermani, *FEBS J.* **2021**, *288*, 5788–5804.

[12] M. Levantino, B. A. Yorke, D. C. F. Monteiro, M. Cammarata, A. R. Pearson, *Curr. Opin. Struct. Biol.* **2015**, *35*, 41–48.

[13] ESRF, 'European Synchrotron Radiation Facility', can be found under https://lightsources.org/lightsources-of-the-world/europe/esrf/, **2024**.

[14] MaxIV, 'The MAX IV facility', can be found under https://www.maxiv.lu.se/about-us/the-max-iv-facility/, **n.d.**

[15] W. A. Hendrickson, *Trends Biochem. Sci.* **2000**, *25*, 637–643.

[16] A. Nocentini, C. T. Supuran, C. Capasso, *J. Enzyme Inhib. Med. Chem.* **2021**, *36*, 1988.

[17] T. L. Rosenberry, *Adv. Enzymol. Relat. Areas Mol. Biol.* **2006**, *43*, 103–218.

[18] A. Bar-Even, E. Noor, Y. Savir, W. Liebermeister, D. Davidi, D. S. Tawfik, R. Milo, *Biochemistry* **2011**, *50*, 4402–4410.

[19] D. C. F. Monteiro, E. Amoah, C. Rogers, A. R. Pearson, *Acta Crystallogr. Sect. D Struct. Biol.* **2021**, *D77*, 1218–1232.

[20] R. Neutzo, R. Wouts, D. Van Der Spoel, E. Weckert, J. Hajdu, *Nature* **2000**, *406*, 752–757.

[21] A. Doerr, *Nat. Methods* **2011**, *8*, 283–283.

[22] A. Ebrahim, T. Moreno-Chicano, M. V. Appleby, A. K. Chaplin, J. H. Beale, D. A. Sherrell, H. M. E. Duyvesteyn, S. Owada, K. Tono, H. Sugimoto, R. W. Strange, J. A. R. Worrall, D. Axford, R. L. Owen, M. A. Hough, *IUCrJ* **2019**, *6*, 543–551.

[23] R. Neutze, G. Brändén, G. F. X. Schertler, *Curr. Opin. Struct. Biol.* **2015**, *33*, 115–125.

[24] J. A. R. Worrall, M. A. Hough, *Curr. Opin. Struct. Biol.* **2022**, *77*, 102486.

[25] H. N. Chapman, P. Fromme, A. Barty, T. A. White, R. A. Kirian, A. Aquila, M. S. Hunter, J. Schulz, D. P. Deponte, U. Weierstall, R. B. Doak, F. R. N. C. Maia, A. V. Martin, I. Schlichting, L. Lomb, N. Coppola, R. L. Shoeman, S. W. Epp, R. Hartmann, D. Rolles, A. Rudenko, L. Foucar, N. Kimmel, G. Weidenspointner, P. Holl, M. Liang, M. Barthelmess, C. Caleman, S. Boutet, M. J. Bogan, J. Krzywinski, C. Bostedt, S. Bajt, L. Gumprecht, B. Rudek, B. Erk, C. Schmidt, A. Hömke, C. Reich, D. Pietschner, L. Ströder, G. Hauser, H. Gorke, J. Ullrich, S. Herrmann, G. Schaller, F. Schopper, H. Soltau, K. U. Kühnel, M. Messerschmidt, J. D. Bozek, S. P. Hau-Riege, M. Frank, C. Y. Hampton, R. G. Sierra, D. Starodub, G. J. Williams, J. Hajdu, N. Timneanu, M. M. Seibert, J. Andreasson, A. Rocker, O. Jönsson, M. Svenda, S. Stern, K. Nass, R. Andritschke, C. D. Schröter, F. Krasniqi, M. Bott, K. E. Schmidt, X. Wang, I. Grotjohann, J. M. Holton, T. R. M. Barends, R. Neutze, S. Marchesini, R. Fromme, S. Schorb, D. Rupp, M. Adolph, T. Gorkhover, I. Andersson, H. Hirsemann, G. Potdevin, H. Graafsma, B. Nilsson, J. C. H. Spence, *Nat. 2011 4707332* **2011**, *470*, 73–77.

[26] S. Pandey, R. Bean, T. Sato, I. Poudyal, J. Bielecki, J. Cruz Villarreal, O. Yefanov, V. Mariani, T. A. White, C. Kupitz, M. Hunter, M. H. Abdellatif, S. Bajt, V. Bondar, A. Echelmeier, D. Doppler, M. Emons, M. Frank, R. Fromme, Y. Gevorkov, G. Giovanetti, M. Jiang, D. Kim, Y. Kim, H. Kirkwood, A. Klimovskaia, J. Knoska, F. H. M. Koua, R. Letrun, S. Lisova, L. Maia, V. Mazalova, D. Meza, T. Michelat, A. Ourmazd, G. Palmer, M. Ramilli, R. Schubert, P. Schwander, A. Silenzi, J. Sztuk-Dambietz, A. Tolstikova, H. N. Chapman, A. Ros, A. Barty, P. Fromme, A. P. Mancuso, M. Schmidt, *Nat. Methods 2019 171* **2019**, *17*, 73–78.

[27] J. Tenboer, S. Basu, N. Zatsepin, K. Pande, D. Milathianaki, M. Frank, M. Hunter, S. Boutet, G. J. Williams, J. E. Koglin, D. Oberthuer, M. Heymann, C. Kupitz, C. Conrad, J. Coe, S. Roy-Chowdhury, U. Weierstall, D. James, D. Wang, T. Grant, A. Barty, O. Yefanov, J. Scales, C. Gati, C. Seuring, V. Srajer, R. Henning, P. Schwander, R. Fromme, A. Ourmazd, K. Moffat, J. J. Van Thor, J. C. H. Spence, P. Fromme, H. N. Chapman, M. Schmidt, *Science (80-.).* **2014**, *346*, 1242–1246.

[28] Y. Shimazu, K. Tono, T. Tanaka, Y. Yamanaka, T. Nakane, C. Mori, K. T. Kimura, T. Fujiwara, M. Sugahara, R. Tanaka, R. B. Doak, T. Shimamura, S. Iwata, E. Nango, M. Yabashi, *J. Appl. Crystallogr.* **2019**, *52*, 1280–1288.

[29] A. M. Orville, *Curr. Opin. Struct. Biol.* **2020**, *65*, 193–208.

[30] D. Wang, U. Weierstall, L. Pollack, J. Spence, *J. Synchrotron Radiat.* **2014**, *21*, 1364–1366.

[31] A. Butryn, P. S. Simon, P. Aller, P. Hinchliffe, R. N. Massad, G. Leen, C. L. Tooke, I. Bogacz, I. S. Kim, A. Bhowmick, A. S. Brewster, N. E. Devenish, J. Brem, J. J. A. G. Kamps, P. A. Lang, P. Rabe, D. Axford, J. H. Beale, B. Davy, A. Ebrahim, J. Orlans, S. L. S. Storm, T. Zhou, S. Owada, R. Tanaka, K. Tono, G. Evans, R. L. Owen, F. A.

Houle, N. K. Sauter, C. J. Schofield, J. Spencer, V. K. Yachandra, J. Yano, J. F. Kern, A. M. Orville, *Nat. Commun.* **2021**, *12*, 1–7.

[32] T. Hori, H. Moriyama, J. Kawaguchi, Y. Hayashi-Iwasaki, T. Oshima, N. Tanaka, *Protein Eng.* **2000**, *13*, 527–533.

[33] A. M. Wolff, E. Nango, I. D. Young, A. S. Brewster, M. Kubo, T. Nomura, M. Sugahara, S. Owada, B. A. Barad, K. Ito, A. Bhowmick, S. Carbajo, T. Hino, J. M. Holton, D. Im, L. J. O'Riordan, T. Tanaka, R. Tanaka, R. G. Sierra, F. Yumoto, K. Tono, S. Iwata, N. K. Sauter, J. S. Fraser, M. C. Thompson, *Nat. Chem.* **2023**, *15*, 1549–1558.

[34] D. R. Hekstra, K. I. White, M. A. Socolich, R. W. Henning, V. Šrajer, R. Ranganathan, *Nature* **2016**, *540*, 400–405.

[35] P. R. Ogilby, *Chem. Soc. Rev.* **2010**, *39*, 3181–3209.

[36] W. T. Borden, R. Hoffmann, T. Stuyver, B. Chen, *J. Am. Chem. Soc.* **2017**, *139*, 9010–9018.

[37] R. Stuhr, P. Bayer, A. J. von Wangelin, *ChemSusChem* **2022**, *15*, 1–17.

[38] P. C. Wietstock, T. Kunz, F. J. Methner, *J. Agric. Food Chem.* **2016**, *64*, 8035–8044.

[39] H. Kautsky, *Trans. Faraday Soc.* **1939**, *35*, 216–219.

[40] C. Schweitzer, R. Schmidt, *Chem. Rev.* **2003**, *103*, 1685–1757.

[41] V. Brega, Y. Yan, S. W. Thomas, *Org. Biomol. Chem.* **2020**, *18*, 9191–9209.

[42] P. Di Mascio, E. J. H. Bechara, M. H. G. Medeiros, K. Briviba, H. Sies, *FEBS Lett.* **1994**, *355*, 287–289.

[43] P. Di Mascio, G. R. Martinez, S. Miyamoto, G. E. Ronsein, M. H. G. Medeiros, J. Cadet, *Chem. Rev.* **2019**, *119*, 2043–2086.

[44] J. Al-Nu'airat, I. Oluwoye, N. Zeinali, M. Altarawneh, B. Z. Dlugogorski, *Chem. Rec.* **2021**, *21*, 315–342.

[45] C. Kim, R. Meskauskiene, K. Apel, C. Laloi, *EMBO Rep.* **2008**, *9*, 435–439.

[46] D. Wagner, D. Przybyla, R. Op den Camp, C. Kim, F. Landgraf, K. P. Lee, M. Würsch, C. Laloi, M. Nater, E. Hideg, K. Apel, *Science.* **2004**, *306*, 1183–1185.

[47] P. Agostinis, K. Berg, K. A. Cengel, T. H. Foster, A. W. Girotti, S. O. Gollnick, S. M. Hahn, M. R. Hamblin, A. Juzeniene, D. Kessel, M. Korbelik, J. Moan, P. Mroz, D. Nowis, J. Piette, B. C. Wilson, J. Golab, *CA. Cancer J. Clin.* **2011**, *61*, 250–281.

[48] R. V. Huis in 't Veld, J. Heuts, S. Ma, L. J. Cruz, F. A. Ossendorp, M. J. Jager, *Pharmaceutics* **2023**, *15*, 1–41.

[49] L. Hong, J. Li, Y. Luo, T. Guo, C. Zhang, S. Ou, Y. Long, Z. Hu, *Biomolecules* **2022**, *12*, 1–20.

[50] B. Li, L. Lin, H. Lin, B. C. Wilson, *J. Biophotonics* **2016**, *9*, 1314–1325.

[51] S. Kolemen, T. Ozdemir, D. Lee, G. M. Kim, T. Karatas, J. Yoon, E. U. Akkaya, *Angew.*

Chemie - Int. Ed. **2016**, *55*, 3606–3610.

[52] H. Lai, J. Yan, S. Liu, Q. Yang, F. Xing, P. Xiao, *Angew. Chemie - Int. Ed.* **2020**, *59*, 10431–10435.

[53] Z. Yuan, S. Yu, F. Cao, Z. Mao, C. Gao, J. Ling, *Polym. Chem.* **2018**, *9*, 2124–2133.

[54] E. Ucar, D. Xi, O. Seven, C. Kaya, X. Peng, W. Sun, E. U. Akkaya, *Chem. Commun.* **2019**, *55*, 13808–13811.

[55] S. Ayan, G. Gunaydin, N. Yesilgul-Mehmetcik, M. E. Gedik, O. Seven, E. U. Akkaya, *Chem. Commun.* **2020**, *56*, 14793–14796.

[56] D. Eisenberg, *Protein Sci.* **1994**, *3*, 1625–1628.

[57] V. J. Thannickal, *Am. J. Respir. Cell Mol. Biol.* **2009**, *40*, 507.

[58] B. Meunier, S. P. de Visser, S. Shaik, *Chem. Rev.* **2004**, *104*, 3947–3980.

[59] H. Basch, K. Mogi, D. G. Musaev, K. Morokuma, *J. Am. Chem. Soc.* **1999**, *121*, 7249–7256.

[60] J. M. Berg, J. L. Tymoczko, G. J. J. Gatto, L. Stryer, *Biochemistry*, W.H. Freeman, New York, **2015**.

[61] M. M. Pereira, M. Santana, M. Teixeira, *Biochim. Biophys. Acta - Bioenerg.* **2001**, *1505*, 185–208.

[62] J. J. Regan, B. E. Ramirez, J. R. Winkler, H. B. Gray, B. G. Malmström, *J. Bioenerg. Biomembr.* **1998**, *30*, 35–39.

[63] D. M. Medvedev, I. Daizadeh, A. A. Stuchebrukhov, *J. Am. Chem. Soc.* **2000**, *122*, 6571–6582.

[64] H. J. Kim, O. Khalimonchuk, P. M. Smith, D. R. Winge, *Biochim. Biophys. Acta* **2012**, *1823*, 1604.

[65] M. Wikström, V. Sharma, *Biochim. Biophys. Acta - Bioenerg.* **2018**, *1859*, 692–698.

[66] V. R. I. Kaila, M. P. Johansson, D. Sundholm, L. Laakkonen, M. Wikström, *Biochim. Biophys. Acta - Bioenerg.* **2009**, *1787*, 221–233.

[67] E. A. Gorbikova, I. Belevich, M. Wikström, M. I. Verkhovsky, *Proc. Natl. Acad. Sci. U. S. A.* **2008**, *105*, 10733–10737.

[68] S. Iwata, C. Ostermeier, B. Ludwig, H. Michel, *Nature* **1995**, *376*, 660–669.

[69] T. Soulimane, G. Buse, M. Dewor, M. E. Than, R. Huber, *Protein Sci.* **2000**, *9*, 2068–2073.

[70] T. Soulimane, G. Buse, G. P. Bourenkov, H. D. Bartunik, R. Huber, M. E. Than, *EMBO J.* **2000**, *19*, 1766–1776.

[71] A. Kannt, T. Soulimane, G. Buse, A. Becker, E. Bamberg, H. Michel, *FEBS Lett.* **1998**, *434*, 17–22.

[72] S. A. Siletsky, I. Belevich, A. Jasaitis, A. A. Konstantinov, M. Wikström, T. Soulimane, M. I. Verkhovsky, *Biochim. Biophys. Acta - Bioenerg.* **2007**, *1767*, 1383–1392.

[73] C. Von Ballmoos, P. Ädelroth, R. B. Gennis, P. Brzezinski, *Biochim. Biophys. Acta - Bioenerg.* **2012**, *1817*, 650–657.

[74] D. Bloch, I. Belevich, A. Jasaitis, C. Ribacka, A. Puustinen, M. I. Verkhovsky, M. Wikström, *Proc. Natl. Acad. Sci. U. S. A.* **2004**, *101*, 529–533.

[75] V. Sharma, K. D. Karlin, M. Wikström, *Proc. Natl. Acad. Sci. U. S. A.* **2013**, *110*, 16844–16849.

[76] C. Von Ballmoos, P. Lachmann, R. B. Gennis, P. Ädelroth, P. Brzezinski, *Biochemistry* **2012**, *51*, 4507–4517.

[77] C. Von Ballmoos, N. Gonska, P. Lachmann, R. B. Gennis, P. Ädelroth, P. Brzezinski, *Proc. Natl. Acad. Sci.* **2015**, *112*, 3397–3402.

[78] X. Cai, C. Y. Son, J. Mao, D. Kaur, Y. Zhang, U. Khaniya, Q. Cui, M. R. Gunner, *Biochim. Biophys. Acta - Bioenerg.* **2020**, *1861*, 148239.

[79] M. R. A. Blomberg, *Front. Chem.* **2021**, *9*, 1–11.

[80] P. V. N. Rajasekharan, *Synthesis (Stuttg).* **1980**, *1*, 1–26.

[81] J. H. Kaplan, B. Forbush, J. F. Hoffman, *Biochemistry* **1978**, *17*, 1929–1935.

[82] H. M. Lee, D. R. Larson, D. S. Lawrence, *ACS Chem. Biol.* **2009**, *4*, 409–427.

[83] G. Mayer, A. Heckel, G. Mayer, A. Heckel, *Angew. Chemie Int. Ed.* **2006**, *45*, 4900–4921.

[84] S. R. Adams, J. P. Y. Kao, R. Y. Tsien, *J. Am. Chem. Soc.* **1989**, *111*, 7957–7968.

[85] J. J. Zaitsev-Doyle, A. Puchert, Y. Pfeifer, H. Yan, B. A. Yorke, H. M. Müller-Werkmeister, C. Uetrecht, J. Rehbein, N. Huse, A. R. Pearson, M. Sans, *RSC Adv.* **2019**, *9*, 8695–8699.

[86] P. Klán, T. Šolomek, C. G. Bochet, A. Blanc, R. Givens, M. Rubina, V. Popik, A. Kostikov, J. Wirz, *Chem. Rev.* **2013**, *113*, 119–191.

[87] S. Hauke, A. K. Dutta, V. B. Eisenbeis, D. Bezold, T. Bittner, C. Wittwer, D. Thakor, I. Pavlovic, C. Schultz, H. J. Jessen, *Chem. Sci.* **2019**, *10*, 2687–2692.

[88] R. Aarhus, K. Gee, H. C. Lee, *J. Biol. Chem.* **1995**, *270*, 7745–7749.

[89] G. C. R. Ellis-Davies, *Angew. Chemie Int. Ed.* **2023**, *62*, 1–12.

[90] A. Barth, J. E. T. Corrie, *Biophys. J.* **2002**, *83*, 2864–2871.

[91] S. Abbruzzetti, S. Sottini, C. Viappiani, J. E. T. Corrie, *J. Am. Chem. Soc.* **2005**, *127*, 9865–9874.

[92] R. J. D. Miller, O. Paré-Labrosse, A. Sarracini, J. E. Besaw, *Nat. Commun.* **2020**, *11*, 1–4.

[93] G. Nass Kovacs, J. P. Colletier, M. L. Grünbein, Y. Yang, T. Stensitzki, A. Batyuk, S. Carbajo, R. B. Doak, D. Ehrenberg, L. Foucar, R. Gasper, A. Gorel, M. Hilpert, M.

Kloos, J. E. Koglin, J. Reinstein, C. M. Roome, R. Schlesinger, M. Seaberg, R. L. Shoeman, M. Stricker, S. Boutet, S. Haacke, J. Heberle, K. Heyne, T. Domratcheva, T. R. M. Barends, I. Schlichting, *Nat. Commun. 2019 101* **2019**, *10*, 1–17.

[94] G. Brändén, R. Neutze, *Science.* **2021**, *373*, 1–13.

[95] T. R. M. Barends, A. Gorel, S. Bhattacharyya, G. Schirò, C. Bacellar, C. Cirelli, J.-P. Colletier, L. Foucar, M. L. Grünbein, E. Hartmann, M. Hilpert, J. M. Holton, P. J. M. Johnson, M. Kloos, G. Knopp, B. Marekha, K. Nass, G. Nass Kovacs, D. Ozerov, M. Stricker, M. Weik, R. B. Doak, R. L. Shoeman, C. J. Milne, M. Huix-Rotllant, M. Cammarata, I. Schlichting, *Nature* **2024**, *626*, 905–911.

[96] S. Namiki, T. Arai, K. Fujimori, *J. Am. Chem. Soc.* **1997**, *119*, 3840–3841.

[97] S. Fallab, *Angew. Chemie Int. Ed. English* **1967**, *6*, 496–507.

[98] A. C. Benniston, L. Zeng, *Dalt. Trans.* **2022**, *51*, 4202–4212.

[99] G. L. Geoffrey, G. S. Hammond, H. B. Gray, *J. Am. Chem. Soc.* **1975**, *97*, 3933–3936.

[100] H. C. Fry, P. G. Hoertz, I. M. Wasser, K. D. Karlin, G. J. Meyer, *J. Am. Chem. Soc.* **2004**, *126*, 16712–16713.

[101] I. Hatzopoulos, H. D. Brauer, M. R. Geisberger, W. A. Herrmann, *J. Organomet. Chem.* **1996**, *520*, 201–209.

[102] I. Hatzopoulos, W. R. Thiel, H. D. Brauer, *J. Photochem. Photobiol. A Chem.* **1997**, *102*, 151–155.

[103] D. M. Wagnerová, K. Lang, *Coord. Chem. Rev.* **2011**, *255*, 2904–2911.

[104] N. Shinohara, S. Matsufuji, W. Okubo, *Polyhedron* **1991**, *10*, 107–112.

[105] D. Valentine, *The Photochemistry of Cobalt(III) and Chromium(III) Complexes in Solution*, John Wiley & Sons, Ltd, **1968**.

[106] J. S. Valentine, D. Valentine, *J. Am. Chem. Soc.* **1971**, *93*, 1111–1117.

[107] J. S. Valentine, D. Valentine, *Inorg. Chem.* **1971**, *10*, 393–395.

[108] M. Kikkawa, Y. Sasaki, S. Kawata, Y. Hatakeyama, F. B. Ueno, K. Saito, *Inorg. Chem.* **1985**, *24*, 4096–4100.

[109] F. Miller, R. G. Wilkins, *J. Am. Chem. Soc.* **1970**, *92*, 2687–2691.

[110] J. Simplicio, R. G. Wilkins, *J. Am. Chem. Soc.* **1967**, *89*, 6092–6095.

[111] V. M. Miskowski, *Comments Inorg. Chem.* **1987**, *6*, 193–207.

[112] R. Macarthur, A. Sucheta, F. F. S. Chongt, O. Einarsdottir, *PNAS* **1995**, *92*, 8105–8109.

[113] C. Ludovici, R. Fröhlich, K. Vogtt, B. Mamat, M. Lübben, *Eur. J. Biochem.* **2002**, *269*, 2630–2637.

[114] N. Van Eps, I. Szundi, O. Einarsdottir, *Biochemistry* **2000**, *39*, 14576–14582.

[115] Ó. Einarsdóttir, C. Funatogawa, T. Soulimane, I. Szundi, *Biochim. Biophys. Acta* **2012**,

1817, 672–679.

[116] I. Szundi, C. Funatogawa, T. Soulimane, Ó. Einarsdóttir, *Biophys. J.* **2020**, *118*, 386–39.

[117] P. Mehrabi, E. C. Schulz, R. Dsouza, H. M. Müller-Werkmeister, F. Tellkamp, R. J. Dwayne Miller, E. F. Pai, *Science.* **2019**, *365*, 1167–1170.

[118] P. W. Y. Chan, A. F. Yakunin, E. A. Edwards, E. F. Pai, *J. Am. Chem. Soc.* **2011**, *133*, 7461–7468.

[119] E. C. Schulz, P. Mehrabi, H. M. Müller-Werkmeister, F. Tellkamp, A. Jha, W. Stuart, E. Persch, R. De Gasparo, F. Diederich, E. F. Pai, R. J. D. Miller, *Nat. Methods* **2018**, *15*, 901–904.

[120] R. S. Givens, K. Stensrud, P. G. Conrad, A. L. Yousef, C. Perera, S. N. Senadheera, D. Heger, J. Wirz, *Can. J. Chem.* **2011**, *89*, 364–384.

[121] M. A. Hough, F. Prischi, J. A. R. Worrall, *Front. Mol. Biosci.* **2023**, *10*, 1–6.

[122] M. Schmidt, *Crystals* **2020**, *10*, 11–15.

[123] T. Tosha, T. Nomura, T. Nishida, N. Saeki, K. Okubayashi, R. Yamagiwa, M. Sugahara, T. Nakane, K. Yamashita, K. Hirata, G. Ueno, T. Kimura, T. Hisano, K. Muramoto, H. Sawai, H. Takeda, E. Mizohata, A. Yamashita, Y. Kanematsu, Y. Takano, E. Nango, R. Tanaka, O. Nureki, O. Shoji, Y. Ikemoto, H. Murakami, S. Owada, K. Tono, M. Yabashi, M. Yamamoto, H. Ago, S. Iwata, H. Sugimoto, Y. Shiro, M. Kubo, *Nat. Commun.* **2017**, *8*, 1–9.

[124] R. Henderson, J. K. Moffat, *Acta Crystallogr. Sect. B* **1971**, *27*, 1414–1420.

[125] C. Wickstrand, G. Katona, T. Nakane, P. Nogly, J. Standfuss, E. Nango, R. Neutze, *Struct. Dyn.* **2020**, *7*, 24701.

[126] H. S. Cho, F. Schotte, V. Stadnytskyi, P. Anfinrud, *Curr. Opin. Struct. Biol.* **2021**, *70*, 99–107.

[127] Y. Lee, H. Lee, H. Ihee, *Chem. Phys. Rev.* **2022**, *3*, 41304.

[128] J. G. Kim, T. W. Kim, J. Kim, H. Ihee, *Acc. Chem. Res.* **2015**, *48*, 2200–2208.

[129] H. Poddar, D. J. Heyes, G. Schirò, M. Weik, D. Leys, N. S. Scrutton, *FEBS J.* **2022**, *289*, 576–595.

[130] H. Ravishankar, M. N. Pedersen, M. Eklund, A. Sitsel, C. Li, A. Duelli, M. Levantino, M. Wulff, A. Barth, C. Olesen, P. Nissen, M. Andersson, *Sci. Adv.* **2020**, *6*, 1–10.

[131] W. W. L. Cheng, J. G. McCoy, A. N. Thompson, C. G. Nichols, C. M. Nimigean, *Proc. Natl. Acad. Sci. U. S. A.* **2011**, *108*, 5272–5277.

[132] D. A. Doyle, J. M. Cabral, R. A. Pfuetzner, A. Kuo, J. M. Gulbis, S. L. Cohen, B. T. Chait, R. MacKinnon, *Science (80-.).* **1998**, *280*, 69–77.

[133] Q. Kuang, P. Purhonen, H. Hebert, *Cell. Mol. Life Sci.* **2015**, *72*, 3677–3693.

[134] A. N. Thompson, D. J. Posson, P. V. Parsa, C. M. Nimigean, *Proc. Natl. Acad. Sci. U. S.*

A. **2008**, *105*, 6900–6905.

[135] M. Varadi, S. Anyango, M. Deshpande, S. Nair, C. Natassia, G. Yordanova, D. Yuan, O. Stroe, G. Wood, A. Laydon, A. Žídek, T. Green, K. Tunyasuvunakool, S. Petersen, J. Jumper, E. Clancy, R. Green, A. Vora, M. Lutfi, M. Figurnov, A. Cowie, N. Hobbs, P. Kohli, G. Kleywegt, E. Birney, D. Hassabis, S. Velankar, *Nucleic Acids Res.* **2022**, *50*, D439–D444.

[136] M. Andersson, J. Vincent, D. van der Spoel, J. Davidsson, R. Neutze, *Structure* **2008**, *16*, 21–28.

[137] J. Trewhella, *Structure* **2022**, *30*, 15–23.

[138] J. Bietsch, M. Olson, G. Wang, *Gels* **2021**, *7*, 134.

[139] P. Dastidar, *Chem. Soc. Rev.* **2008**, *37*, 2699–2715.

[140] J. H. Van Esch, *Langmuir* **2009**, *25*, 8392–8394.

[141] A. R. Hirst, I. A. Coates, T. R. Boucheteau, J. F. Miravet, B. Escuder, V. Castelletto, I. W. Hamley, D. K. Smith, *J. Am. Chem. Soc.* **2008**, *130*, 9113–9121.

[142] D. J. Adams, *J. Am. Chem. Soc.* **2022**, *144*, 11047–11053.

[143] A. Axelsson, L. Ta, H. Sundén, *European J. Org. Chem.* **2016**, *2016*, 3339–3343.

[144] H. Sundén, L. Ta, A. Axelsson, *JoVE (Journal Vis. Exp.* **2015**, *2015*, e53213.

[145] A. Axelsson, L. Ta, H. Sundén, *Catalysts* **2015**, *5*, 2052–2067.

[146] L. Ta, A. Axelsson, J. Bijl, M. Haukka, H. Sundén, *Chem. – A Eur. J.* **2014**, *20*, 13889–13893.

[147] P. C. Chiang, J. Kaeobamrung, J. W. Bode, *J. Am. Chem. Soc.* **2007**, *129*, 3520–3521.

[148] C. Sauvée, A. Ström, M. Haukka, H. Sundén, *Chem. - A Eur. J.* **2018**, *24*, 8071–8075.

[149] M. D. Johnstone, C. W. Hsu, N. Hochbaum, J. Andréasson, H. Sundén, *Chem. Commun.* **2020**, *56*, 988–991.

[150] C.-W. Hsu, C. Sauvée, H. Sundén, J. Andréasson, *Chem. Sci.* **2018**, *9*, 8019–8023.

[151] S. C. Zacharias, M. Kamlar, H. Sundén, *Ind. Eng. Chem. Res.* **2021**, *60*, 10056–10063.

[152] D. F. Barbosa De Mattos, A. Dreos, M. D. Johnstone, A. Runemark, C. Sauvée, V. Gray, K. Moth-Poulsen, H. Sundén, M. Abrahamsson, *J. Chem. Phys.* **2020**, *153*, 1–9.

[153] M. Vakili, H. Han, C. Schmidt, A. Wrona, M. Kloos, I. de Diego, K. Dörner, T. Geng, C. Kim, F. H. M. Koua, D. V. M. Melo, M. Rappas, A. Round, E. Round, M. Sikorski, J. Valerio, T. Zhou, K. Lorenzen, J. Schulz, *J. Appl. Crystallogr.* **2023**, *56*, 1038–1045.

[154] J. Park, K. H. Nam, *Trends Anal. Chem.* **2024**, *172*, 117554.

[155] R. Andersson, C. Safari, P. Bath, R. Bosman, A. Shilova, P. Dahl, S. Ghosh, A. Dunge, R. Kjeldsen-Jensen, J. Nan, R. L. Shoeman, M. Kloos, R. B. Doak, U. Mueller, R. Neutze, G. Brändén, *Acta Crystallogr. Sect. D Struct. Biol.* **2019**, *75*, 937–946.

[156] S. Ghosh, D. Zoric, P. Dahl, M. Bjelčic, J. Johannesson, E. Sandelin, P. Borjesson, A. Björling, A. Banacore, P. Edlund, O. Aurelius, M. Milas, J. Nan, A. Shilova, A. Gonzalez, U. Mueller, G. Brändén, R. Neutze, *J. Appl. Cryst.* **2023**, *56*, 56.

[157] C. Safari, S. Ghosh, R. Andersson, J. Johannesson, P. Båth, O. Uwangue, P. Dahl, D. Zoric, E. Sandelin, A. Vallejos, E. Nango, R. Tanaka, R. Bosman, P. Börjesson, E. Dunevall, G. Hammarin, G. Ortolani, M. Panman, T. Tanaka, A. Yamashita, T. Arima, M. Sugahara, M. Suzuki, T. Masuda, H. Takeda, R. Yamagiwa, K. Oda, M. Fukuda, T. Tosha, H. Naitow, S. Owada, K. Tono, O. Nureki, S. Iwata, R. Neutze, G. Brändén, *Sci. Adv.* **2023**, *9*, 1–12.

[158] I. Ishigami, A. Lewis-Ballester, A. Echelmeier, G. Brehm, N. A. Zatsepin, T. D. Grant, J. D. Coe, S. Lisova, G. Nelson, S. Zhang, Z. F. Dobson, S. Boutet, R. G. Sierra, A. Batyuk, P. Fromme, R. Fromme, J. C. H. Spence, A. Ros, S. R. Yeh, D. L. Rousseau, *Proc. Natl. Acad. Sci. U. S. A.* **2019**, *116*, 3572–3577.

[159] F. Kolbe, S. Safarian, Ż. Piórek, S. Welsch, H. Müller, H. Michel, *Nat. Commun.* **2021**, *12*, 6903.

[160] C. Ostermeier, A. Harrenga, U. Ermler, H. Michel, *Proc. Natl. Acad. Sci.* **1997**, *94*, 10547–10553.

[161] T. Tiefenbrunn, W. Liu, Y. Chen, V. Katritch, C. D. Stout, J. A. Fee, V. Cherezov, *PLoS One* **2011**, *6*, e22348.

[162] R. Andersson, C. Safari, R. Dods, E. Nango, R. Tanaka, A. Yamashita, T. Nakane, K. Tono, Y. Joti, P. Båth, E. Dunevall, R. Bosman, O. Nureki, S. Iwata, R. Neutze, G. Brändén, *Sci. Rep.* **2017**, *7*, 4518.

[163] W.-G. Han Du, D. McRee, A. W. Götz, L. Noodleman, *Inorg. Chem.* **2020**, *59*, 8906–8915.

[164] M. Fabian, D. Jancura, G. Palmer, *J. Biol. Chem.* **2004**, *279*, 16170–16177.

[165] E. Forte, M. C. Barone, M. Brunori, P. Sarti, A. Giuffrè, *Biochemistry* **2002**, *41*, 13046–13052.

[166] S. Yoshikawa, K. Shinzawa-Itoh, R. Nakashima, R. Yaono, E. Yamashita, N. Inoue, M. Yao, M. J. Fei, C. P. Libeu, T. Mizushima, H. Yamaguchi, T. Tomizaki, T. Tsukihara, *Science (80-.).* **1998**, *280*, 1723–1729.

[167] A. L. Woelke, A. Wagner, G. Galstyan, T. Meyer, E. W. Knapp, *Biophys. J.* **2014**, *107*, 2177–2184.

[168] T. Oshima, K. Imahori, *Int. J. Syst. Bacteriol.* **1974**, *24*, 102–112.

[169] M. Roeßler, X. Sewald, V. Müller, *FEMS Microbiol. Lett.* **2003**, *225*, 161–165.

[170] J. C. I. I. I. Lukesh, M. J. Palte, R. T. Raines, *J. Am. Chem. Soc.* **2012**, *134*, 4057–4059.

[171] J. Park, S. Park, J. Kim, G. Park, Y. Cho, K. H. Nam, *Sci. Rep.* **2019**, *9*, 2525.

[172] G. Kovácsová, M. L. Grünbein, M. Kloos, T. R. M. Barends, R. Schlesinger, J. Heberle, W. Kabsch, R. L. Shoeman, R. B. Doak, I. Schlichting, *IUCrJ* **2017**, *4*, 400–410.

[173] A. Mahmoud Asadirad, Z. Erno, N. R. Branda, *Chem. Commun.* **2013**, *49*, 5639–5641.

[174] D. Dutta, J. Wang, X. Li, Q. Zhou, Z. Ge, *Small* **2022**, *18*, 2202369.

[175] W. Fudickar, T. Linker, *ChemPhotoChem* **2018**, *2*, 548–558.

[176] W. Fudickar, T. Linker, *J. Org. Chem.* **2017**, *82*, 9258–9262.

[177] W. Fudickar, T. Linker, *J. Am. Chem. Soc.* **2012**, *134*, 15071–15082.

[178] D. M. Gill, L. Male, A. M. Jones, *Chem. Commun.* **2019**, *55*, 4319–4322.

[179] K. T. Lau, R. Shepherd, D. Diamond, D. Diamond, *Sensors* **2006**, *6*, 848–859.

[180] M. Wulff, A. Plech, L. Eybert, R. Randler, F. Schotte, P. Anfinrud, *Faraday Discuss.* **2003**, *122*, 13–26.

[181] M. Cammarata, L. Eybert, F. Ewald, W. Reichenbach, M. Wulff, P. Anfinrud, F. Schotte, A. Plech, Q. Kong, M. Lorenc, B. Lindenau, J. Räbiger, S. Polachowski, *Rev. Sci. Instrum.* **2009**, *80*, 15101.